LABORATORY EXPERIMENTS AND NUMERICAL MODELING OF WAVE ATTENUATION THROUGH ARTIFICIAL VEGETATION

A Thesis

by

LAUREN NICOLE AUGUSTIN

Submitted to the Office of Graduate Studies of
Texas A&M University
in partial fulfillment of the requirements for the degree of

MASTER OF SCIENCE

December 2007

Major Subject: Ocean Engineering

LABORATORY EXPERIMENTS AND NUMERICAL MODELING OF WAVE ATTENUATION THROUGH ARTIFICIAL VEGETATION

A Thesis

by

LAUREN NICOLE AUGUSTIN

Submitted to the Office of Graduate Studies of
Texas A&M University
in partial fulfillment of the requirements for the degree of

MASTER OF SCIENCE

Approved by:

Co-Chairs of Committee,	Patrick Lynett
	Jennifer Irish
Committee Members,	Billy Edge
	Achim Stössel
Head of Department,	David Rosowsky

December 2007

Major Subject: Ocean Engineering

ABSTRACT

Laboratory Experiments and Numerical Modeling of Wave Attenuation Through Artificial Vegetation. (December 2007)

Lauren Nicole Augustin, B.S., Texas A&M University

Co-Chairs of Advisory Committee: Dr. Patrick Lynett

Dr. Jennifer Irish

It is commonly known that coastal vegetation dissipates energy and aids in shoreline protection by damping incoming waves and depositing sediment in vegetated regions. However, this critical role of vegetation to dampen wave forces is not fully understood at present. A series of laboratory experiments were conducted in the Haynes Coastal Laboratory and 2-D flume at Texas A&M University to examine different vegetative scenarios and analyze the wave damping effects of incident wave height, stem density, wave period, plant type, and water depth with respect to stem length.

In wetland regions vegetation is one of the main factors influencing hydraulic roughness. Traditional open-channel flow equations, including the Manning and Darcy-Weisbach friction factor approach, have been successfully applied to determine bottom friction coefficients for flows in the presence of vegetation. There have been numerous relationships derived relating the friction factor to different flow regime boundary layers

to try and derive a wave friction factor for estimating energy dissipation due to bottom bed roughness. The boundary layer problem is fairly complex, and studies relating the wave friction factor to vegetation roughness elements are sparse. In this thesis the friction factor is being applied to estimate the energy dissipation under waves due to artificial vegetation. The friction factor is tuned to the laboratory experiments through the use of the numerical model COULWAVE so that the pipe flow formulation can be reasonably applied to wave problems. A numerical friction factor is found for each case through an iterative process and empirical relationships are derived relating the friction factor for submerged and emergent plant conditions to the Ursell number. These relationships can be used to reasonably estimate a wave friction factor for practical engineering purposes.

This thesis quantitatively analyzes wave damping due to the effects of wave period, incident wave height, horizontal stem density, water depth relative to stem length, and plant type for a 6 m plant bed length. A friction factor is then determined numerically for each of the laboratory experiments, and a set of equations is derived for predicting a roughness coefficient for vegetation densities ranging between 97 stems/m^2 and 162 stems/m^2.

ACKNOWLEDGEMENTS

First and foremost, I would like to thank my advisor, Dr. Patrick Lynett, for his continuous support throughout my academic career at Texas A&M. Despite his many other professional commitments he has always been there to guide and motivate me. His encouragement and wisdom has truly inspired me. I would also like to thank Dr. Jennifer Irish for being the co-chair of my committee, and for giving me the opportunity to work on this project. Without her enthusiasm, motivation, and guidance this project would have not been possible. Working with both Dr. Lynett and Dr. Irish has been a very enjoyable experience and I look forward to future collaborations. I am very grateful to my thesis committee members, Dr. Billy Edge and Dr. Achim Stössel, for their contributions and for taking the time to review this work. I want to especially thank Dr. Billy Edge for allowing me to use the Haynes Coastal Laboratory to conduct my experiments. Without this opportunity a large portion of this work would have not been possible. I would also like to thank Dr. Jim Kaihatu for his discussions and contributions to this study. I cannot express enough how grateful I am to Greg Balsemeier for assisting me in the lab. Without his invaluable help it would have been impossible to achieve my research goals on time. I would also like to thank Oscar and Carmen Cruze for helping me in the Haynes Lab, despite their other academic and work commitments. Additionally, many thanks to Dave Piazza for helping with the construction of the artificial wetlands in both the basin and in the laboratory flume. Finally, I would like to express my utmost appreciation to my friends and family for the ongoing support throughout my thesis work, without you none of this would have been possible.

NOMENCLATURE

h	Water depth
η	Free surface elevation
k	Wave number
L	Wavelength
A	Wave amplitude
A_o	Incident or approaching wave amplitude
H_i	Incident or approaching wave height
H_{mo}	Zero moment wave height
H_m	Mean wave height
H_s	Significant wave height
H_{rms}	Root-mean-square wave height
d	Plant stem diameter
t_v	Plant thickness
b_v	Plant width
F_x	Horizontal force
F_z	Vertical force
t	Time
T	Wave period
u	Horizontal particle velocity of fluid
w	Vertical particle velocity of fluid
u_r	Relative horizontal velocity between vegetation and fluid
a_f	Fluid acceleration

a_r	Relative acceleration between vegetation and fluid
A_p	Projected area of plant stem
ρ	Density of fluid
ρ_v	Density of vegetation
V	Volume of plant stem
C_M	Inertia coefficient
C_D	Drag coefficient
C_R	Reflection coefficient
F_D	Drag force
F_T	Total force
v	Kinematic viscosity of fluid
K	Wave attenuation coefficient
σ	Angular frequency of wave
f	Darcy-Weisbach friction factor
f_N	Numerically determined friction factor
$f_N^{(S)}$	Numerical friction factor for submerged plant conditions
$f_N^{(E)}$	Numerical friction factor for emergent plant conditions
g	Gravitational acceleration
S_v	Plant spacing
s	Distance above plant bed
l_p	Length of plant stem
b_v	Plant area per unit height
N	Number of vegetation stems per unit area

f_p	Peak frequency
γ_b	Adjusting parameter from Thornton and Guza (1983) model
E	Energy density
c_g	Group celerity
ϵ_v	Energy dissipation due to vegetation
ϵ_b	Energy dissipation due to wave breaking
ϵ_D	Energy dissipation due to drag
p	Dynamic pressure
p_{atm}	Atmospheric pressure
k_i	Imaginary wave number
f_s	Sample frequency
x	Horizontal coordinate in space, positive in direction of wave propagation
z	Vertical coordinate in space
R	Reflected wave amplitude
T	Transmitted wave amplitude
ϱ	Ensemble parameter
M	Mass transport
S_{ij}	Radiation stress
λ	Portion of water depth occupied by stem
r	Ratio of wave group celerity to phase speed
αh	Mean vegetation height
S_η	Unidirectional frequency spectrum
B	Adjusting parameter from Thornton and Guza (1983) model

δ	Damping factor
Q	Rate of water discharge
n	Manning roughness coefficient
C	Chezy coefficient
R_h	Hydraulic radius
S	Slope of water surface
A_c	Cross-sectional area
τ_b	Basal shear stress
C_f	Generalized non-dimensional friction factor

TABLE OF CONTENTS

Page

Page

LIST OF FIGURES

Page

Page

Page

Page

LIST OF TABLES

Page

CHAPTER I

INTRODUCTION

1.1. Importance of Coastal Vegetation

Beaches are one of our most important natural resources, and once destroyed repair is a difficult, costly, and a repetitive, if not an impossible process. The prevention of erosion of our coastlines requires an understanding of wave motion, nearshore hydrodynamics, beach morphology, the movement of beach sediment, and the effects of wetland vegetation. Until recently, shoreline protection typically involved constructing hard structures such as jetties and breakwaters to dissipate and reflect wave energy. These methods disrupt regional and local sediment transport and alter nearshore hydrodynamics and circulation patterns. The latest trends in coastal engineering are focusing on more non-intrusive forms of shore protection such as vegetation, which protects the shoreline and provides a natural habitat for many different species of fish, amphibians, shellfish, insects and birds. Wetlands are one of the most productive ecosystems in the world with valuable natural resources that provide important benefits to people and the environment. Aquatic vegetation helps regulate water levels, improve water quality, reduce flood and storm damages, provide important fish and wildlife habitats, and support recreational activities.

This thesis follows the style of the *Journal of Geophysical Research*

Additionally, vegetation directly increases the durability of shorelines through the root systems and enhances the storage of sand in dunes (Dean, 1978). Until recently the importance and function of wetlands was not well understood, and the amount of wetlands being degraded and lost annually was approximately 70,000 to 90,000 acres (EPA, 2007). Because of the destruction of wetlands, our coasts are becoming more vulnerable to the damages resulting from hurricane storm surge and other extreme weather events. In 2005 Hurricane Katrina and Rita caused record storm surge and damage, resulting in over 1500 deaths, and more than $80 billion in total property damages (Knabb *et al*. 2006) and 300 km^2 of lost land and wetlands (U.S. Geological Survey 2006). In addition to extreme weather events, wetlands may also provide protection against sea level rise. Vegetation is known to dissipate incoming wave energy and trap sediment, which in turn can help build a shoreline upward and accrete the beach seaward, maintaining itself above the rising sea. It is predicted that increasing rates of glacial melting, combined with thermal expansion of the ocean's water, will raise sea levels potentially 1-2 m within the next 100 years (Komar, 1998). Sea level rise will inundate low-lying coasts, making more areas susceptible to coastal flooding by storm surge. While we cannot stop sea level rise, it is possible to restore natural wetlands and construct new wetlands that may help reduce flood damage. Wetlands naturally store water spreading it more evenly across the floodplain and help slow the speed of flood waters, thus lowering flood heights and reducing erosion.

1.2. Motivation

It is commonly known that vegetation dissipates energy and aids in shoreline protection by damping incoming waves and depositing sediment in vegetated regions. The hydrodynamic processes in wetland ecosystems are one of the most important governing factors, therefore the interaction between water waves and vegetation needs to be quantified (Asano *et al*., 1992). However, this critical role of vegetation to dampen wave forces is not fully understood at present. Extreme weather events and accelerated sea level rise projections based on climate change research may result in increased levels of flooding of vegetated regions (American Society of Civil Engineers Task Committee on Sea Level and its Effects on Bays and Estuaries, 1992), therefore the need to understand these vegetation mechanisms is urgent. In order to address this urgent need, a series of laboratory experiments were conducted to examine different vegetative scenarios and qualitatively analyze the wave damping effects of each. However, in these experiments only waves are considered, while wind and currents that accompany storm surge are neglected. Additionally, the attenuation due to vegetation roughness for each experiment is estimated through the determination of a nondimensional friction factor. The estimation of vegetation roughness coefficients are an important factor in the calibration and validation of ocean and river hydraulic models.

The objectives of this research are as follows:

- Conduct controlled laboratory flume tests on an array of artificial wetland scenarios for emergent and submerged plant conditions

- Analyze monochromatic and spectral wave characteristics, including wave height decay
- Determine dependence of wave and vegetation parameters on wave attenuation
- Numerically determine a friction factor for each vegetation scenario using the COULWAVE Boussinesq model

1.3. Thesis Content

This thesis is divided into six chapters. Chapter I presents a general overview of coastal vegetation and discusses the need for improved understanding in the area of vegetative damping research. The first section of this chapter contains an introduction to wetlands and explains why vegetation is an important asset to our shorelines. Section two includes the motivation and objectives of the research presented in this thesis. Chapter II is divided into three parts and presents a background of theory and a review of relevant literature. Wave attenuation theories for flow through emergent and submerged vegetation are discussed in section two and section three presents a brief overview of common open-channel flow approaches applied for predicting vegetation roughness. In Chapter III, the experimental setup, equipment, and data collection procedures are outlined. A discussion of the data reduction process is also presented. Chapter IV is divided into two parts, and presents the data analysis procedures and experimental results for the Haynes Coastal basin and flume experiments. Influences of wave characteristics and vegetation parameters on wave attenuation are discussed. Chapter V includes a brief introduction to the COULWAVE Boussinesq model and

presents the vegetation friction factors simulated for each laboratory vegetation scenario. Empirical equations are derived for estimating a friction factor value for emergent and submerged plant conditions. Conclusions and suggestions for future work are contained in Chapter VI.

CHAPTER II

BACKGROUND AND LITERATURE REVIEW

2.1. Introduction

Wave attenuation by emergent and submerged vegetation is a function of plant characteristics (geometry, stem density, spatial coverage, buoyancy, stiffness) as well as water depth, wave period, and wave height. In general, the damping of surface waves is caused by the energy loss through work performed on the plants (Mork, 1996). Numerous models exist that attempt to relate the interactions between waves and vegetative plants to explain the damping effects of vegetative fields. A definition sketch of the typical vegetation model is shown below in Figure 1, where S_v is the plant spacing, d is the plant diameter, l_p is the length of the plant stem, h is the water depth, s is the inundation depth of the vegetation, and F_x is the horizontal force exerted on the plant.

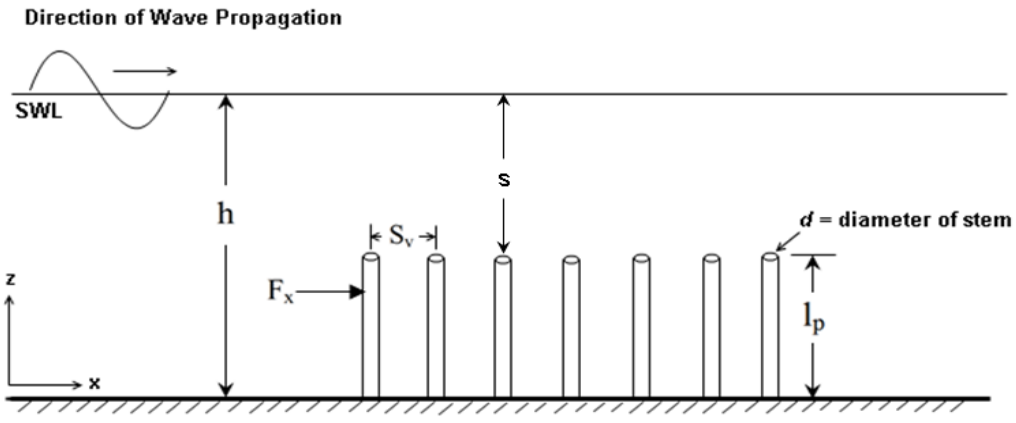

Figure 1. Definition sketch of wave and plant parameters.

Interaction of fluid flow in aquatic vegetation is dynamic because the structure of the plant field changes with time as it is exposed to the physical forcing of wave action and water flow (Mendez and Losada, 2004). The first hydrodynamic model developed by Price et al. (1968) simulated the effects of seaweed as a high viscous layer. Mork (1996) extended the idea of the high viscous layer and developed a theory for kelp plants that took into account not only viscous drag, but form drag for the canopy layer and the lower vegetative area. Vegetation has also been modeled as a high friction area by Camfield (1983) who studied wind-wave growth over shallow flooded regions. Numerous models predict wave attenuation using the conservation of wave energy equation and account for vegetation effects in an energy dissipation term (Dalrymple *et al*. 1984, Mendez and Losada 2004), while others simulate the drag forces induced by the waves along the stem of the plant (Kobayashi *et al.,* 1993). All of these methods ultimately end up with a solution for the exponential decay in wave height through the vegetation field. Each model has its own advantages and disadvantages, depending on how the wave force on the plant is represented. Unfortunately, the variety of wetland plants is extensive and trying to find a generalized method for modeling the behavior of plant dissipation is practically impossible (Mendez and Losada, 2004). The vast majority of vegetation flow studies focus on a single species of vegetation localized in a particular region.

2.2. Wave Attenuation Theory

Price *et al.* (1968) was the first to propose a simple hydrodynamic model to predict wave attenuation due to submerged artificial polypropylene seaweed. He

conducted experiments in the laboratory and in the field to observe how seaweed affected incoming wave heights and on-shore mass transport of sediment. A field of 12.7 cm (5 in) long polypropylene "pony tails" was assembled on a 14.2 cm (5.6 in) grid offshore of a model beach and subject to 7.6 cm (3 in) waves with a 1.3 s period. Price observed that the seaweed dampened the waves by approximately 4 percent due to energy dissipation at the bed. The model assumes that the water-seaweed layer is of higher viscosity than the water layer above the vegetation. This idea is suggested because the plant stems stay near vertical close to the sea bed. The modulus of wave attenuation (K) derived by Price *et al.* is given as,

$$K = \left(\frac{2\upsilon}{\sigma}\right)^{\frac{1}{2}} \frac{k^2}{2kh + \sinh 2kh} \tag{2.1}$$

where υ is the fluid viscosity, σ is the angular wave frequency, and k is the wave number. The model assumes that the wave height decays exponentially relative to the wave attenuation modulus. The wave amplitude as it propagates through the vegetation field is then expressed as

$$A = A_o e^{-Kx} \cos(kx - \sigma t) \tag{2.2}$$

where A_o is the amplitude of the approaching incident wave. Price concluded that wave attenuation arises principally from viscous shearing stress in the horizontal plane at the sea bed, and at that the time it was thought this model could be reasonably applied over a wide range of conditions.

An energy dissipation model was developed by Dalrymple *et al.* (1984) which represented vegetative plants as an array of slender, vertical, rigid cylinders. This theory

is derived from the conservation of energy equation and linear wave theory and assumes that waves are propagating over a flat bottom. Energy loss due to the presence of the rigid cylinders is accounted for in a bulk drag coefficient term (C_D). If flexible members are to be considered, the drag coefficient should take on different values in order to try and compensate for plant motion. The model can be applied to either emergent or submerged plant conditions by specifying the elevation of the top of the plant relative to the bottom ($s=h-l_p$). Energy dissipation due to drag (ϵ_D) is evaluated as a function of the drag force (F_D) so that,

$$\epsilon_D = F_D u = 2\rho \frac{C_D}{3\pi} \frac{d}{k} \frac{\left(sinh^3 ks + 3\, sinh\, ks\right)}{3\, cosh^3 kh} \left(\frac{gk}{\sigma}\right)^3 \left(\frac{1}{S_v{}^2}\right) \tag{2.3}$$

where u is the horizontal fluid velocity and g is the acceleration due to gravity. The dissipation is evaluated over the length of the plant and the solution for the wave amplitude decay through the vegetation field is given by,

$$A = A_o \left(\frac{1}{1 + \delta x}\right) \tag{2.4}$$

where δ is a damping factor given by:

$$\delta = \frac{2C_D}{3\pi} \left(\frac{d}{S_v}\right) \left(\frac{A_o}{S_v}\right) \left(sinh^3 ks + 3\, sinh\, ks\right) \left[\frac{4k}{3\, sinh\, kh(sinh\, 2kh + 2kh)}\right] \tag{2.5}$$

The method developed by Dalrymple *et al.* (1984) was extended to an empirical model for wave damping and wave breaking over variable depth vegetation fields by Mendez and Losada (2004). This model was the first to incorporate both monochromatic and random waves, consider wave breaking, and include a calibration parameter to account for plant type. Similar to the formulation in Dalrymple *et al.* (1984), this empirical model also accounts for plant motion in the drag coefficient (C_D). Even though swaying

motion is neglected, C_D can be adjusted so that the model can be applied for rigid or flexible plants. The horizontal plant-induced drag force (F_x) per unit volume is expressed as

$$F_x=\frac{1}{2}\rho C_D b_v N u|u| \tag{2.6}$$

where b_v is the plant area per unit height of each vegetation stand normal to u, and N is the number of vegetation stems per unit horizontal area. The energy conservation equation is extended to include the energy dissipation resulting from breaking $\langle \varepsilon_b \rangle$ and from the presence of vegetation $\langle \varepsilon_v \rangle$,

$$\frac{\partial Ec_g}{\partial x} = -\langle \varepsilon_b \rangle - \langle \varepsilon_v \rangle \tag{2.7}$$

in which

$$\langle \varepsilon_b \rangle = \frac{3\sqrt{\pi}}{16}\rho g \frac{B^3 f_p}{\gamma_b^4 h^5} H_{rms}^7 \tag{2.8}$$

$$\langle \varepsilon_v \rangle = \frac{1}{2\sqrt{\pi}}\rho C_D b_v N \left(\frac{kg}{2\sigma}\right)^3 \times \frac{\sinh^3 k\propto h + 3\sinh k\propto h}{3k\cosh^3 kh} H_{rms}^3 \tag{2.9}$$

where H_{rms} is the root-mean-square wave height, B and γ_b are adjusting parameters from the Thornton and Guza (1983) model, E is the energy density, αh is the mean vegetation height, f_p is the peak frequency, and c_g is the group celerity. The method has been validated by artificial laboratory kelp experiments for the species *Laminaria Hyperborea*, and is assumed appropriate for representing wave transformation and damping over submerged vegetative fields of variable depths.

Mork (1996) studied the kelp plant called *Laminaria Hyperborea* and proposed a simple, linear model based on the assumption that rotational and dissipative effects are important in the canopy level, and that friction due to shear stresses and form drag are

important in the lower layer of the kelp vegetation. Mork assumed that the force acting on each kelp plant was a sum of the viscous shear stress and form drag and observed that each kelp stipe acted as an elastic spring with bending similar to that of a cantilever beam. Mork observed that 70% to 85% of the total wave energy was reduced over a field 258 m long (0.27 to 0.33% per m), where the highest amount of attenuation occurred during shallow depths associated with low tide. His observations also supported that the kelp fronds were more effective at dissipating wave energy than stipes due to greater form drag.

Kobayashi *et al.* (1993) presents a model based on the continuity and depth integrated, time averaged momentum equations, as opposed to the typical energy balance approach. In this model, it is assumed that the force acting on the plant is distributed over depth and is a function of the linear drag force. The method analyzes the regions above and below the vegetation over a plane and horizontal bottom. In the region below the vegetation the momentum equations per unit water volume are given by,

$$\rho \frac{\partial u}{\partial t} = -\frac{\partial p}{\partial x} - F_x \tag{2.10}$$

$$\rho \frac{\partial w}{\partial t} = -\frac{\partial p}{\partial z} - F_z \tag{2.11}$$

where F_x and F_z are the horizontal and vertical drag forces acting on the vegetation, p is the dynamic pressure, and w is the vertical particle velocity. The horizontal resisting force acting on the vegetation is estimated assuming slender, rigid vertical cylinders as presented by Dalrymple *et al.* (1984), see equation 2.6. This force is linearized in order to find an analytical solution for the decay of wave height. The decay in wave amplitude is then expressed by

$$A = A_o \exp(-Kx) \tag{2.12}$$

where *K* is an exponential decay coefficient which can be written in terms of the complex wave number. Koboyashi *et al.* (1993) determined *K* through a regression analysis by fitting values to experimental data.

Mendez *et al.* (1999) extended the previous wave damping theories developed by Kobayashi *et al.* (1993) and Dubi and Torum (1995) to include random waves. The formulation solves for the flow through the vegetation field and includes the total wave field in front, along and leeward of the vegetation by dividing the vegetation field up into four regions. The theory offers the ability to analyze either emergent or submerged vegetation, however only region 2 (above vegetation) is applicable if the vegetation is non-emergent. The model assumes linear wave theory over a plane and horizontal bottom. Incident and reflected waves are considered, where *T* is the transmitted wave amplitude, *R* is the reflected wave amplitude, and *A* and *B* are wave amplitudes in the vegetation region, which are solved for using an iterative method. The effect of the vegetation is included in the linearized momentum equations in terms of a force, $\vec{F}$, acting on the vegetation and is expressed as

$$\frac{\partial \vec{u}_4}{\partial t} = -\frac{1}{\rho}\nabla p_4 - \frac{1}{\rho}\vec{F} \tag{2.13}$$

where $\vec{u}_4=(u_4,w_4)$ and is the velocity in the vegetation region, p_4 is the dynamic pressure in the vegetation section, and $\vec{F} = (F_x, F_z)$. The model also includes the effects of vegetation motion and provides a means to analyze free surface oscillations, velocity, acceleration, and pressure fields inside and outside the vegetation field, as well as the

wave-induced forces and moments. The forces acting on vegetation can be expressed in a formulation similar to that of the Morison equation:

$$F_x = \frac{1}{2}\rho C_D(z)N|u_r|(u_r) + \rho b_v(z)t_v(z)N\left[C_M(z)\dot{u}_4 - \left(C_M(z)-1\right)\ddot{\xi}\right] \quad (2.14)$$

$$F_z \cong 0 \quad (2.15)$$

where u_r is the relative velocity between the fluid flow and vegetation motion, C_M is the inertia coefficient, and $\ddot{\xi}$ is time derivative of the vegetation velocity. The motion of vegetation is modeled by a harmonic oscillation where plants are allowed to move independently. Similar to other theories, interaction between plant stems is not included. The model solves for the velocity associated with the fluid flow and vegetation motion and iterates until the velocity field in fluid converges with that in the vegetation. Once the velocities are known the time varying overturning forces and moments acting on the vegetation stems can be calculated to analyze plant mortality and breakage. The theory is extended to include random waves by defining a unidirectional frequency spectrum, S_η. Overall, this theory has been shown to provide a better fit to experimental data than previous theories because it includes the total wave field, including both incident and reflected waves.

Lima *et al.* (2006) developed a finite-difference numerical model based on experiments that were conducted with fixed length, flexible stretches of nylon rope in a laboratory flume. The nylon rope was used to simulate aquatic vegetation and is mathematically modeled as a string of nodes. The effect of each plant stem is included as an average resisting force in the time-averaged, depth-integrated momentum equation:

$$\frac{\partial}{\partial t}M_i+\frac{\partial}{\partial x_j}\left(u_iM_j\right)=p_{atm}-\rho_f g(h+\bar{\eta})\frac{\partial\bar{\eta}}{\partial x_i}-\frac{\partial}{\partial x_j}S_{ij}+\frac{1}{T}\int_0^T F_i dt \quad (2.16)$$

where the overbar stands for time average over one wave period, M_i is the total mass transport, S_{ij} are the radiation stresses, p_{atm} is atmospheric pressure, and F_i is the average resisting force of the plant stems acting on the fluid. Unlike previous theories, the total resisting force of the vegetation is not a summation of the individual effects of each plant stem. A nondimensional ensemble coefficient is added to the total force formulation which is a function of the stem density and vegetation flow parameters. The model breaks each plant stem into segments and determines the total hydrodynamic force, horizontal displacement and vertical displacement at each node by using a finite difference scheme. Vegetation motion is accounted for in the Morison equation where the total force (F_T) is expressed as:

$$F_T=\frac{1}{2}C_D\rho A_p u_r|u_r|+C_m\rho V a_r+\rho V a_f \quad (2.17)$$

where A_p is the projected stem area in the direction of fluid flow, a_r is the relative acceleration, and a_f is the fluid acceleration. An algebraic wave height decay coefficient (K) is then found:

$$K=7.916\frac{L^2\lambda^4}{gT^2(4r-1)l^2}\frac{\rho_v}{\rho}\phi^{5/2}N^{5/4} \quad (2.18)$$

where λ is the portion of the water depth occupied by the plant stem, ϕ is the velocity potential and r is the ratio between wave group celerity and phase velocity. The model was calibrated by observing the plant motion on video and marking points every 5 cm along the stem. Knowing the position of the points in time allowed for the calculation of velocity and acceleration along the stem so that the drag coefficient could be estimated

using equation 2.18. Lima *et al.* found that once the model was calibrated, it was possible to obtain satisfactory results for the hydrodynamic force time series, velocities and positions of stems.

2.3. Vegetative Bottom Roughness for Open Channel Flow

There are various methods available to estimate the bottom roughness for uniform flow in an open channel. The three most common approaches used in practice are Chezy's equation, Manning's equation and the Darcy-Weisbach equation. All of the formulations find a roughness coefficient related to the average velocity of the flow, $\bar{u}$. Chezy's equation is given by

$$\frac{Q}{A_c} = \bar{u} = C\sqrt{R_h S} \tag{2.19}$$

where Q is the rate of water discharge, C is the Chezy roughness coefficient [units of $L^{1/2}/T$], R_h is the hydraulic radius, and S is the slope of the water surface. Experiments have shown that the hydraulic radius dependence of open channel flow is not very accurate in the Chezy equation. For this reason Manning developed a more accurate modified equation for describing the flow in prismatic open channels. The Manning's equation in SI units is given by

$$\frac{Q}{A_c} = \bar{u} = \frac{1}{n} R_h^{2/3} S^{1/2} \tag{2.20}$$

where n is the Manning's roughness factor in units of $s/m^{1/3}$. The Darcy-Weisbach equation originally developed for pipe flow theory is expressed as

$$\bar{u}^2 = \frac{8gR_h S}{f} \tag{2.21}$$

where *f* is the non-dimensional Darcy-Weisbach friction factor. A more generalized version of the Darcy Weisbach equation is written as

$$\bar{u}=\frac{\sqrt{gR_hS}}{C_f^{1/2}} \tag{2.22}$$

and

$$\tau_b = \rho C_f \bar{u}^2 \tag{2.23}$$

which relates the generalized non-dimensional friction factor, C_f, to the basal shear stress, τ_b, assuming that the hydraulic radius is equivalent to that of the water depth. Both the friction factor for pipe flow and Manning coefficient relate the wall shear stress to the material of the bounding surface (Munson *et al.* 2002), therefore there are various relationships available that describe *n* in terms of the pipe friction factor, *f*. For a wide shallow channel, the relationship in metric units between Manning's *n* and the Darcy-Weisbach friction factor *f* is given by

$$n = \sqrt{f}\left(\frac{h^{1/3}}{8g}\right) \tag{2.24}$$

Vegetation is one of the main factors influencing hydraulic roughness, with other factors being sediment grain size, bottom bathymetry, sediment transport, variations in channel width and depth, channel curvature, and flow obstructions. According to Kadlec (1990) the Manning equation assumes that flow is fully turbulent, which is usually not the case in wetland flow areas during daily conditions; however, during storm conditions flow is likely to be turbulent. Many studies have found that the Manning coefficient is strongly dependent on factors including the depth, vegetation density, and Reynolds number. The Darcy-Weisbach approach is suitable for flows that range from laminar to

turbulent flow, but is also dependent on various parameters such as depth, slope, and vegetation type (Kadlec, 1990). Despite the assumption of turbulent flow, the Manning equation is the most widely used in practice. Tshirky (2000) presents typical values of the Manning coefficient for different flow scenarios. For flow that is shallow compared to the vegetation height the Manning *n* takes on a value in the range of 0.25 and 0.3. As vegetation is submerged, plant stems begin to oscillate and interact, resulting in an increase in *n* value up to 0.4. Once the flow reaches a turbulent state, plant stems are flattened against the bed and the value of the Manning *n* decreases. Both the Manning and Darcy-Weisbach open channel flow equations have been successfully applied to flows in the presence of vegetation in the field and in the laboratory. Chen (1976) investigated laminar sheet flow over a shallow grassed channel and analyzed two species of turf grasses, Kentucky Blue grass and Bermuda grass. The grasses were planted in 0.3 m (1 ft) of soil inside a long narrow flume. Chen varied the bed slope and flow rates over the vegetation and measured the corresponding discharge and depth of flow at the end of the plant bed. He then calculated the friction factor for each experimental case and found that *f* increases with bed slope, and decreases with Reynolds number. It was concluded that the roughness coefficient for any species of turf grass could be reasonably represented a friction factor, and that the value would be a few orders of magnitude greater than that of a concrete surface.

The Darcy-Weisbach friction factor is developed for steady pipe flow, and is not meant to represent bottom friction dealing with the unsteady turbulent boundary layers that are present under waves. There have been numerous relationships derived relating

the friction factor to different flow regime boundary layers to try and derive a wave friction factor for estimating energy dissipation due to bottom bed roughness. The boundary layer problem is fairly complex and studies relating the wave friction factor to vegetation roughness elements are sparse. In this thesis, the friction factor is being adopted from the steady pipe flow theory and is being applied to estimate the energy dissipation under waves due to artificial vegetation. The friction factor will then be tuned to the laboratory experiments so that the pipe flow formulation can be reasonably applied to wave problems.

There have been numerous studies done relating the Manning coefficient to different types of vegetation roughness. In an effort to improve the relationship between the Manning equation and functional flow parameters, Kouwen *et al.* (1969) derived a quasi-theoretical formula for flow retardance in vegetated channels that could be calibrated according to vegetation density and plant flexibility. The method is based on experiments conducted in a flume with flexible plastic elements. The slope of the water surface, depth of flow, average deflected height of vegetation, and velocity profiles were measured for varying bed slopes and water depths. Experiments found that the Manning coefficient is largely dependent on relative roughness, the ratio of water depth to the deflected height of the vegetation element.

In a subsequent study, Kouwen and Unny (1973) analyzed three different flow regimes over flexible plastic strips in a laboratory flume and derived an equation for calculating the vegetation friction factor based on relative roughness and plant flexibility. Experiments found that the local friction factor was a constant value when the

plastic strips were in an erect (stationary) or waving condition, and decreased significantly when the strips were prone (flat against the bed). The study concluded that for stationary and waving plant conditions the friction factor was primarily a function of the relative roughness, but for prone strips, most likely occurring during turbulent flow, the friction factor was dependent on Reynolds number. There have been countless other studies done that confirm the dependence of plant flexibility and the importance of vegetation height in relation to the flow depth for estimating roughness coefficients. Despite these finding, the majority of hydraulic models assume rigid emergent elements (Kouwen and Fathi-Maghadam, 1997). A model developed by Kouwen and Fathi-Maghadam (1997) included the effects of plant flexibility and confirmed that the assumption of rigid vegetation, commonly used in practice, leads to large errors when estimating vegetation roughness.

CHAPTER III

EXPERIMENTAL SETUP

3.1. Introduction

Two sets of experiments were conducted in the 3-D basin at the Haynes Coastal Engineering Laboratory and in a 2-D flume at Texas A&M University to assess the effects of water depth, wave period and stem density (number of stems per unit area) on wave attenuation through artificial vegetation. Experiments in the Haynes Coastal Laboratory investigated irregular waves over flexible vegetation for both emergent and submerged plant conditions. A 4.6 m (15 ft) wide flume was constructed inside the basin where two different stem density arrangements were analyzed. For each irregular wave test the spectral wave height was held constant, while the peak period and water depth were varied.

Both rigid wooden dowels and flexible foam members were analyzed in a narrow 0.9 m (3 ft) wide flume using regular monochromatic waves. Wave height, stem density, wave period, plant rigidity, and water depth were varied during the runs to investigate the importance of each factor on wave damping. Wave periods representative of nearshore wind waves were chosen for testing, which ranged from 1.5 to 2.0 s. Additionally, two separate depths were analyzed, the first with the vegetation near emergent conditions (h=0.3 m), and the other with the vegetation fully submerged (h=0.4 m) where the vegetation stems were 0.3 m in length. Depths and periods analyzed were equivalent in both the basin and flume experiments for experiment similarity.

3.2. Test Layout and Design

3.2.1. Two-dimensional Flume

Monochromatic waves were analyzed over different vegetative scenarios in a laboratory flume 30.5 m (100 ft) long, 0.9 m (3 ft) wide, and 1.2 m (4 ft) deep. A SEASIM (RSW 90-85) Rolling Seal absorbing paddle wavemaker was used for generating waves at one end of the flume and a 3 m long rubber horsehair beach was constructed at the opposite end to absorb wave energy and reduce reflection effects (Figure 3). The vegetation field was placed approximately 13.1 m (43 ft) from the wavemaker, and extended 6 m (20 ft) down the length of the tank. Five SEASIM 2 resistance wire probe electronic wave gages were used to measure the free surface oscillations in the vegetation field for each test run. The gages were spaced equally 1.5 m (5 ft) apart from the beginning to the end of the field. Figure 2 shows the position of each gage, with the lines representing 1.5 m increments.

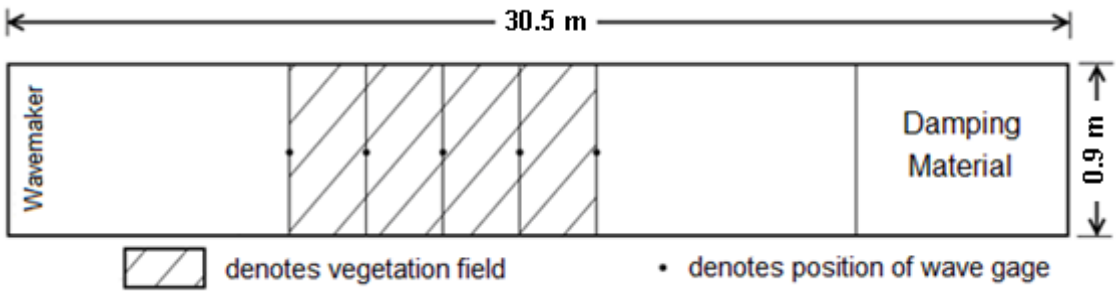

Figure 2. Plan view of 2D wave flume layout

Four different test scenarios were attempted using rigid and flexible vegetation elements, however only 3 were successful due to construction and durability issues within the time allotted for experimentation. The first experiment consisted of a flexible polyethylene

foam vegetation field constructed on a 10.2 cm x 10.2 cm grid. The diameter of both the wooden dowels and flexible foam was 12 mm (0.5 in). The 10.2 cm (4 in) spacing gave a stem per unit area (N) of 97 stems/m^2. For the second set of experiments the stem density was doubled by placing a stem in the center of each 10.2 cm square. See layout two in Figure 3 for a diagram of the stem spacing for both layouts. For layout 2 the plant per unit area density was 162 stems/m^2. The 13.2 cm (4 in) spacing was chosen because Nepf showed this condition did not result in sheltering.

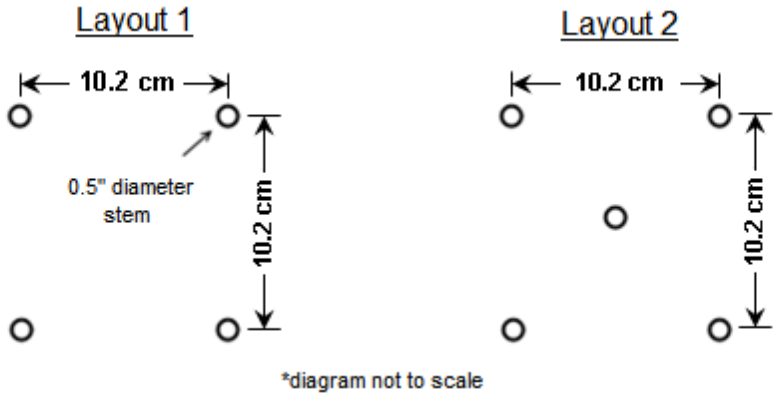

Figure 3. Experimental design layouts for plant stems

The third vegetative scenario was constructed out of rigid cylindrical dowels using stem layout 2. Table 1 summarizes the stem density and plant type for the three experimental cases.

Table 1. Summary of stem density and plant type for flume experiments

Type	97 stems/m^2	162 stems/m^2
Rigid dowels	X	X
Flexible foam	X	-

After approximately four days of testing the plywood and dowels became saturated with water, weakening the bond between the surface of the dowels and the wooden bottom of the flume. The original idea was to remove the center dowel from the constructed grid and conduct tests using Layout 1 with rigid stems. In order to have successfully completed the last scenario an entire new false bottom would have to have been constructed, which time constraints did not allow for.

To run tests at the desired water depth, the bottom of the flume was raised in order to overcome wavemaker limitations. A five inch false bottom was constructed out of ¾" plywood and was secured to the bottom of the flume using wooden 2x4's and lead weights. A small ramp, 1.2 m in length, was built to shoal waves up to the desired depth because the bottom could not be extended all the way to the edge of the wavemaker. Approximately 3 m were left to allow clearance for the drain. A side view of the flume bottom with the ramp and false bottom is shown below in Figure 4. To ensure a good seal and prevent bubbles, the sides and seems of the plywood were sealed with silicone gel.

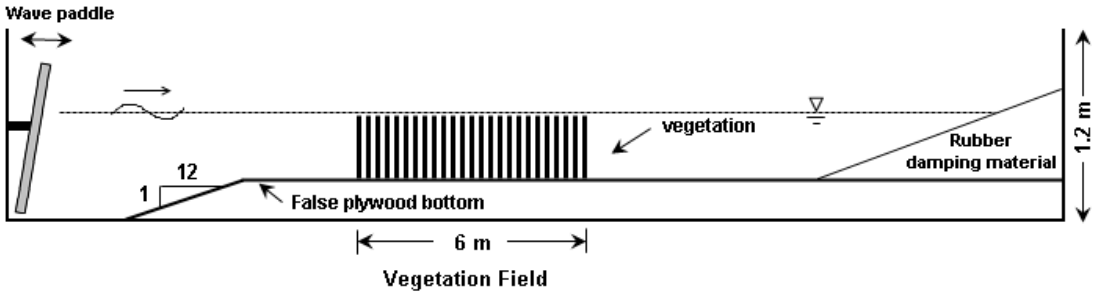

Figure 4. Side view of wave flume layout

3.2.2. Haynes Coastal Basin

Spectral wave experiments were conducted on flexible vegetation elements in the 3-D Haynes Coastal Engineering Laboratory. The basin is 22.9 m (75 ft) wide, 30.5 m (100 ft) long and 1.2 m (4 ft) deep, and has a 42 paddle wave maker at one end and a rock beach for wave absorption approximately 3 m long at the opposite end (Figure 5). A 4.6 m (15 ft) wide flume was constructed along one side of the basin and enclosed with concrete blocks. The blocks were approximately 4.5 m long, 20 cm wide, and 60 cm tall, and were placed inside the basin using a 3 ton overhead crane. Openings were left at the beginning and end of the flume to dissipate energy and minimize reflection within the experiment region. Additionally, rubber horsehair was placed in front of the first concrete block.

Figure 5. Front and end of concrete flume in 3-D basin

The vegetation field was placed near the center of the flume and was 6 m (20 ft) long and 4.6 m (15 ft) wide . The experimental layout is shown in Figure 6.

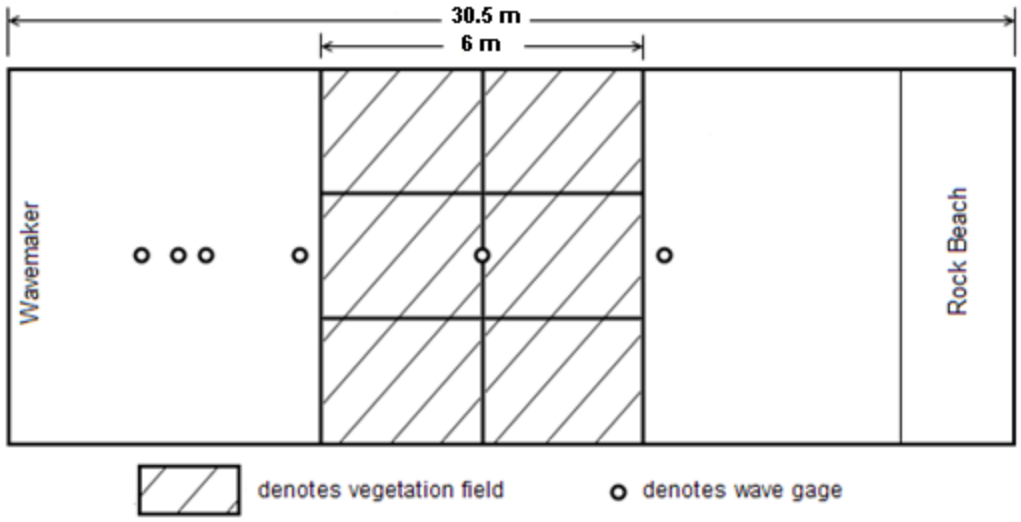

Figure 6. Position of wave gages and vegetation field in 3-D basin

The vegetation was assembled on 6 galvanized metal sheets (denoted in Figure 6 by black lines) and placed in the flume side by side to create the vegetation field. Eleven paddles were used for wave generation to produce waves in the flume region only. This helped prevent recirculation of energy and minimized reflection throughout the basin, removing any unwanted 3-D effects. Test runs were randomly repeated to ensure a controlled environment. Six capacitance wave gages were used for measuring the free surface oscillations in each test run. The first three gages were placed towards the wavemaker (Figure 7) to analyze reflection in the flume, while the other three gages were placed at the beginning, middle and end of the artificial vegetation field, spaced 3.3 m (11 ft) apart. To measure reflection a three probe least squares approach was used as described by Mansard & Funke (1980). Probe spacings for each experiment run were calculated using the input wavelength.

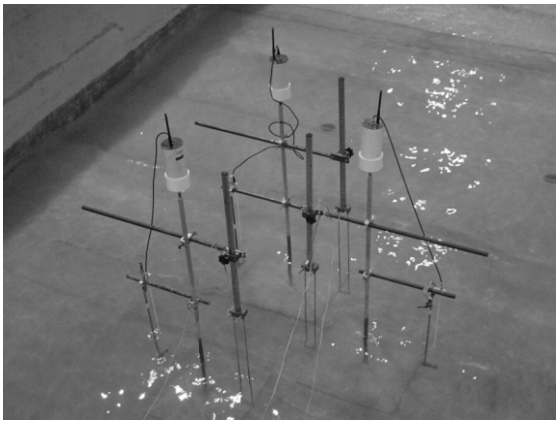

Figure 7. Capacitance wave gages used to measure basin reflection

Two density arrangements were tested and are shown in Figure 8. The first set-up consisted of 6 sheets with the elements equally spaced using layout 1 (Figure 5). This gave the vegetation field a uniform plant density of 97 stems/m^2. For the second arrangement, the front middle steel sheet, closest to the wave maker, was removed and replaced with a vegetation field constructed using layout 2, giving a plant density of 162 stems/m^2.

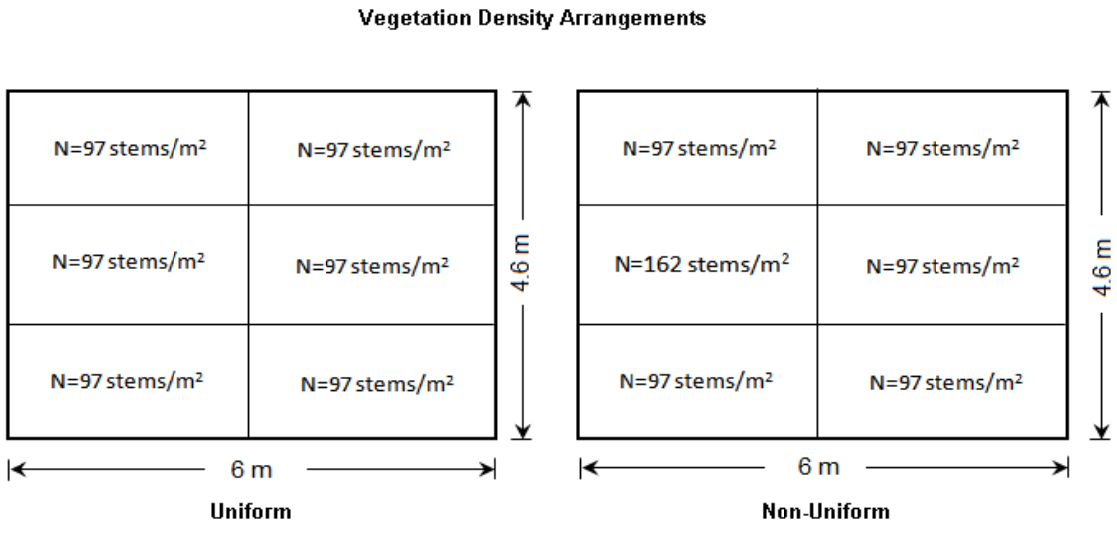

Figure 8. Vegetation density arrangements for basin experiments, wave maker to left

Nepf (2004) defines a nondimensional parameter, *ad*, which is the product of the leaf area density, *a* [m^{-1}] and stem diameter *d* of the plant. This parameter represents the volume of the fluid that is occupied by plant stems. Values of *ad* for each experimental case is presented below in Table 2. Experiments conducted for this thesis only analyzed *ad* values ranging between .01 and .03. It has been found that the volume fraction of vegetation in freshwater marshes can be as high as 15%, and as high as 45% in the root systems of mangrove swamps (Nepf 2004, Fox *et al*., 2002, Mazda *et al*., 1997).

Table 2. Volume of fluid occupied by plant stems for each experimental case

N [stems/m^2]	h [m]	*ad*
97	0.3	0.02
162	0.3	0.03
97	0.4	0.01
162	0.4	0.02

3.3. Artificial Wetland Construction

Polyethylene foam, commonly used for window insulation, was selected to represent the flexible artificial vegetation elements. The foam is low density, highly flexible and has a skin-like outer texture. The synthetic foam stems was selected based on three main characteristics: (1) the foam stems were able to maintain themselves vertically by buoyancy alone when submerged, (2) the foam was available in the same diameter as the cylindrical wooden dowels, (3) a large quantity could be purchased for a relatively low price. The density and other mechanical properties of the foam are listed below in Table 3.

Table 3. Physical properties of polyethylene foam

Diameter [mm]	Density [kg/m^3]	Tensile Strength [kPa]
12	32	344.7

The foam was cut into pieces 0.3 m long and glued to galvanized steel sheets using Liquid Nails™, a strong construction adhesive. The steel sheets were marked before gluing to ensure even grid spacing. Construction of artificial vegetation fields in the Haynes basin is shown below in Figure 9.

Figure 9. Artificial wetland construction at Haynes Coastal Laboratory, Texas A&M University (left to right: Dave Piazza, Lauren Augustin)

Wooden cylindrical dowels were also cut into sections 0.3 m in length. Both the foam and dowels were 12 mm (½") in diameter. Dowel experiments were only conducted in the narrow 2-D flume and were glued directly to the plywood bottom, as opposed to steel sheets, using a strong adhesive similar to super glue with an activator spray. The activator spray allowed for an instant bond so the dowels would stay vertical. Figure 10

shows the artificial vegetation field in the 2D wave flume constructed out of the rigid, cylindrical elements.

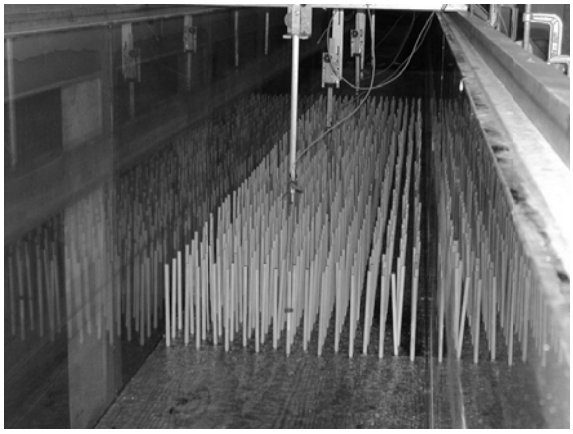

Figure 10. Artificial wetland constructed out of cylindrical dowels in the 2D wave flume

According to Nepf (2004) the morphology of cylindrical cylinders is a reasonable approximation in shape and rigidity for the marsh grasses *Juncus roemerianus* (Needle Rush) and *Spartina alterniflora* (Smooth Cordgrass). Needle Rush is shown in Figure 11, and is a long tubular stem with a sharp point, and is common at marsh borders where the elevation is above the normal high tide.

Figure 11. Schemetic of Juncus roemerianus taken from Schoettle (1996)

Figure 12 shows a clump of *Spartina alterniflora*, a smooth saltwater cordgrass that colonizes in tidal marshes. The stems are rigid and hollow and range between 0.9 m (3 ft) to 1.5 m (5 ft) tall.

Figure 12. Spartina alterniflora (courtesy of the United States Department of Agriculture)

3.4. Data Acquisition and Collection Procedures

3.4.1. Haynes Coastal Basin

Six wireless capacitance wave gages were used for data collection in the Haynes Coastal basin. Each gage was mounted on a horizontal bar connected to a vertical stand and placed in the test region. The capacitance gages consist of a thin insulated wire that is held taut by a metal bow. The insulated wire is connected to a transducer box mounted above the bow via a coaxial cable. Because the transducer boxes are wireless they were fully charged before each set of experiments. Gages were calibrated using the LabVIEW Multiple Channel Data Acquistion System to obtain a relationship between the voltage output signal from the probe and the water surface elevation. Calibration points were chosen based on the water depth and wave height so that the calibration spanned all water levels of interest. The calibration procedure consists of moving each probe up and down equal spacings to different water levels. When the water level is completely still the gain and offset of the gage is collected, and the probe is moved to the next point. If gages are not properly calibrated all data can be skewed.

Irregular waves were generated using a TMA shallow water spectrum with a spreading factor of 2. The LabVIEW program was utilized for collecting all time series data. The free surface elevation was recorded for each wave probe at a sampling rate of 25 Hz. Each spectral experiment was run for a duration of 1210 seconds to ensure a long enough wave record for accurate spectral analysis. Regular monochromatic waves were also generated over each experimental set-up. The monochromatic waves were sampled at 25 Hz and collected over a duration of 130 s.

3.4.2. 2-D Wave Flume

Eight SEASIM Seagauge resisitance wave gages were used for data collection in wave flume experiments. Each gage consists of two stainless steel wire probes 400 mm long. Probes were connected to a Seagauge amplifier to convert the voltage signals into water level measurements. The amplifier was connected to a computer equipped with the LabVIEW data acquisition system for data collection. The free surface elevation was sampled at a frequency of 25 Hz over a duration of 620 s, approximately 10 minutes. The LabVIEW signal driver program was used to generate sinusoidal voltage signals to the wavemaker. The signal is built according to a specified voltage input and cannot be generated by simply specifying a wave amplitude, thus it was impossible to keep wave heights constant from run to run. The inability to reproduce wave conditions in the flume is most likely due to the hydraulics and mechanical response of the wave maker, due to the age and lack of maintenance on the system. Physical characteristics of the flume, including side seams and a slightly varying width may have also caused disturbances in the wave characteristics.

3.5. Data Reduction

The collected data in the basin and flume required some data reduction to ensure accurate and efficient data processing. The frequencies that the wireless capacitance gages used in the 3D basin operated on were occasionally interfered with, introducing large spikes into the measured wave record. The main source of frequency disturbance occurred from a large overhead crane that was operating during experimentation. The noise was removed from the wave record by using a simple linear interpolation

smoothing scheme. Water levels that exceeded a reasonable threshold were interpolated until an acceptable value was reached. An example of a time series before and after smoothing is shown below in Figure 13.

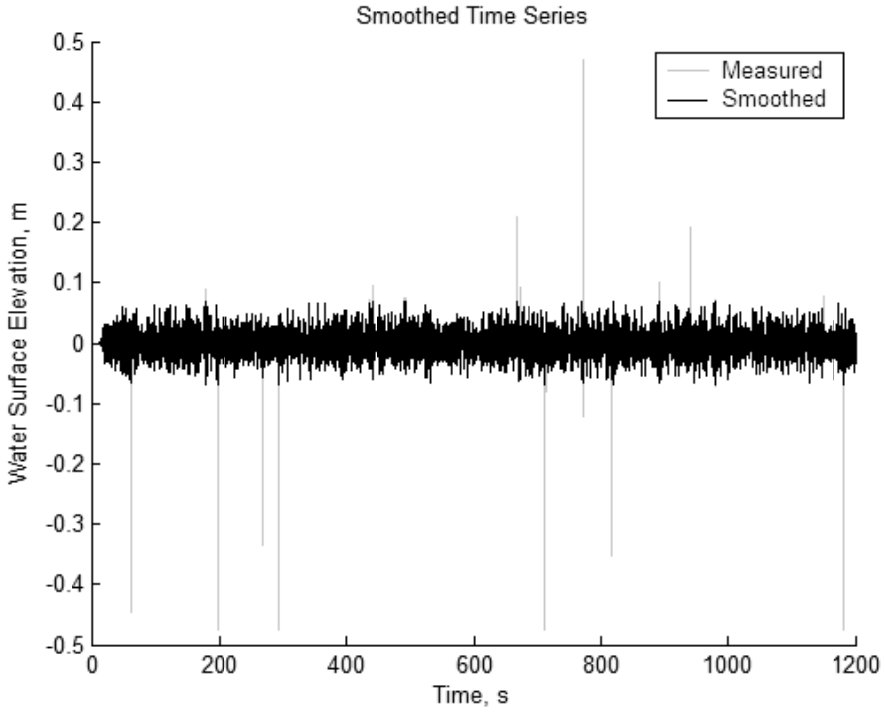

Figure 13. Example of measured free surface elevation time series before and after smoothing

For both 2D wave flume and 3D basin experiments the data acquisition system was initiated as soon as the waves were generated. Because it takes varying time for the waves to reach each individual probe, a portion of the beginning and end of each time series was removed to eliminate possible sources of error during analysis. Each time series was adjusted accordingly until a complete and accurate representation of the wave record was obtained.

CHAPTER IV

EXPERIMENTAL RESULTS

4.1. Time Domain Analysis: 2-D Flume

A wave-by-wave analysis was performed on each free surface time series measured in the wave flume. Each time series was divided up into segments of individual waves determined by a zero-upcrossing analysis. Individual wave segments were defined as the water level variation between two successive upcrossing points of the time series relative to the mean water line. The wave height was then calculated as the difference between the maximum and minimum points in the segment. Once all the individual waves in the time series were found, the mean wave height was statistically calculated.

The average wave height was plotted for each of the five probe points in the vegetation field. It was observed during wave flume experimentation that the second gage would fall out of calibration, and values obtained during data analysis did not fit the trends of the other data points. Therefore, the second gage was considered to be dysfunctional and was eliminated from the time domain analysis. For easier graphical representation the wave height is plotted normalized by the control wave height at the local gage at which it was measured. An example normalized wave height plot including the control, flexible and rigid cases for H_i=9 cm, h=0.3 m and T=1.5 s is shown below in Figure 14. Figure 15 shows a normalized plot for the submerged vegetation case with H_i=10 cm and T=2.0 s. Normalized wave height plots for all flume cases can be referenced in Appendix A.

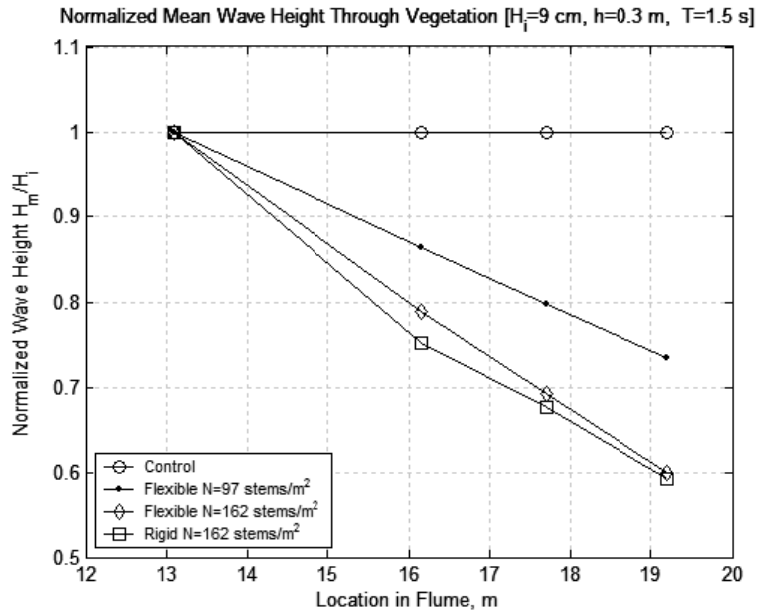

Figure 14. Example plot of normalized wave heights through emergent vegetation field in 2D wave flume

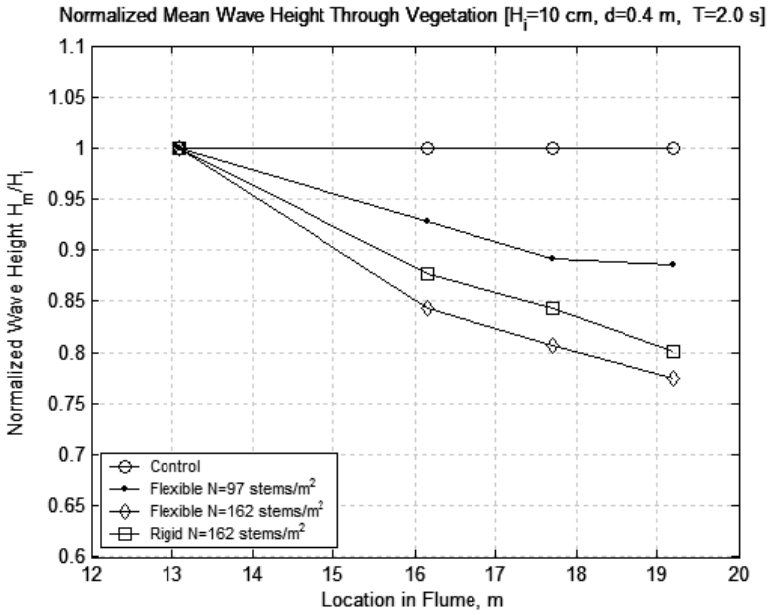

Figure 15. Example plot of normalized wave heights through submerged vegetation field in 2D wave flume

To investigate the influence of incident wave height on damping, multiple wave heights were analyzed for each test scenario. Figures 16 and 17 show plots of the incident wave height versus percent wave height decay for the flexible and rigid vegetation experiments. It was observed that as the wave height of the incident wave increased, the amount of attenuation due to vegetation roughness increased linearly. However, the dependency of attenuation on wave height appeared to be small when compared to other factors such as water depth and stem density. The stem density in the cases shown below are N=162 stems/m^2.

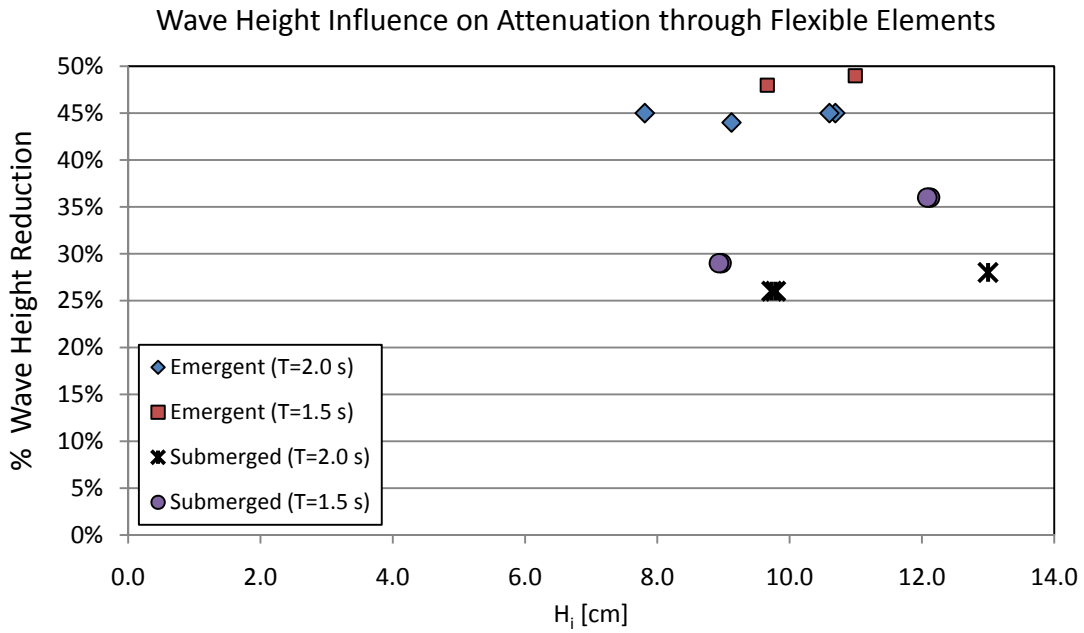

Figure 16. Incident wave height plotted against the percent wave height decay for flexible stems, 2D wave flume

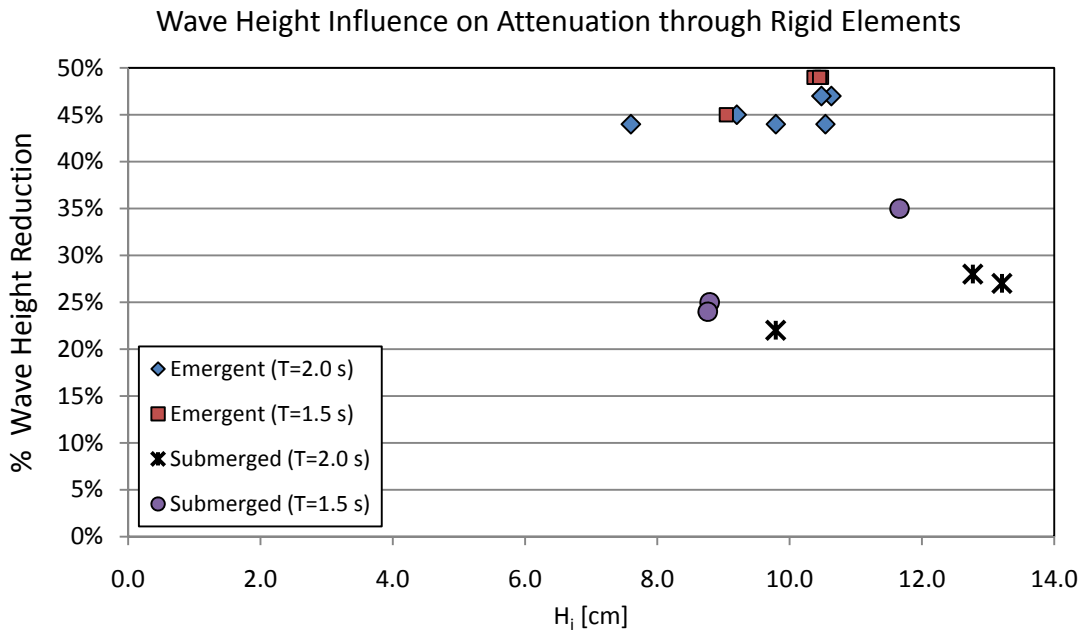

Figure 17. Incident wave height plotted against the percent wave height decay for rigid stems, 2D wave flume

Two wave periods were analyzed for each test case, 1.5 s and 2.0 s. Experiments showed an inverse linear relationship between the percent of wave attenuation and wave period. This is unusual because waves with longer periods are expected to show a higher amount energy dissipation because they are subject to frictional dissipation over a greater distance (Bretschneider *et al.* 1954). However, in all cases the 1.5 s period showed increased damping compared to the 2.0 s period. The percent wave height decay is plotted against the wave period for the rigid and flexible vegetation cases in Figures 18 and 19. Emergent and submerged conditions are depicted to show that the amount of attenuation is more dependent on the water depth with respect to plant stem height than period.

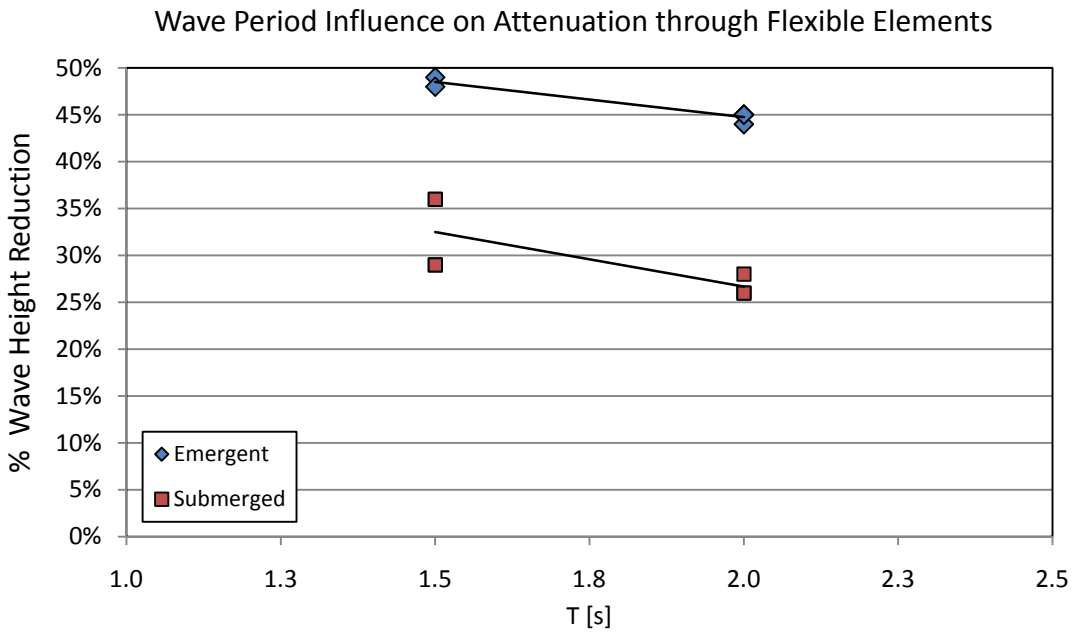

Figure 18. Wave period plotted against percent wave height decay for flexible vegetation, 2D wave flume

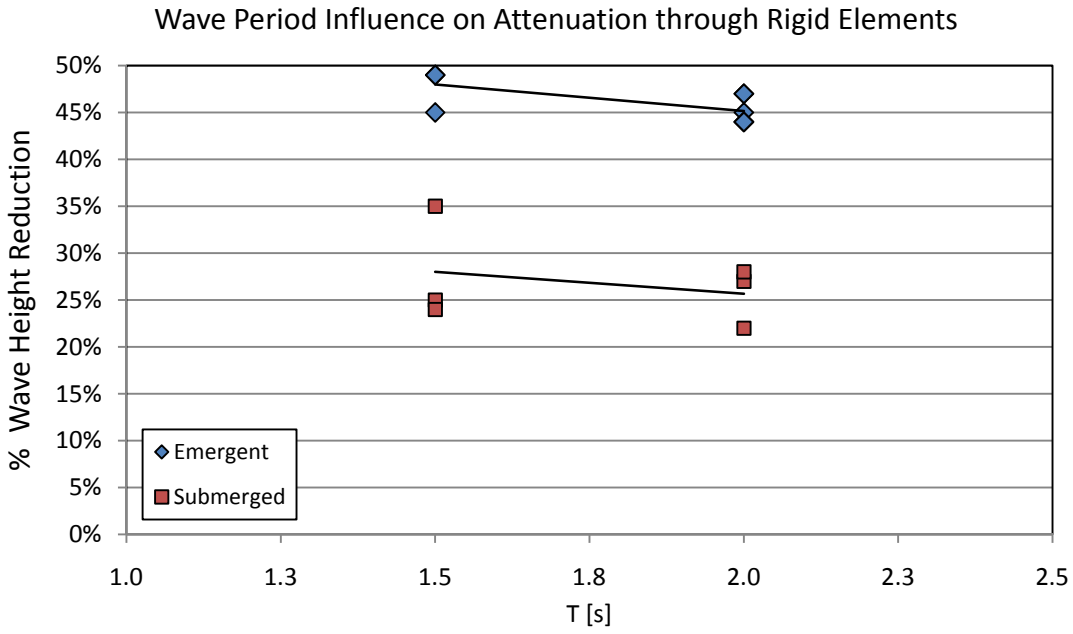

Figure 19. Wave period plotted against percent wave height decay for rigid vegetation, 2D wave flume

The total average percent energy loss and average energy loss per meter of vegetation for all densities, including both flexible and rigid elements is summarized below in Tables 4-6. For near emergent conditions the wave height was reduced an average of 5 – 8% per meter of wave propagation, while submerged vegetation only damped waves between 3 – 6%. The dependency of stem density for emergent and submerged plant conditions is graphically depicted in Figures 20 and 21, where wave height decay is plotted against the dimensionless parameter, *H/h*. As expected, increased plant density resulted in a greater amount of energy dissipation for both emergent and submerged cases.

Table 4. Wave height decay results for rigid vegetation elements in 2D wave flume

h [m]	T [s]	% Wave Height Decay per meter	Total % Wave Height Decay	N [stems/m^2]	Stiffness
0.3	1.5	8%	48%	162	Rigid
0.3	2.0	8%	46%	162	Rigid
0.4	1.5	5%	28%	162	Rigid
0.4	2.0	4%	26%	162	Rigid

Table 5. Wave height decay results for dense flexible vegetation in 2D wave flume

h [m]	T [s]	% Wave Height Decay per meter	Total % Wave Height Decay	N [stems/m^2]	Stiffness
0.3	1.5	8%	49%	162	Flexible
0.3	2.0	8%	45%	162	Flexible
0.4	1.5	6%	33%	162	Flexible
0.4	2.0	5%	27%	162	Flexible

Table 6. Results of wave height decay for less dense flexible vegetation in 2D wave flume

h [m]	T [s]	% Wave Height Decay per meter	Total % Wave Height Decay	N [stems/m^2]	Stiffness
0.3	1.5	5%	32%	97	Flexible
0.3	2.0	5%	31%	97	Flexible
0.4	1.5	4%	21%	97	Flexible
0.4	2.0	3%	15%	97	Flexible

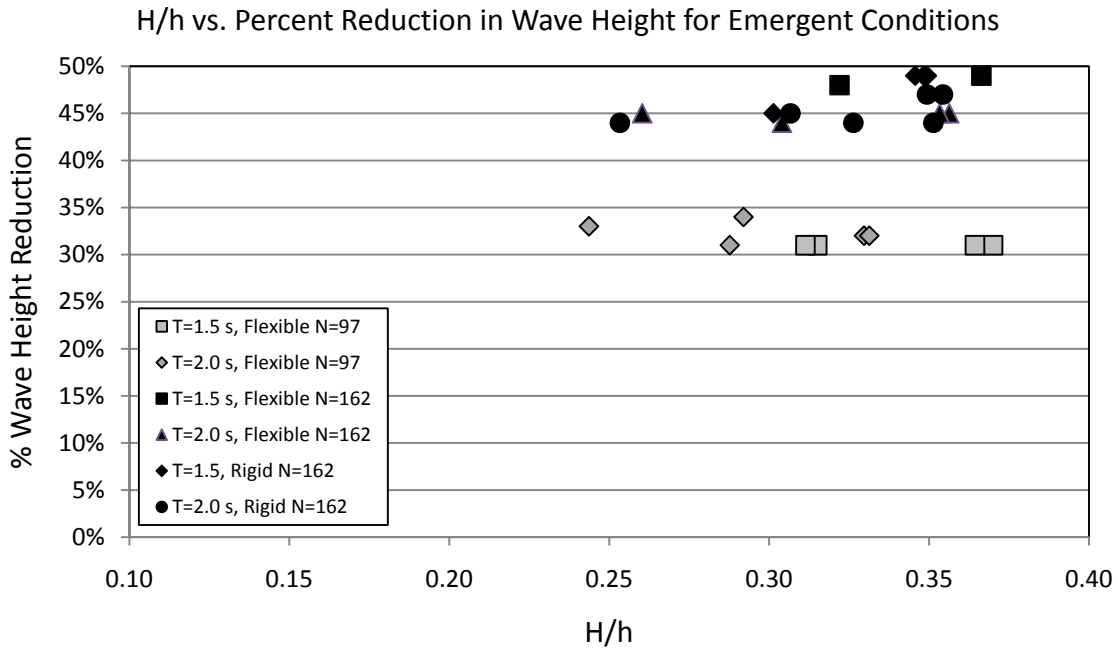

Figure 20. Percent wave height decay plotted against wave steepness for emergent conditions in 2D wave flume

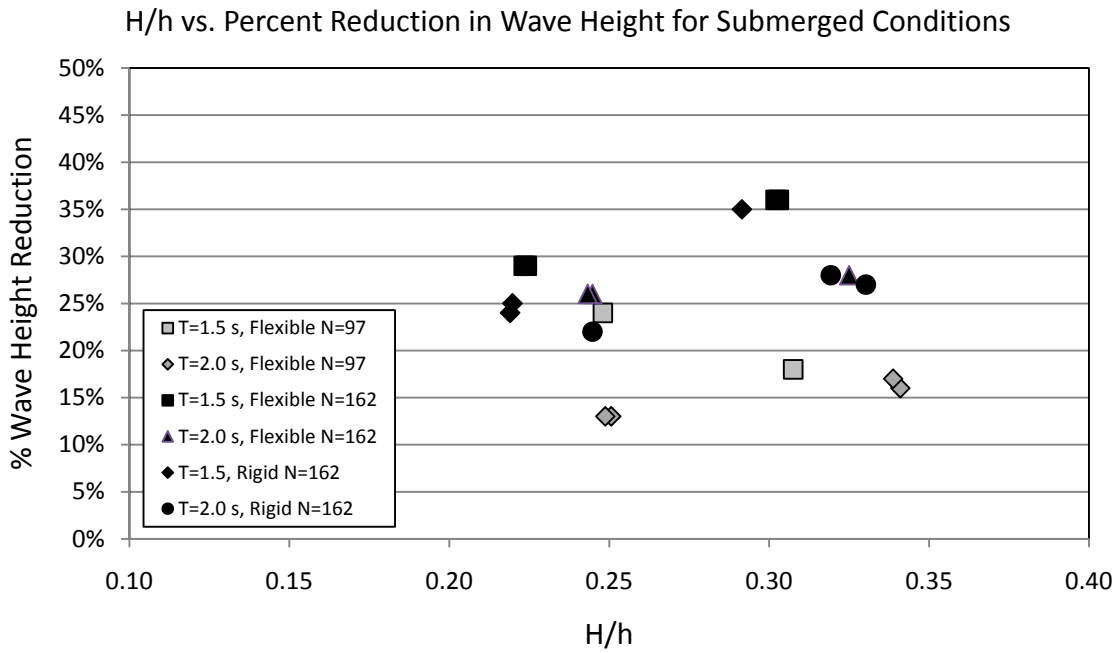

Figure 21. Percent wave height decay plotted against wave steepness for submerged conditions in 2D wave flume

The wave height decay followed the same trends for all the experimental cases and appeared to be more dependent on water depth with respect to stem length and stem density, rather than incoming wave height and period. For both rigid and flexible cases the attenuation increased linearly with respect to larger wave heights, but decreased for longer approaching waves. From the values in Tables 4-6 the effect of the plant type also appeared to play a role in the amount of wave attenuation, with flexible members reducing the wave height by an extra 1-4% compared to rigid members. When subject to oscillating waves in the tank the flexible members showed slight to moderate swaying motion, while rigid elements remained erect (stationary). The actual deflection and amount of bending of the polyethylene foam was not calculated, but a video of the plant motion can be referenced in electron supplement contained in Appendix E. Intuitively,

flexible vegetation should dissipate a higher amount of energy due to the increased form drag and ability to absorb a higher amount of oncoming momentum from the flow.

It should be mentioned that standing waves were observed in the tank and may have contributed some error into water level measurements, and therefore percent wave height decay calculations. However, all experiments were completed twice to ensure they were repeatable and accurate representations of the conditions being tested. To attempt and eliminate bias from unwanted reflection, control conditions were subtracted from the vegetation conditions for wave height decay calculations. Since the wave gages that were used were fairly old, their sensitivity could have diminished which would also result in less accurate data. Slight bows in wave probes may have also introduced nonlinearity errors into the wave record.

4.2. Frequency Domain Analysis: 3-D Basin

Irregular waves were investigated over a 6 m flexible plant bed length to determine the influence of water depth, stem density and wave period on wave attenuation. Four experiments were conducted for each vegetation arrangement and included both emergent and submerged plant stem scenarios. A summary of wave conditions for each experiment is given below in Table 7. A shallow water TMA spectrum, with a spreading factor of 2, was chosen to generate the irregular waves. This spectrum is also used as the input in the COULWAVE Boussinesq model, which will be utilized later to find a friction factor for each plant field.

Table 7. Summary of wave parameters for spectral experiments.

H_{rms} (cm)	h (m)	T (s)	f_s (Hz)	Sample Time (s)	Spectrum Type
8.5	0.3	1.5	25	1210	TMA
8.5	0.3	2.0	25	1210	TMA
8.5	0.4	1.5	25	1210	TMA
8.5	0.4	2.0	25	1210	TMA

The spectral wave data was obtained from each of the water elevation time series using VARSPEC, a variance spectral density program contained in the GEDAP (General Experiment Control and Data Acquisition Package) software package. VARSPEC uses the time series input file and outputs the spectral density in binary form. All binary files were converted to ASCII for further data processing. An example of the typical wave elevation time series output is shown in Figure 22.

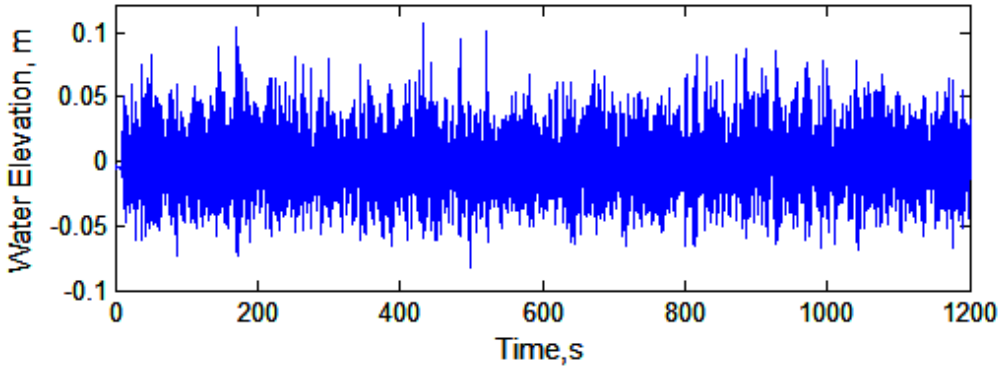

Figure 22. Typical water elevation time series output from GEDAP

The spectral plots were then smoothed using Bartlett averaging over 5 frequency bands with Matlabd for easier interpretation. An example of the smoothed spectrum for a control case without vegetation is shown in Figure 23. The gages are in order according

to their position in the vegetation field. Therefore, gage 1, gage 2, and gage 3 correspond to the beginning, middle and end of vegetation field, respectively.

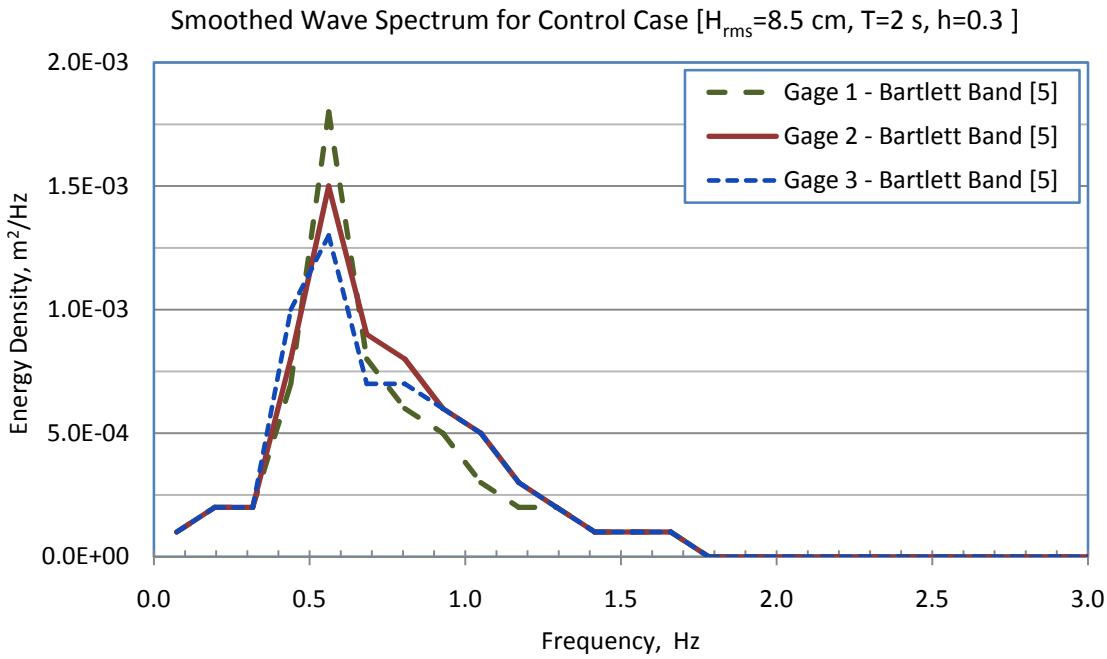

Figure 23. Example of Bartlett smoothed wave spectrum for control case [Hrms=8.5 cm, T=2 s, h=0.3 m]

The band averaged spectral plots for all basin experiments can be referenced in Appendix C. The peak period and zero moment wave height, H_{m0}, were also calculated from the spectral analysis. The peak period is associated with the frequency band that contains the most energy. Assuming the wave heights follow a Rayleigh distribution, the spectral wave height, H_{m0}, value is calculated from the total energy in the spectrum and is expressed as

$$H_{m0} = 4\sqrt{m_0} \tag{4.1}$$

where m_0 is the area under the spectral curve. The H_{m0} value is assumed to be approximately equal to the significant wave height. For data analysis the spectral

moment wave heights were converted to the root-mean-square wave height, H_{rms}, using the relation

$$H_{rms} = \frac{H_{m0}}{1.416} \tag{4.2}$$

Reflection in the basin, resulting from the wall opposite of the wave maker, was calculated for each control case prior to putting the plant field into the flume. The reflection analysis was completed using the REFLS program in the GEDAP software package, which uses the least squares method of Mansard & Funke (1980) to separate the incident and reflected wave trains from the measured spectra. The free surface time series was measured at three points for the reflection analysis. Each probe was spaced according to the wavelength. The wavelength was calculated using the significant spectral wave height, peak period and water depth with the linear dispersion relation,

$$\sigma^2 = gktanh(kh) \tag{4.3}$$

where k is the wave number, h is water depth and σ is the angular frequency of the wave. The reflection coefficient in the basin varied between 0.22 and 0.35 for the control cases (without vegetation). For reference, Appendix B contains a table of the reflection coefficients for laboratory case. Because of the high amount of reflection from the rock beach, control runs were repeated to ensure they were accurate representations of conditions in the basin. To attempt to eliminate bias from reflection, the control wave heights were subtracted from wave heights measured in subsequent runs through the vegetation field. For easier graphical representation of the data, the wave heights were normalized using the control case wave height local to the gage at which they were measured. The spectral wave height decay for each group of experimental conditions is

shown below in Figures 24 – 27. In agreement with the experiments conducted in the flume, the amount of attenuation was found to be more dependent on the ratio between plant stem length and water depth and stem density, rather than wave period over the range of conditions tested. It should be mentioned that only short wave periods, similar to that of wind waves, were considered in these experiments.

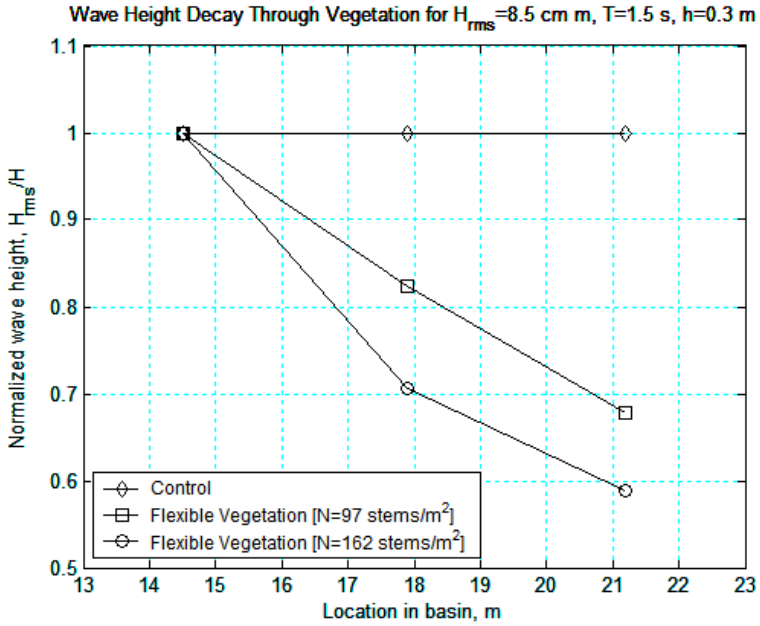

Figure 24. Wave height decay through emergent vegetation for TMA generated spectrum

[H_{rms} = 8.5 cm, T = 1.5 s]

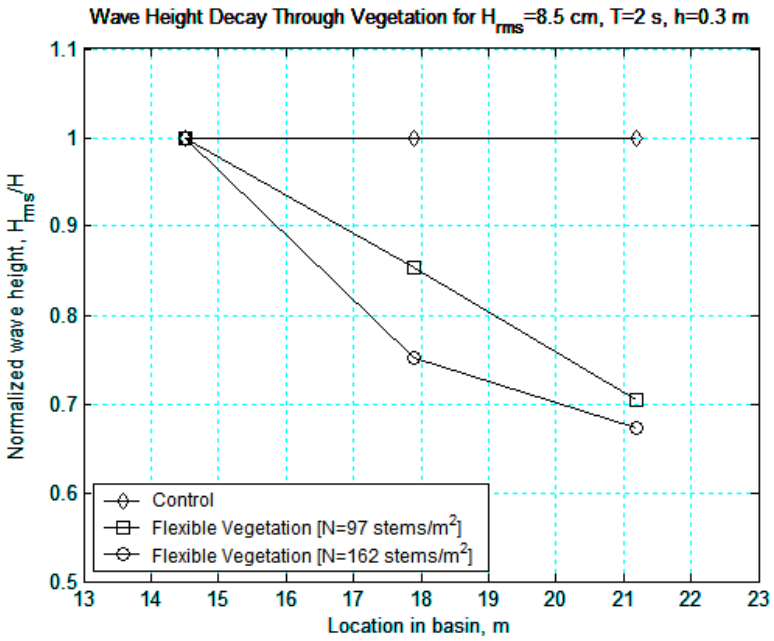

Figure 25. Wave height decay through emergent vegetation for TMA generated spectrum

[H_{rms} = 8.5 cm, T = 2 s]

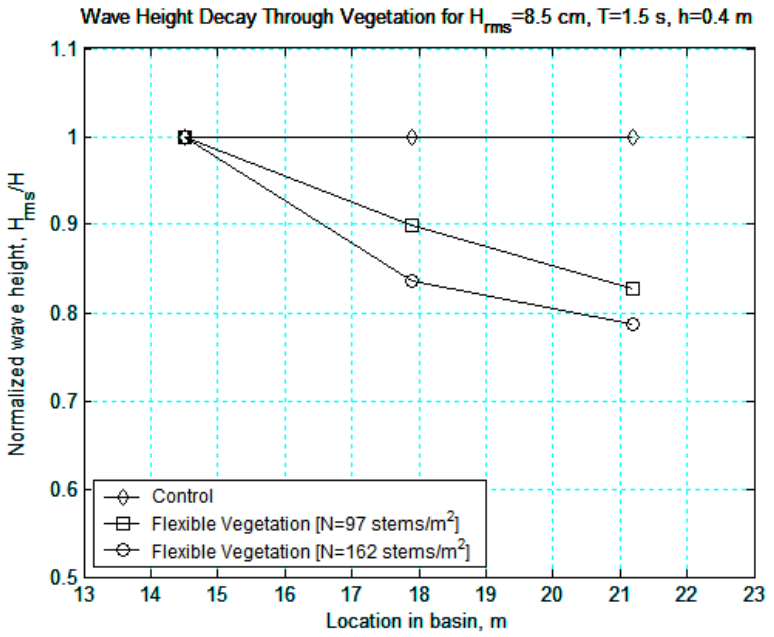

Figure 26. Wave height decay through submerged vegetation for TMA generated spectrum

[H_{rms} = 8.5 cm, T = 1.5 s]

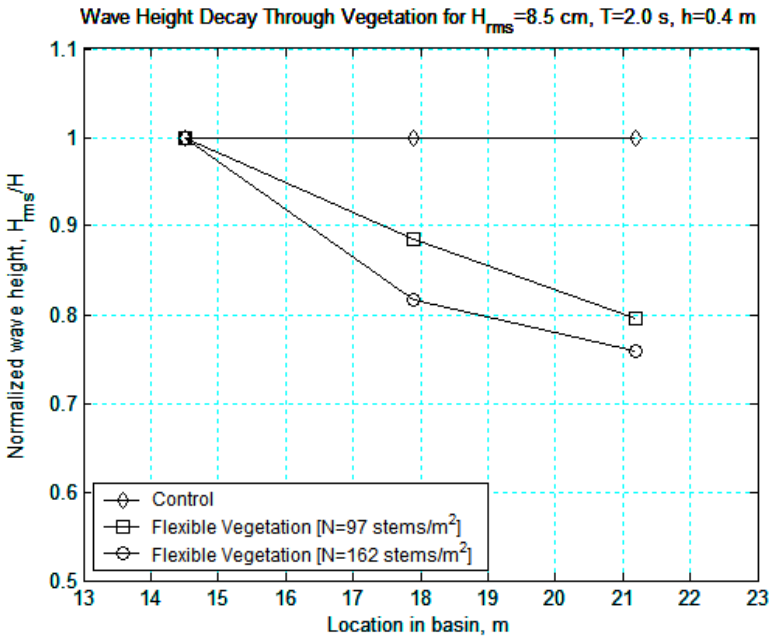

Figure 27. Wave height decay through submerged vegetation for TMA generated spectrum [H_{rms} = 8.5 cm, T = 2 s]

The dependency of wave attenuation on the ration between stem length and water depth can be seen below in Figure 28. The percent decrease in wave height is plotted against the dimensionless parameter *H/h*, the ratio of wave steepness to relative water depth. For emergent conditions, *H/h* is equal to 0.4, and for submerged vegetation *H/h* is equivalent to 0.3. The incident root-mean-square wave height was 8.5 cm for all cases, as shown earlier in Table 7. Experiments where plants occupied the entire water depth (l_p=*h*) showed an average wave height reduction of 30 - 40% percent along the 6 m length of the vegetation field. Experiments with submerged plant conditions showed a wave height decrease of approximately 20-27%. Table 8 presents the energy attenuation for the first 3 m and last 3 m of the vegetation field, in addition to the total percent wave height decay. In general, a higher amount of energy was dissipated in the first half of the

plant bed in experiments where the initial 3 m of the vegetation was more dense (N=162 stems/m^2). This is expected not only due to the increase in stem density but also because the initial wave energy impacts the first 3 m, lowering the velocity of fluid flow which results in a reduction of drag on the plant stems further down the field.

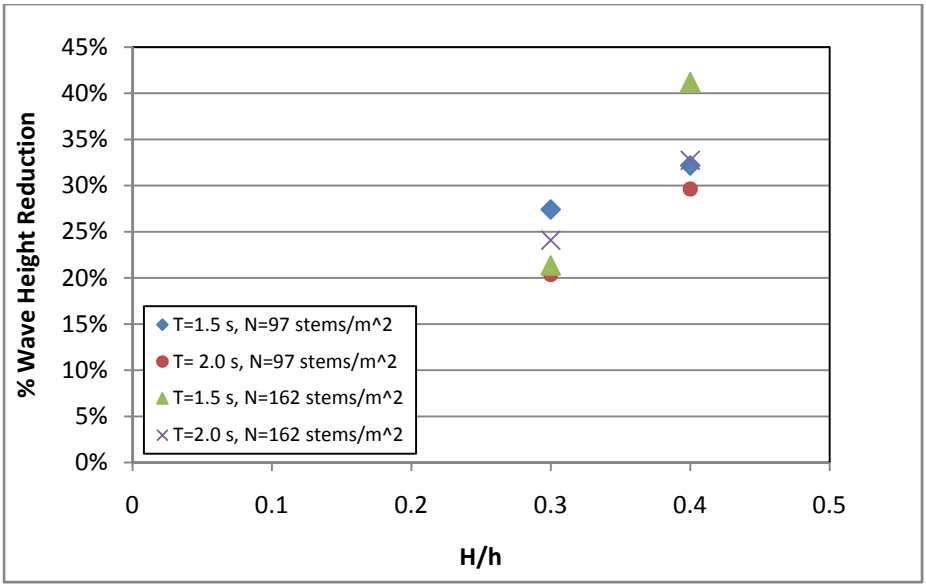

Figure 28. Percent wave height reduction versus H/h for spectral experiments

Table 8. Percent energy loss through first 3 m and last 3 m of vegetation field

H_{rms}	T	h	N	Percent Wave Height Reduction		
[cm]	[s]	[m]	[stems/m^2]	First 3m	Last 3 m	Total
8.5	2.0	0.3	97	14.7%	14.9%	29.6%
8.5	2.0	0.3	162	24.9%	7.9%	32.8%
8.5	2.0	0.4	97	11.5%	8.8%	20.4%
8.5	2.0	0.4	162	18.4%	5.7%	24.1%
8.5	1.5	0.3	97	17.6%	14.6%	32.2%
8.5	1.5	0.3	162	29.4%	11.8%	41.2%
8.5	1.5	0.4	97	10.1%	17.4%	27.4%
8.5	1.5	0.4	162	16.3%	5.0%	21.4%

In addition to spectral waves, monochromatic waves with a height of 8 cm were also generated over each experimental case. The monochromatic and irregular wave experiments followed the same general trends. Wave traces for the two different densities are shown below in Figure 29. The gages are in order from the beginning to the end of the plant field.

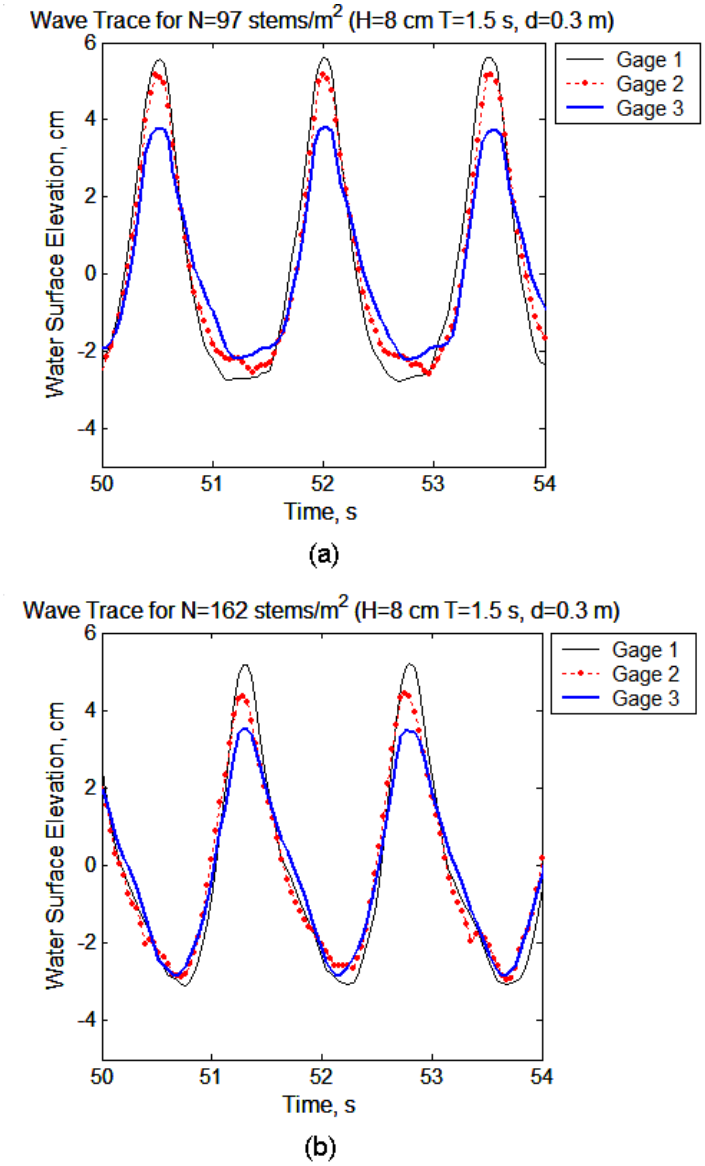

Figure 29. Monochromatic wave traces over vegetation

CHAPTER V

NUMERICAL MODELING OF VEGETATION FRICTION FACTOR USING COULWAVE

5.1. Introduction to COULWAVE Boussinesq Model

The numerical model COULWAVE (Cornell University Long and Intermediate Wave Model) was applied to simulate the physical experiments conducted in the basin and the flume. The model was developed by Lynett (Texas A&M) and Liu (Cornell) during the late 1990's. COULWAVE (Lynett *et al.*, 2002) is based on the modified Boussinesq equations and simulates wave propagation from intermediate to shallow water depths. The fundamental assumption of the depth-averaged model is that the ratio of the wavelength to water depth is large. When the depth is greater than one-fifth of the equivalent deep water wavelength the modified equations are no longer valid. The Boussinesq type equations are known to be accurate from fairly deep water to the shoreline (Wei *et al.*,1995), and have shown to give good predictions of field data (Elgar and Guza, 1985) and laboratory data (Goring, 1978 & Liu *et al.*, 1985), as long as the frequency dispersion and nonlinear effects are weak. The governing equations of the model are derived from the Navier Stokes equations that govern the conservation of momentum and conservation of mass in fluid flow. The 1-D depth-averaged, modified Boussinesq equations are given by

$$\zeta_t + E = 0 \tag{5.1}$$

$$\vec{u}_{\alpha t} + F = 0 \tag{5.2}$$

where

$$E = \nabla\cdot[(h+\zeta)\vec{u}_\alpha] -$$

$$\nabla\cdot\left\{(h+\zeta)\times\left[\left(\frac{1}{6}\left(\zeta^2-\zeta h+h^2\right)-\frac{1}{2}z_\alpha^2\right)\nabla(\nabla\cdot\vec{u}_\alpha)+\left[\frac{1}{2}\left(\zeta-h\right)-z_\alpha\right]\nabla[\nabla\cdot(h\vec{u}_\alpha)]\right]\right\} \quad (5.3)$$

$$F = \vec{u}_\alpha\cdot\nabla\vec{u}_\alpha + g\nabla\zeta + \left\{\frac{1}{2}z_\alpha^2\nabla(\nabla\cdot\vec{u}_{\alpha t}) + z_\alpha\nabla[\nabla\cdot(h\vec{u}_{\alpha t})]\right\} +$$

$$\{[\nabla\cdot(h\vec{u}_\alpha)]\nabla[\nabla\cdot(h\vec{u}_\alpha)] - \nabla\left[\zeta\left(\nabla\cdot(h\vec{u}_{\alpha t})\right)\right] + (\vec{u}_\alpha\cdot\nabla z_\alpha)\nabla[\nabla\cdot(h\vec{u}_\alpha)]\} +$$

$$\left\{z_\alpha\nabla\left[\vec{u}_\alpha\cdot\nabla\left(\nabla\cdot(h\vec{u}_\alpha)\right)\right] + z_\alpha(\vec{u}_\alpha\cdot\nabla z_\alpha)\nabla(\nabla\cdot\vec{u}_\alpha) + \frac{z_\alpha^2}{2}\nabla[\vec{u}_\alpha\cdot\nabla(\nabla\cdot\vec{u}_\alpha)]\right\} +$$

$$\nabla\left\{-\frac{\zeta^2}{2}\nabla\cdot\vec{u}_{\alpha t} - \zeta\vec{u}_\alpha\cdot\nabla[\nabla\cdot(h\vec{u}_\alpha)] + \zeta[\nabla\cdot(h\vec{u}_\alpha)]\nabla\cdot\vec{u}_\alpha\right\} +$$

$$\nabla\left\{\frac{\zeta^2}{2}\left[(\nabla\cdot\vec{u}_\alpha)^2 - \vec{u}_\alpha\cdot\nabla(\nabla\cdot\vec{u}_\alpha)\right]\right\} + R_b \quad (5.4)$$

where ζ is the free surface elevation, ∇ is the gradient operator, $\vec{u}_\alpha$ is the fluid velocity vector at the reference water depth $z_\alpha = -0.531h$, and R_b is a quadratic term accounting for bottom friction. The COULWAVE model is applied to determine a representative friction factor for each laboratory vegetation experiment. Frictional effects are calculated using the quadratic term R_b given by

$$R_b = f\frac{u_b|u_b|}{H} \quad (5.5)$$

where u_b is the horizontal velocity at the bed, and f is the non-dimensional Darcy-Weisbach friction factor. The nondimensional friction factor is being adopted from pipe flow theory and tuned to fit the measured laboratory data. Instead of the steady free-stream velocity profiles associated with pipe flow, the instantaneous velocities under the

wave are being used to determine the numerical friction factor associated with the presence of the vegetation roughness elements.

5.2. Numerical Modeling of Vegetation Friction Factor

The purpose of this numerical analysis is to determine the friction factor *f* related to the effects of vegetation roughness for each experiment. The model was modified to agree with the characteristics of the physical setup in each laboratory. COULWAVE was adjusted to allow for propagation of two-dimensional waves over a distance of 30.5 m (100 ft), equal to the length of both laboratory facilities. The model analysis was divided up into two parts and simulated all laboratory experiments, including both irregular and monochromatic wave conditions. Simulations were run with spectral waves over a flat bottom, and with regular waves over an irregular bottom described earlier in Chapter III under the flume experimental setup. A quadratic friction factor was used to model the vegetation roughness along the length of the vegetation field. A separate friction factor was specified for areas outside the vegetation field to appropriately account for the reduced energy dissipation due to bottom friction. A value of 0.001 was assumed outside of the vegetated region because energy losses due to friction from the bottom and side walls should be very small. In the vegetation field the friction factor was assumed to account only for the presence of the vegetation elements. To simulate the basin experiments the TMA spectral wave conditions were generated using Matlab and specified as an input into the COULWAVE model. The target significant wave height used for all the spectral cases was 0.12 m, and a value of 2 was used for the spectral spreading factor. For regular wave simulations, the wave height and wavelength were

the specified user inputs. Each model simulation was run for a duration of 200 s, and was assumed to be long enough for an accurate wave record. COULWAVE incorporates a numerical ‘sponge layer’ at the end of the grid that absorbs all energy at the end of the flume, thereby removing reflection from the numerical simulation. The distance of the sponge layer boundary condition is equivalent to one wavelength. To get a spatial idea of the wave propagation in the model, a plot of the free surface as a function of time is shown below in Figure 30 for the flume setup. It can be seen that the wave height is damped over the vegetation region beginning at the 13.1 m point, extending 6 m to the end of the field at 19.2 m. An example of the free surface as a function of time for the irregular wave case is shown in Figure 31. The effect of the mean water level due to the presence of vegetation was also investigated. Model results showed a significant rise in mean water level at the start of the vegetation field and then a slight setdown once waves exited the plant field. As the friction factor was increased, the water level setup in the vegetation also increased.

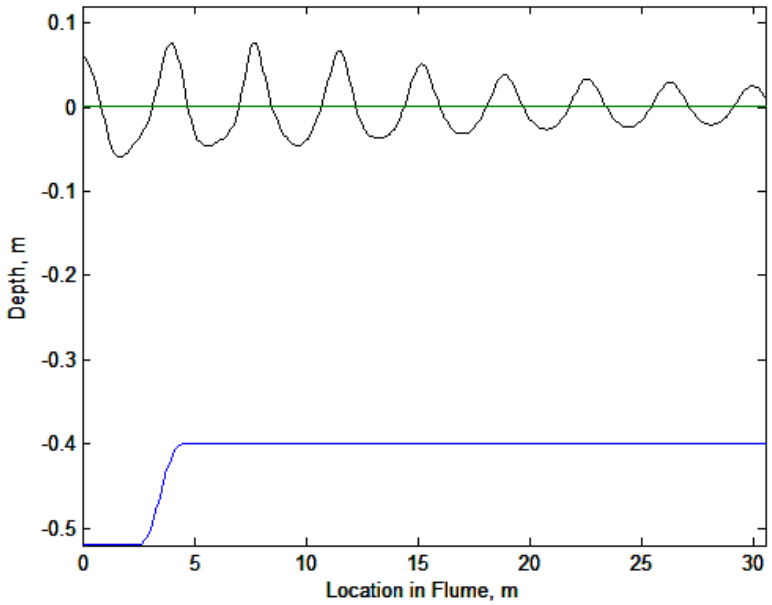

Figure 30. Example of COULWAVE surface elevation as a function of time for regular wave case

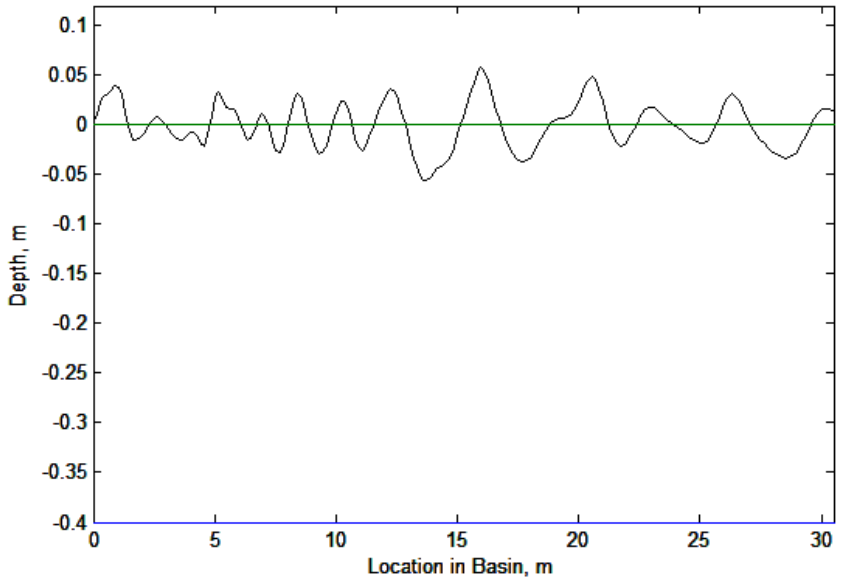

Figure 31. Example of COULWAVE surface elevation as a function of time for irregular wave case

The friction factor was determined for each experimental case through an iterative process. A friction factor value was chosen based on the total amount of energy

dissipated through the vegetation field. An example of the modeled friction factor versus the measured experimental data for emergent and submerged plant conditions are shown in Figures 32 and 33. Numerical friction factor plots for each of the experimental runs can be referenced in Appendix D.

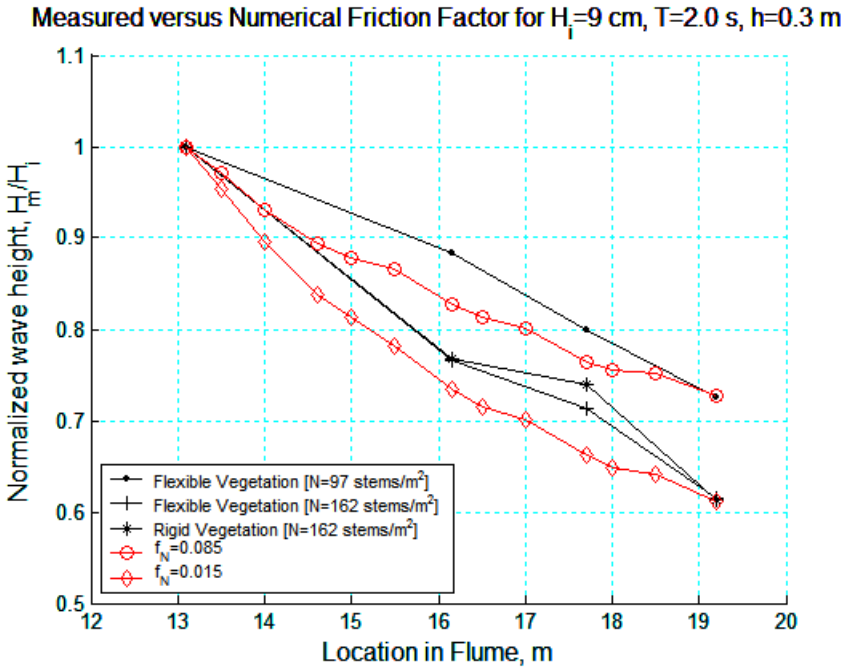

Figure 32. Example of output free surface elevation time series from COULWAVE model normalized by the initial wave height for emergent plant conditions

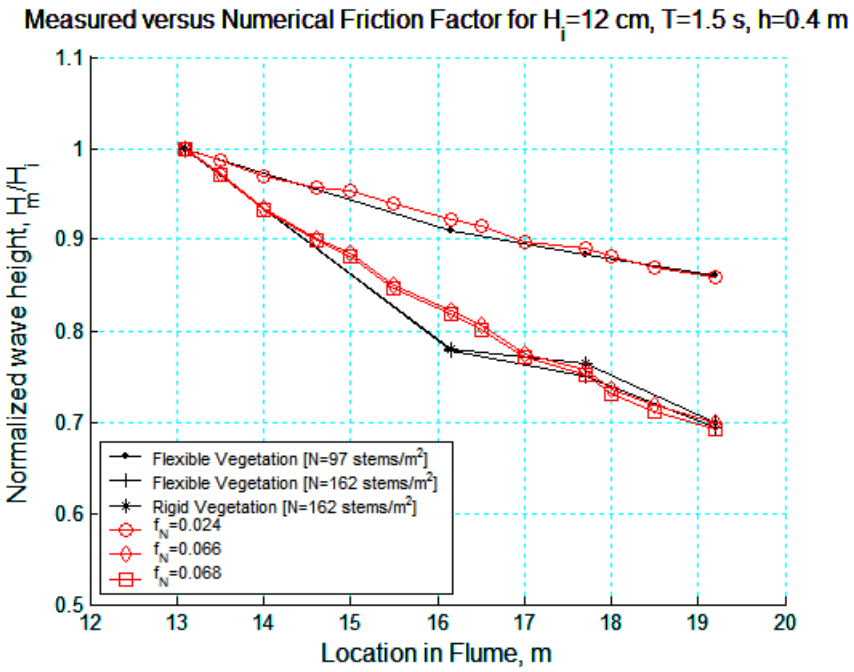

Figure 33. Example of output free surface elevation time series from COULWAVE model normalized by the initial wave height for submerged plant conditions

Because of the large amount of experiments, the friction factor is presented graphically. The friction factor for all experimental cases, including emergent and submerged plant conditions, is plotted against the dimensionless Ursell number below in Figure 34. The Ursell number is given by

$$U_R = \frac{L^2 H}{h^3} \tag{5.6}$$

Shallower water depths with greater periods yield higher Ursell numbers compared to deeper water depths. For submerged conditions the friction factor tends to increase with increasing Ursell number. The increasing trend shows the dependency of water depth and wave period on the friction factor value. Emergent conditions are fairly scattered, most likely due to the friction factor's dependence on other flow parameters. Figure 35

shows the friction factor found for isolated cases where the vegetation density was equal to 97 stems/m^2.

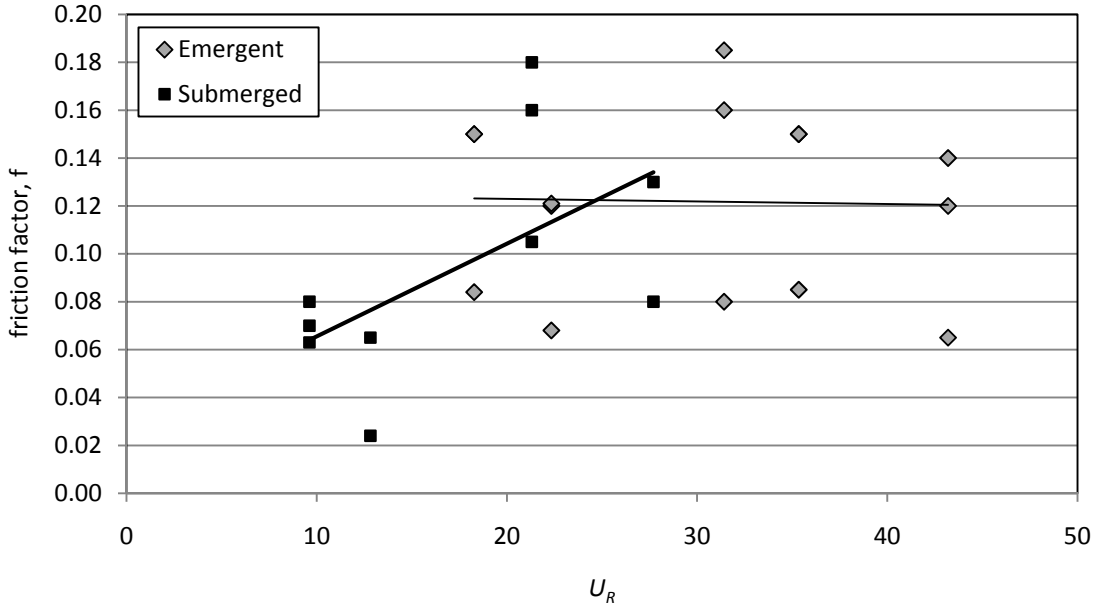

Figure 34. Numerically determined friction factor versus Ursell number

The values of friction factor increased for the higher plant density, but were not observed to depend on plant flexibility. The attenuation effects of the rigid and flexible vegetation elements appeared to be very similar and in some of the experimental cases yielded the same friction factor value. The flexible and rigid cases are shown in Figure 36. Overall, the same trends are followed for all the experiments and yielded reasonable results considering the initial steady friction factor assumption. The average percent error for the regression lines is 16%. A larger percentage of error was observed for the regression lines fitted to submerged plant conditions. This is most likely due to influence of the ratio of stem length to water depth on wave damping, which is not accounted for in the friction factor formulation. The total average percent error for emergent regression lines

was only 10%, which is quite good considering the assumptions made. Percentages for each fitted regression line are displayed in Figures 35 and 36. More data points are needed to statistically determine an accurate sample correlation coefficient for each of the regression lines. From the data collected it appears that modeling vegetation roughness using a friction factor is a reasonable approximation as long as the limitations are known. In Figures 35 and 36 there is a distinct transition zone between the U_R values ranging between 20 and 30 where the emergent and submerged conditions meet.

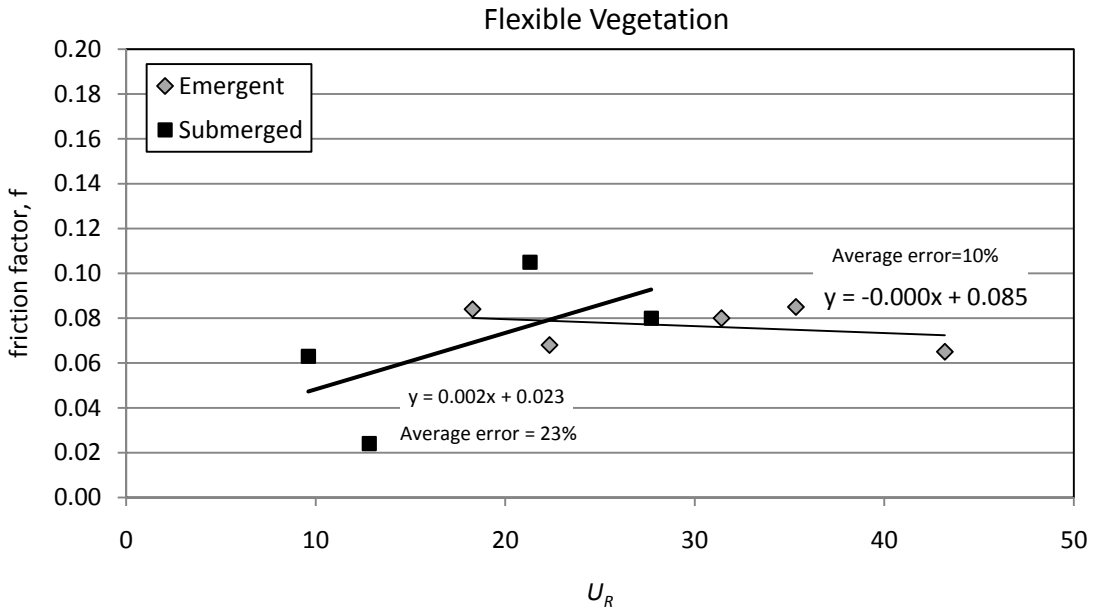

Figure 35. Friction factor versus Ursell parameter for flexible plants with a density of N=97 stems/m^2

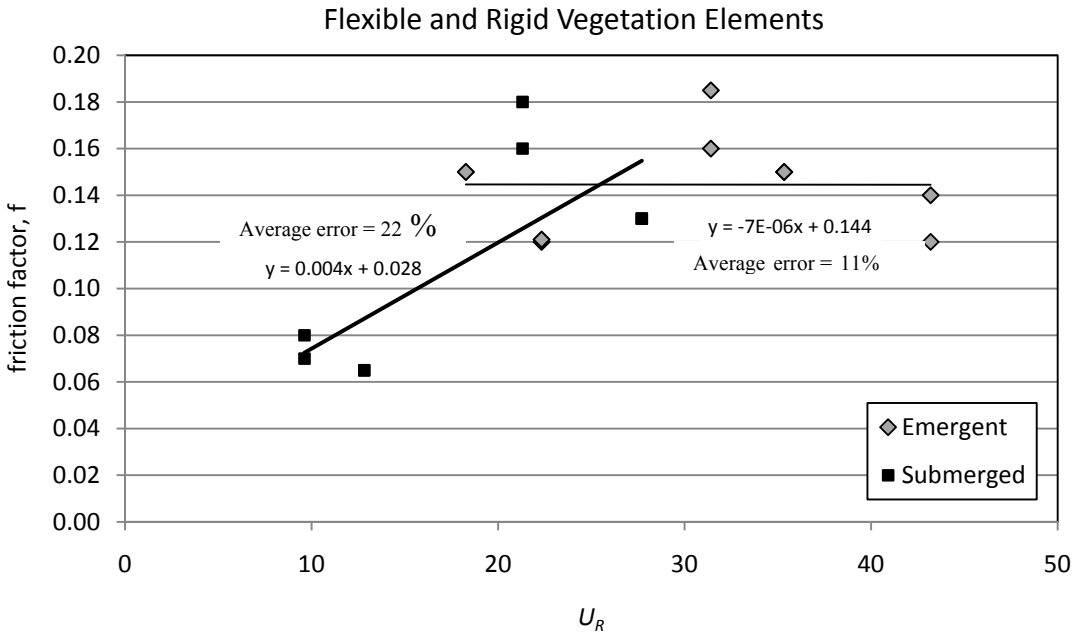

Figure 36. Friction factor versus Ursell number for flexible and rigid plants with a density of *N*=162 stems/m^2

A set of equations for each zone is formulated from the regression lines to estimate a wave friction factor for stem density values ranging over the tested conditions, between 97 stems/m^2 and 162 stems/m^2. The numerically derived empirical wave friction factor equations for submerged, $f_N^{(S)}$, and emergent, $f_N^{(E)}$, plant conditions are given by

$$f_N^{(S)} = 0.002\left(1+\frac{N-97}{65}\right)U_R + 0.005\frac{(N-97)}{65} + 0.023 \quad (5.7)$$

$$f_N^{(E)} = -7E\text{-}06\left(\frac{N-97}{65}\right)U_R + 0.059\frac{(N-97)}{65} + 0.085 \quad (5.8)$$

These equations are derived from the rigid and flexible plants and should be able to be applied to rigid vegetation or flexible vegetation with limited swaying motion for practical engineering purposes. However, plants that are extremely flexible are not valid in the above equations because a large amount of bending will result in a significantly

lower friction factor than is predicted. The friction factor becomes highly dependent on the Reynolds number when the flow velocity is high enough to bend the plant stems so that they are near parallel with the bed (Figure 37).

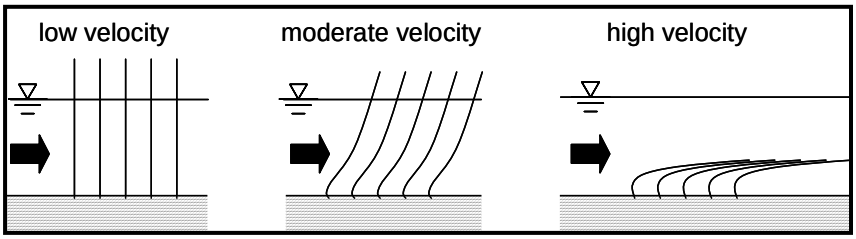

Figure 37. Schematic of plant shape as velocity increases, with arrows indicating the direction of fluid flow

CHAPTER VI

CONCLUSIONS

Experiments found that near emergent conditions resulted in a higher amount of wave attenuation compared to submerged conditions. Emergent conditions are most prevalent in marsh and wetland systems and are expected to result in a higher amount of wave attenuation because the plant stem occupies the entire depth of the water column. The wave height decay followed the same trends for all the experimental cases and appeared to be more dependent on the ratio of stem length to water depth and stem density, rather than incoming wave height and period. Vegetation density also influenced wave attenuation, with denser layout attenuating the wave height by 12 – 17% more than the less dense layout. Plant flexibility appeared to play a role in the amount of wave attenuation, with flexible members reducing the wave height by an extra 1-4% compared to rigid members. Motion of the flexible elements is an important factor when considering the effects of plant rigidity on wave attenuation. If the plants are subject to high velocities the stem can become prone near the bed. Prone plants are not as effective as dissipating energy as plants that demonstrate a slight to moderate swaying motion. The attenuation effects of the rigid and flexible vegetation elements appeared to be very similar in the laboratory experiments and in some of the cases yielded the same friction factors. Intuitively, flexible vegetation should dissipate a higher amount of energy due to the increased form drag and ability to absorb a higher amount of oncoming momentum from the flow.

The COULWAVE model was shown to accurately simulate the experimental cases using the friction factor approach. The values of the numerical friction factor for the conditions tested ranged between 0.02 and 0.2, which is equivalent to a Manning's n value of 0.13 and .03, respectively. Values were found to be primarily dependent on the height of the vegetation relative to the water depth. It was observed for submerged plant conditions, the friction factor increased with larger periods, concluding the attenuation in submerged plants is highly dependent on the wavelength of the approaching wave. Modeling vegetation roughness through the use of a dimensionless friction factor was found to provide a reasonable estimate for the amount of wave attenuation that may occur through vegetation fields. Unfortunately, the friction factor is strongly dependent on many factors and would generally require field data if it was desired to determine a friction factor for a particular site. To avoid the necessity of field data empirical equations were derived from the numerical regression lines. The derived equations for both emergent and submerged plant conditions can be applied to estimate wave damping for practical engineering purposes if the stem density ranges between 97 stems/m^2 and 162 stems/m^2.

Recommendations for future study are focused on further improving our understanding of vegetation roughness, and the physical processes that cause wave attenuation through emergent and submerged vegetation. The following lists recommendations, based on the research from this thesis:

- Conduct laboratory measurements on a wider variety of stem diameters, stem densities, and varying plant bed lengths to determine how distance affects total wave height decay.
- Collect real wetland plant specimens and construct a vegetation field inside a laboratory flume. Measure attenuation and determine a damping coefficient for a particular species from existing attenuation theory.
- Scale experiments or collect field data to analyze attenuation for longer wave periods. The main concern is that the periods analyzed in this study are not long enough to accurately represent nearshore wind waves. Periods should be in the range of 3 s, as opposed to 1.5 - 2 s.
- Conduct experiments over a wider range of submerged and emergent conditions to validate friction factor equations and develop correlation coefficients for the friction factor regression lines. This study did not consist of enough sample points to accurately determine correlation statistics.
- Numerically model wake effects of each individual plant stem to determine total wave attenuation and compare to the friction factor approach. Interaction between stems is a very complex process and is most likely a significant factor contributing to the total amount of wave attenuation through flexible vegetation elements. Plant interaction is typically ignored in analytical attenuation models.

REFERENCES

Asano, T., Deguchi, H., and N. Kobayashi (1992), Interaction between water waves and Vegetation, Chapter 207, *Proc. Intern. Coastal Eng. Conf., 23rd , ASCE, 3,* 2710-2723.

ASCE Task Committee on Sea Level Rise and its Effects on Bays and Estuaries (1992), Effects of sea level rise on bays and estuaries, *J. Hydraul. Eng.*, *118*(1), 1-10.

Bretschneider, C. L., and R.O. Reid (1954), Modification of wave height due to bottom friction, percolation, and refraction, *US Beach Erosion Board, Corps of Eng., Tech. Mem., 45*.

Camfield, F. E. (1983), Wind wave growth with high friction, *J. Waterway, Port, Coastal, Ocean Eng.*, *109*(1), 115-117.

Chen, C. L. (1976), Flow resistance in broad shallow grassed channels, *J. Hydraul. Eng., 102*(3), 307-322.

Dalrymple, R. A., Kirby, J. T., and P.A. Hwang (1984), Wave refraction due to areas of energy dissipation, *J. Waterways, Port., Coastal, Ocean Eng., 110*(1), 67-79.

Dean, R. G. (1978), Effects of vegetation on shoreline erosional processes, Wetland Functions and Values: The State of Our Understanding, *American Water Resources Assoc.*, 415-426.

Dubi, A., and A. Torum (1995), Wave damping by kelp vegetation, *Proc. of the Twenty-Fourth Coastal Eng. Conf.,* edited by B.L. Edge, pp. 142-156, ASCE, New York.

Elgar, S., and R.T. Guza (1985), Observations of bispectra of shoaling surface gravity waves, *J. Fluid Mech., 161*, 425-448.

Fox, A.M., Haller, W.T., and J.P. Cuda (2002), Impacts of carbohydrate depletion by repeated clipping on the production of subterranean turions by dioecious hydrilla. *J. Aquatic Plant Manag.*, *40,* 99-104.

Goring, D.G. (1978), Tsunamis-the propagation of long waves onto a shelf, *Rep. KH-R-38,* California Institute of Technology.

Kadlec, R.H. (1990), Overland flow in wetlands: vegetation resistance, *J. Hydraul. Eng.*, *116*, 691-707.

Knabb, R.D., Rhome, J.R., and D.P. Brown (2006), Tropical cyclone report Hurricane Katrina 23-30 August 2005. *National Hurricane Center Report*, 43 pp.

Kobayashi, N., Raichlen, A. W., and T. Asano (1993), Wave attenuation by vegetation, *J. Waterways, Port, Coastal, Ocean Eng. Div., 199*(1), 30-48.

Komar, P.D. (1998), *Beach Processes and Sedimentation*, 2nd ed., 544 pp., Simon and Schuster, Upper Saddle River, N.J.

Kouwen, N., Unny, T.E., and H.M. Hill (1969), Flow retardance in vegetated channels, *J. Irr. Drainage Div.*, *95*(IRE), 329-342.

Kouwen, N., and T. Unny (1973), Flexible roughness in open channels, *J. Hydraul. Div.*, *99*(HY5), 713-728.

Kouwen, N. and M. Fathi-Maghadam (1997), Nonrigid, nonsubmerged, vegetative roughness on floodplains, *J. Hydraul. Eng.*, 51-57.

Lima, S.F., Neves, C.F., and N.M.L. Rosauro (2006), Damping of gravity waves by fields of flexible vegetation, *Proc. Intern. Coastal Eng. Conf., 30th, 1*, San Diego, California, 491-503.

Liu, P.L.-F., Yoon, S.B. and J.T. Kirby (1985), Nonlinear refraction-diffraction of waves in shallow water, *J. Fluid Mech., 153*, 184-201.

Lynett, P., Wu, T.-R., and P. L.-F. Liu (2002), Modeling Wave Runup with Depth-Integrated Equations, *Coastal Eng., 46*(2), 89-107.

Mansard, E.P.D, and E.R. Funke (1980), The measurement of incident and reflected spectra using a least squares method, *Proc. Coastal Eng. Conf.*, *17th , 1,* 154-172.

Mazda, Y., Wolanski, E., King, B., Sase, A., Ohtsuka, D., and M. Magi (1997), Drag force due to vegetation in mangrove swamps," *Mangroves and Marshes, 1,* 193-199.

Mendez, F. J., Losada, I. J., and M.A. Losada (1999), Hydrodynamics induced by wind waves in a vegetation field, *J. Geophys. Res., 104(C8),* 18383-18396.

Mendez, F. J., and I.J. Losada (2004), An empirical model to estimate the propagation of random breaking and nonbreaking waves over vegetation fields, *Coastal Eng., 51*, 103-118.

Mork, M. (1996), Wave attenuation due to bottom vegetation, in *Waves and nonlinear processes in hydrodynamics,* pp. 371-382, Kluwer Academic Publishers.

Munson, B.R., Okiishi, T.H., and D.F. Young (2002), *Fundamentals of Fluid Mechanics, 4th ed.*, John Wiley & Sons, Inc.

Nepf, H.M. (2004), Vegetated Flow Dynamics, in *Ecogeomorphology of tidal marshes*, *Coastal and Estuarine Studies, 59,* edited by S. Fagherazzi, M. Marani, and L. Blum, pp. 137-164.

Price, W. A., Tomlinson, K. W., and J.N. Hunt (1968), The effect of artificial seaweed in promoting the build-up of beaches, *Proc. Coastal Eng. Conf.*, *11th, 1,* 570-578.

Schoettle, T. (1996), *A Guide to a Georgia Barrier Island,* Watermarks Publishing, St. Simons Island, Georgia.

Thornton, E.B., and R.T. Guza (1983), Transformation of wave height distribution, *J. Geophys. Res., 88* (C10), 5925-5938.

Tshirky, P.A. (2000), An investigation of wave attenuation by emergent, freshwater, wetland vegetation, Ph.D. Thesis, Queen's University, Kingston, Ontario, Canada.

U.S. Environmental Protection Agency, EPA, *America's Wetlands*, 16 July 2007, <http://www.epa.gov/OWOW/wetlands/vital/toc.html>

U.S. Geological Survey (2006), USGS reports on latest land-water changes for southeastern Louisiana, February 2006, *U.S. Dept. of the Interior, U.S. Geol. Survey*.

Wei, G., Kirby, J. T, Grilli, S.T., and R. Subramanya (1995), A fully nonlinear Boussinesq model for surface waves. I. Highly nonlinear, unsteady waves, *J. Fluid Mech., 294,* 71-92.

APPENDIX A

LOCALLY NORMALIZED WAVE HEIGHT PLOTS

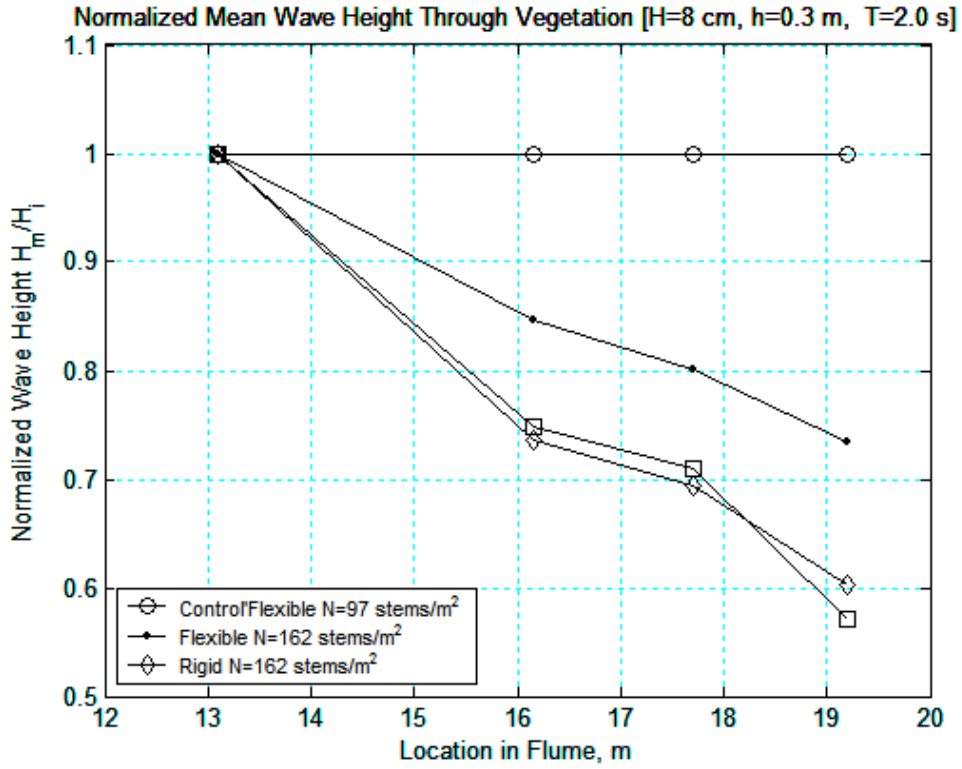
Normalized Mean Wave Height Through Vegetation [H=8 cm, h=0.3 m, T=2.0 s]
Normalized Wave Height H_m/H_i
Location in Flume, m
Control'Flexible N=97 stems/m^2
Flexible N=162 stems/m^2
Rigid N=162 stems/m^2

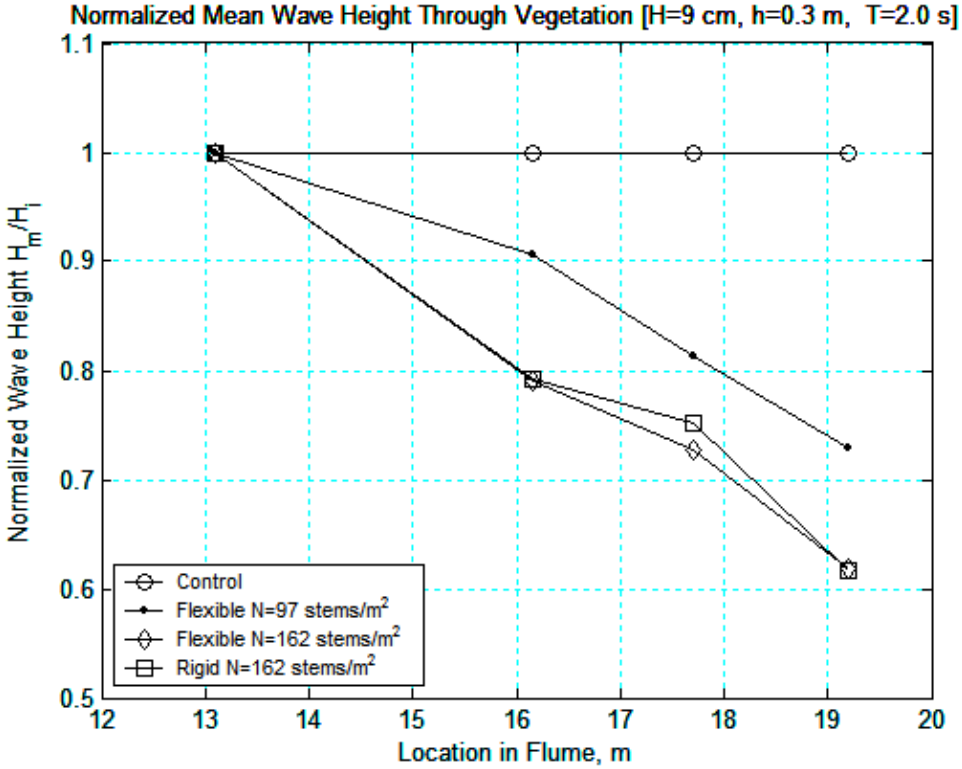
Normalized Mean Wave Height Through Vegetation [H=9 cm, h=0.3 m, T=2.0 s]
Normalized Wave Height H_m/H_i
Location in Flume, m
Control
Flexible N=97 stems/m^2
Flexible N=162 stems/m^2
Rigid N=162 stems/m^2

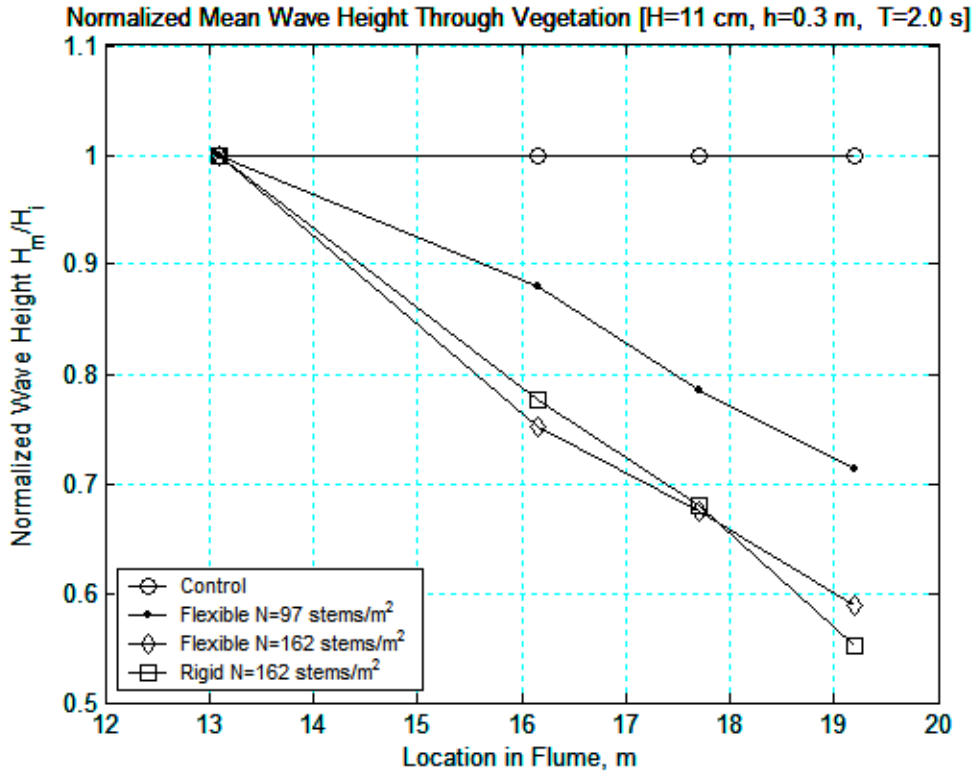
Normalized Mean Wave Height Through Vegetation [H=11 cm, h=0.3 m, T=2.0 s]
Normalized Wave Height H_m/H_i
Location in Flume, m
1.1
1
0.9
0.8
0.7
0.6
0.5
12
13
14
15
16
17
18
19
20
Control
Flexible N=97 stems/m^2
Flexible N=162 stems/m^2
Rigid N=162 stems/m^2

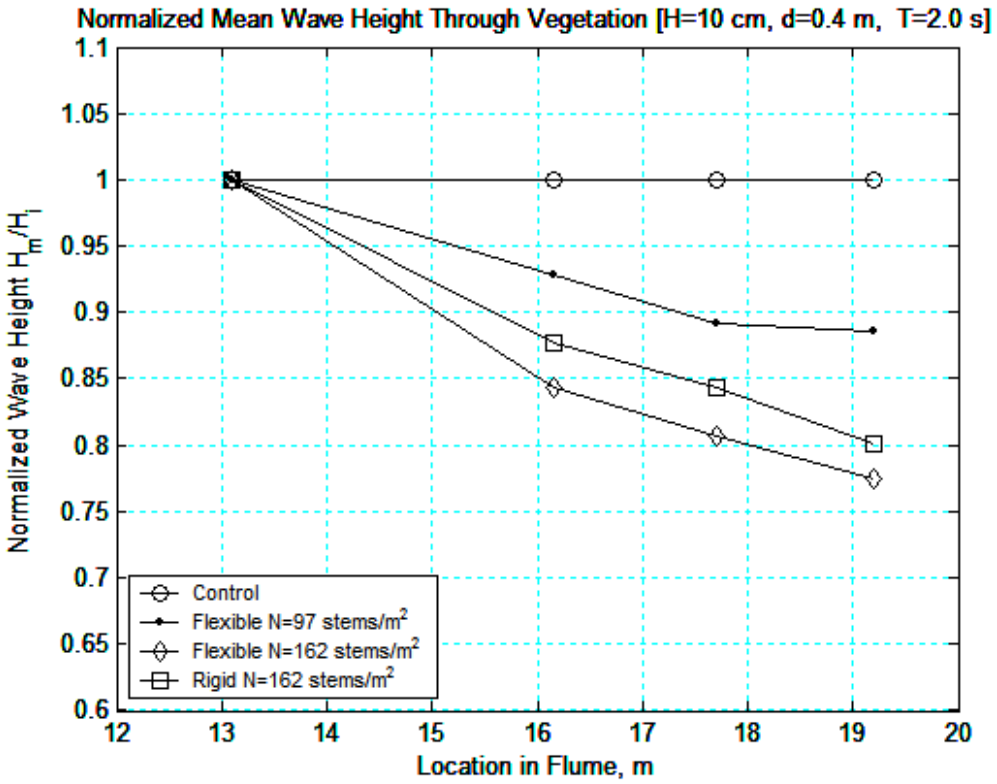
Normalized Mean Wave Height Through Vegetation [H=10 cm, d=0.4 m, T=2.0 s]
Normalized Wave Height H_m/H_i
Location in Flume, m
Control
Flexible N=97 stems/m^2
Flexible N=162 stems/m^2
Rigid N=162 stems/m^2

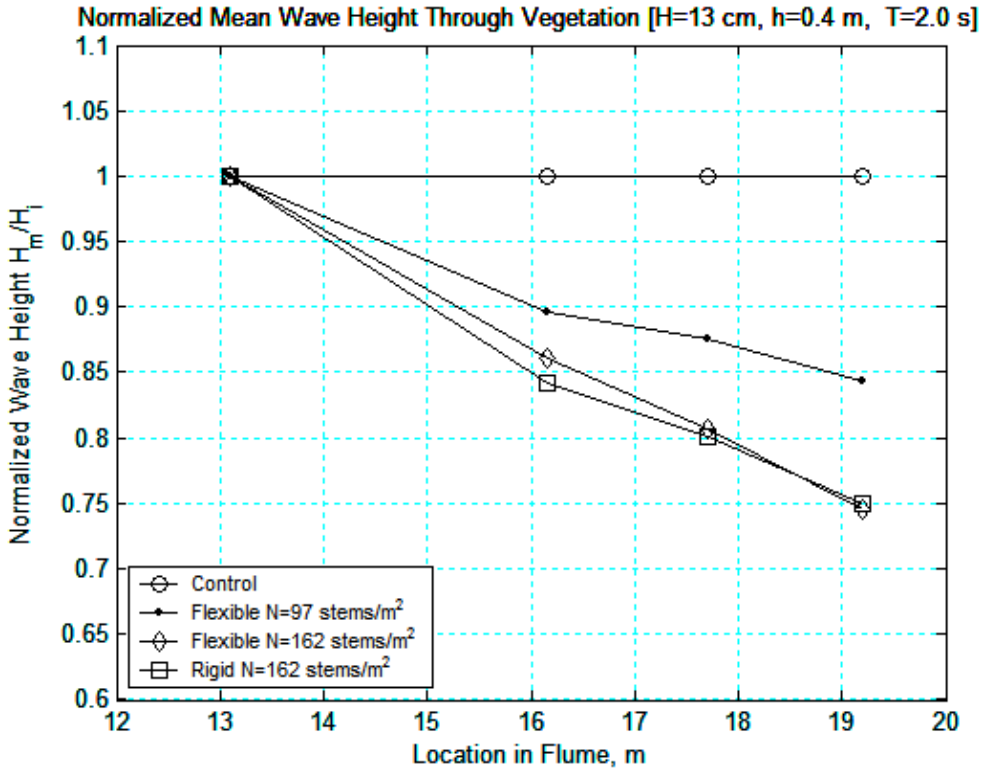
Normalized Mean Wave Height Through Vegetation [H=13 cm, h=0.4 m, T=2.0 s]
Normalized Wave Height H_m/H_i
Location in Flume, m
Control
Flexible N=97 stems/m^2
Flexible N=162 stems/m^2
Rigid N=162 stems/m^2

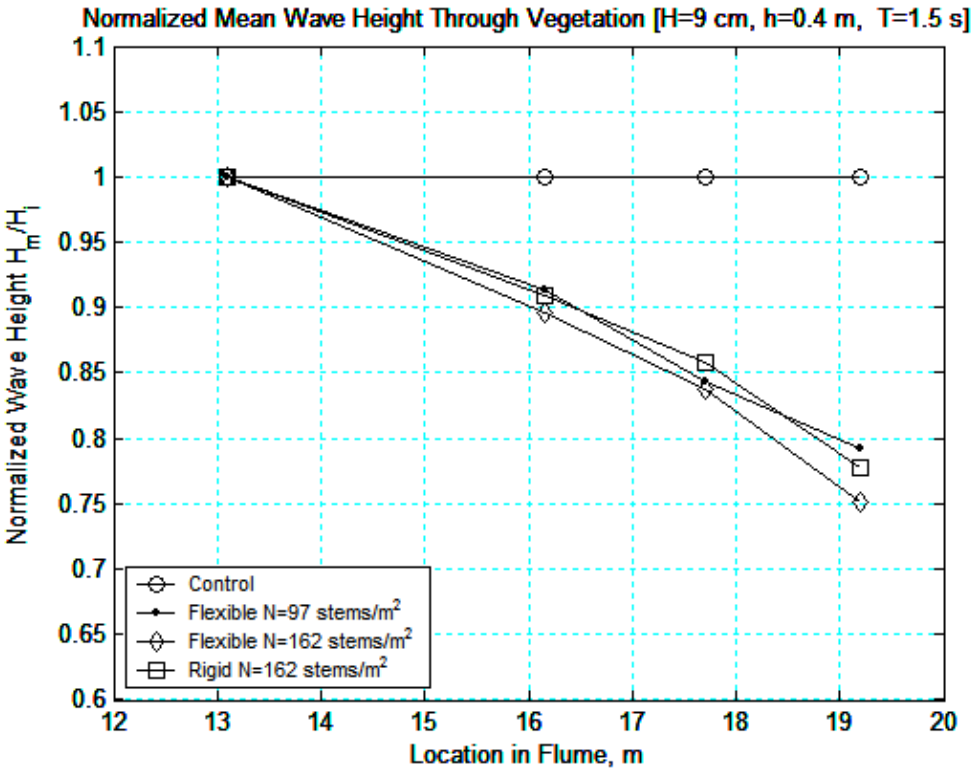
Normalized Mean Wave Height Through Vegetation [H=9 cm, h=0.4 m, T=1.5 s]
Normalized Wave Height H_m/H_i
Location in Flume, m
Control
Flexible N=97 stems/m^2
Flexible N=162 stems/m^2
Rigid N=162 stems/m^2

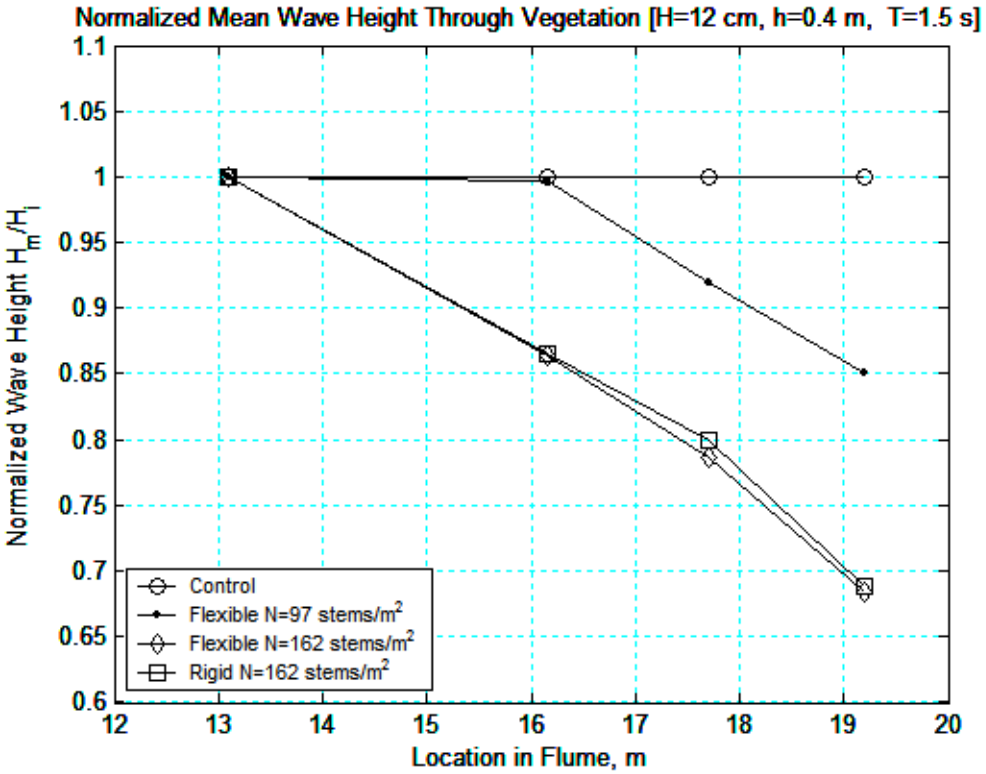
Normalized Mean Wave Height Through Vegetation [H=12 cm, h=0.4 m, T=1.5 s]
Normalized Wave Height H_m/H_i
Location in Flume, m
Control
Flexible N=97 stems/m^2
Flexible N=162 stems/m^2
Rigid N=162 stems/m^2

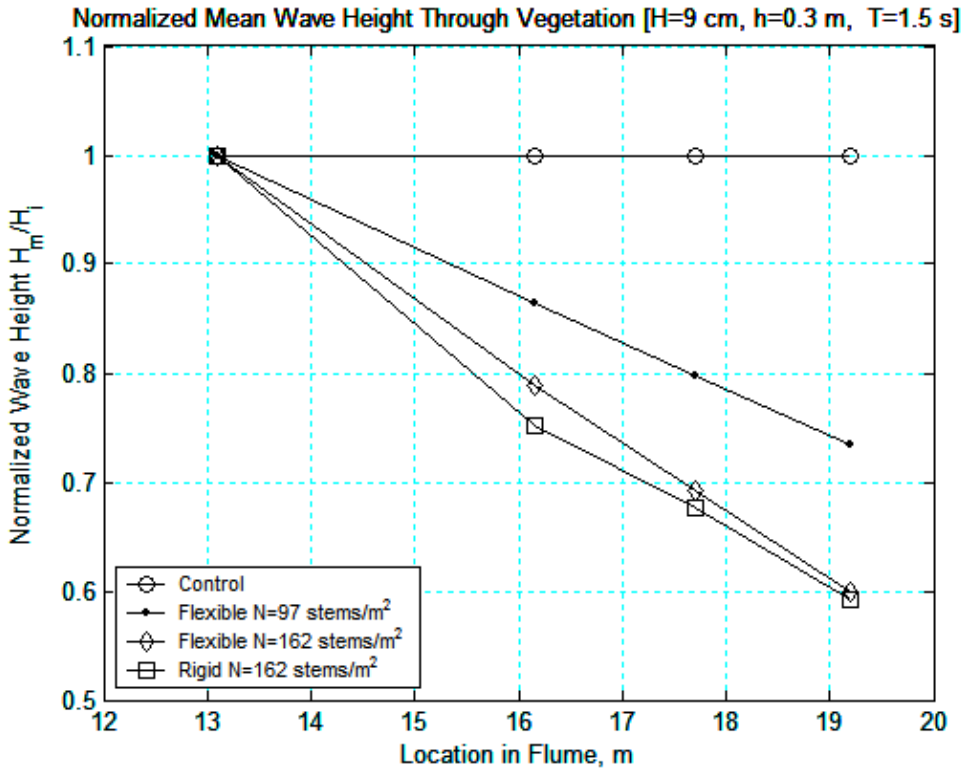
Normalized Mean Wave Height Through Vegetation [H=9 cm, h=0.3 m, T=1.5 s]
Normalized Wave Height H_m/H_i
Location in Flume, m
Control
Flexible N=97 stems/m^2
Flexible N=162 stems/m^2
Rigid N=162 stems/m^2

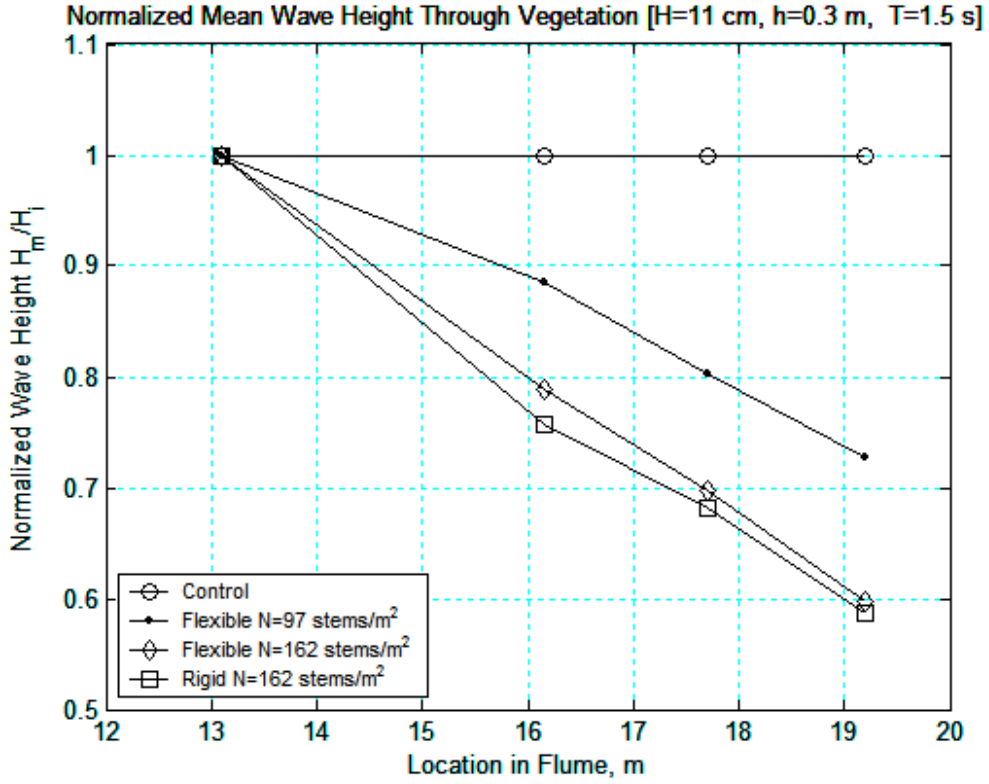
Normalized Mean Wave Height Through Vegetation [H=11 cm, h=0.3 m, T=1.5 s]
Normalized Wave Height H_m/H_i
Location in Flume, m
Control
Flexible N=97 stems/m^2
Flexible N=162 stems/m^2
Rigid N=162 stems/m^2

APPENDIX B

BASIN REFLECTION COEFFICIENTS

Hrms [cm]	T [s]	h [m]	N [stems/m^2]	C_R	Wave Type
8.5	2.0	0.3	0	0.377	TMA
8.5	2.0	0.3	0	0.327	TMA
8.5	2.0	0.3	97	0.341	TMA
8.5	2.0	0.3	162	0.270	TMA
8.5	2.0	0.3	162	0.286	TMA
8.5	2.0	0.4	0	0.255	TMA
8.5	2.0	0.4	97	0.240	TMA
8.5	2.0	0.4	162	0.200	TMA
8.5	1.5	0.3	0	0.355	TMA
8.5	1.5	0.3	97	0.285	TMA
8.5	1.5	0.3	97	0.264	TMA
8.5	1.5	0.3	162	0.226	TMA
8.5	1.5	0.3	162	0.221	TMA
8.5	1.5	0.4	0	0.282	TMA
8.5	1.5	0.4	0	0.302	TMA
8.5	1.5	0.4	97	0.244	TMA
8.5	1.5	0.4	97	0.239	TMA
8.5	1.5	0.4	162	0.227	TMA
8.5	1.5	0.4	162	0.228	TMA

APPENDIX C

WAVE SPECTRUM PLOTS

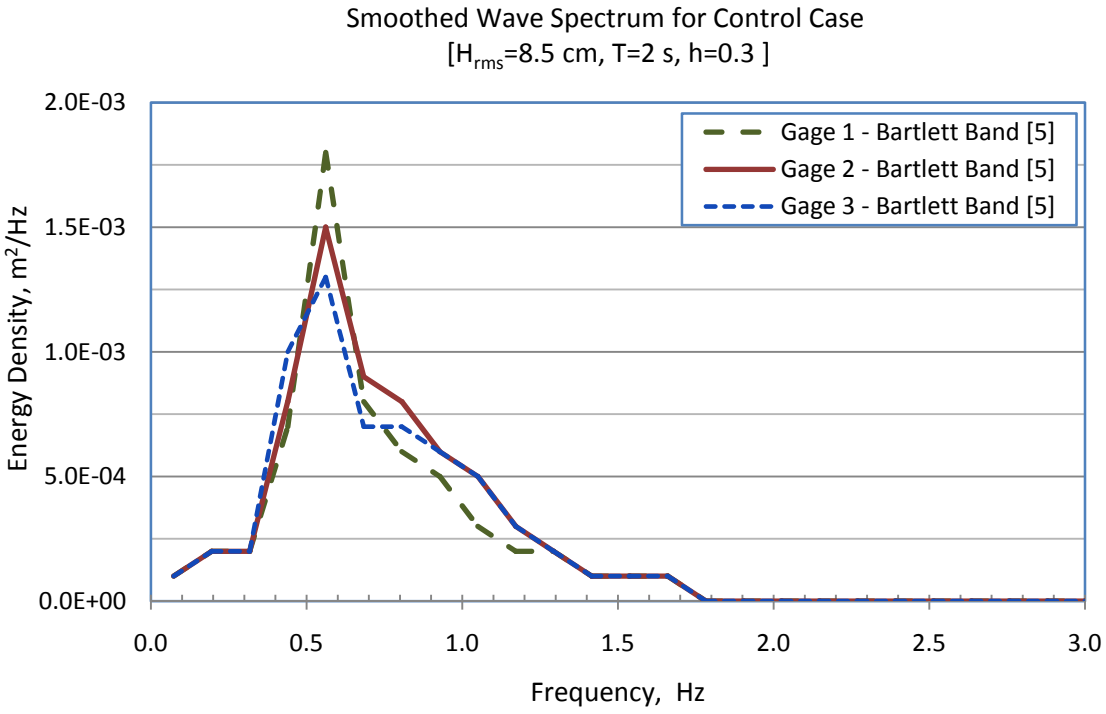
Smoothed Wave Spectrum for Control Case
[Hrms=8.5 cm, T=2 s, h=0.3]
Energy Density, m2/Hz
2.0E-03
1.5E-03
1.0E-03
5.0E-04
0.0E+00
0.0
0.5
1.0
1.5
2.0
2.5
3.0
Frequency, Hz
Gage 1 - Bartlett Band [5]
Gage 2 - Bartlett Band [5]
Gage 3 - Bartlett Band [5]

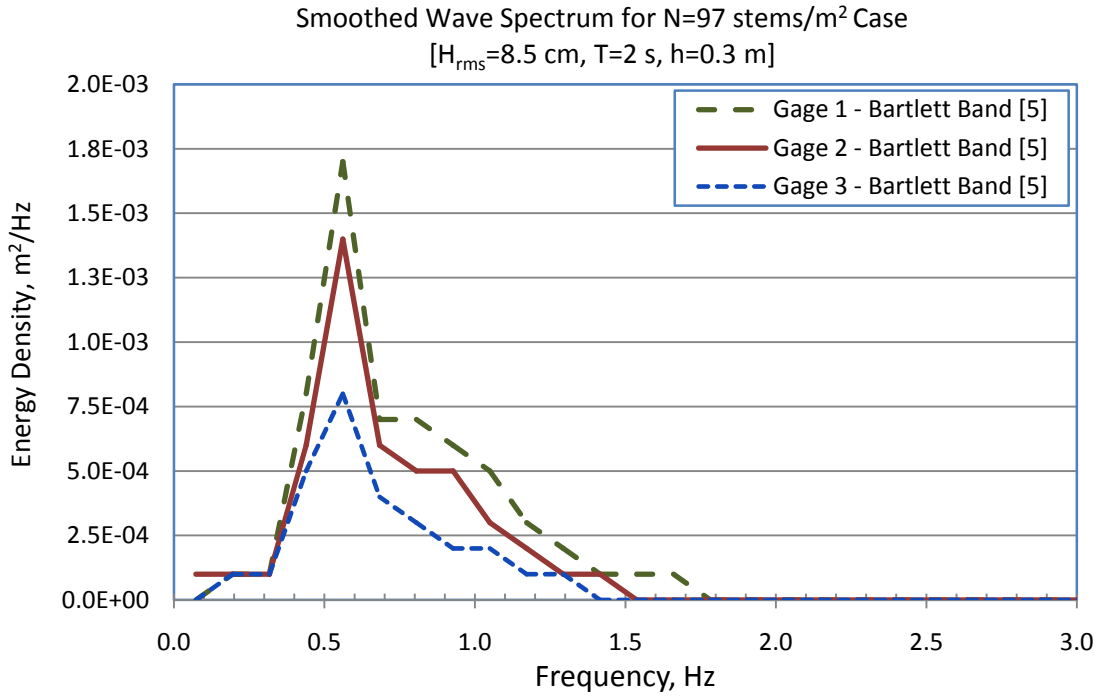
Smoothed Wave Spectrum for N=97 stems/m2 Case
[Hrms=8.5 cm, T=2 s, h=0.3 m]
Energy Density, m2/Hz
2.0E-03
1.8E-03
1.5E-03
1.3E-03
1.0E-03
7.5E-04
5.0E-04
2.5E-04
0.0E+00
0.0
0.5
1.0
1.5
2.0
2.5
3.0
Frequency, Hz
Gage 1 - Bartlett Band [5]
Gage 2 - Bartlett Band [5]
Gage 3 - Bartlett Band [5]

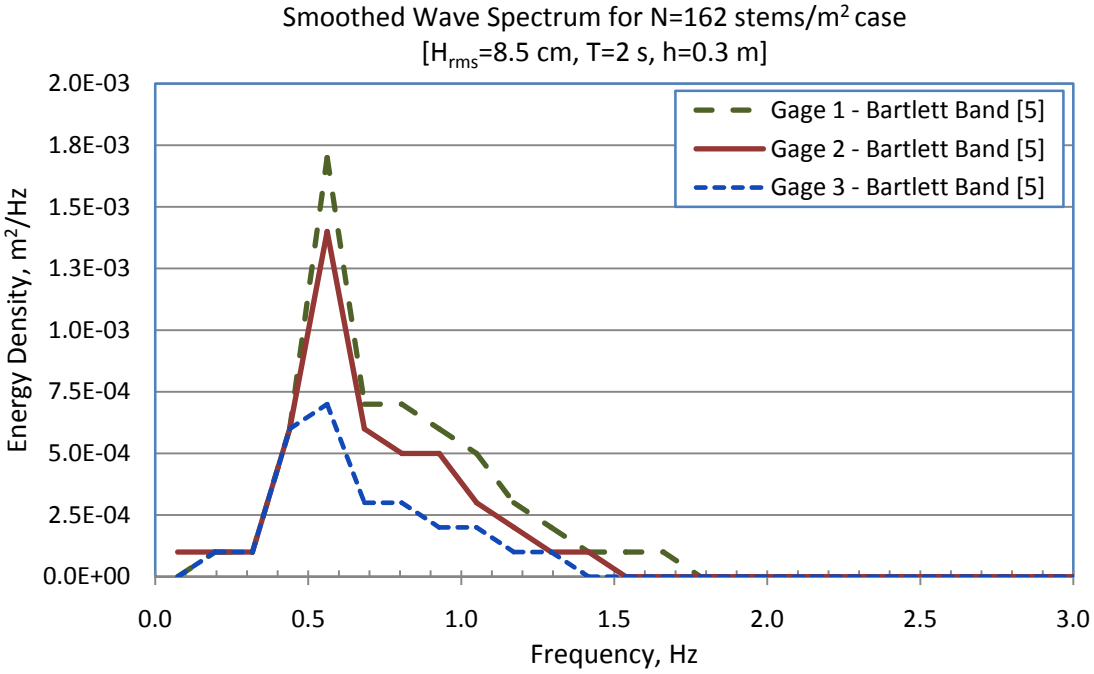
Smoothed Wave Spectrum for N=162 stems/m² case
[H_rms=8.5 cm, T=2 s, h=0.3 m]
Energy Density, m²/Hz
2.0E-03
1.8E-03
1.5E-03
1.3E-03
1.0E-03
7.5E-04
5.0E-04
2.5E-04
0.0E+00
0.0
0.5
1.0
1.5
2.0
2.5
3.0
Frequency, Hz
Gage 1 - Bartlett Band [5]
Gage 2 - Bartlett Band [5]
Gage 3 - Bartlett Band [5]

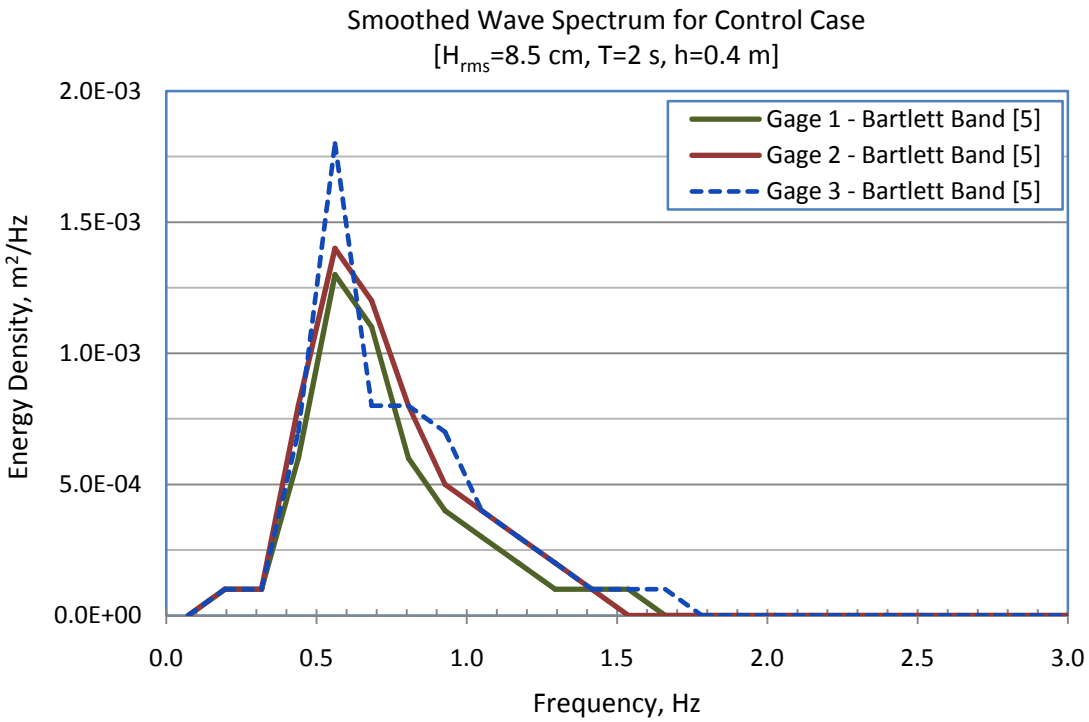
Smoothed Wave Spectrum for Control Case
[H_rms=8.5 cm, T=2 s, h=0.4 m]
Energy Density, m²/Hz
2.0E-03
1.5E-03
1.0E-03
5.0E-04
0.0E+00
0.0
0.5
1.0
1.5
2.0
2.5
3.0
Frequency, Hz
Gage 1 - Bartlett Band [5]
Gage 2 - Bartlett Band [5]
Gage 3 - Bartlett Band [5]

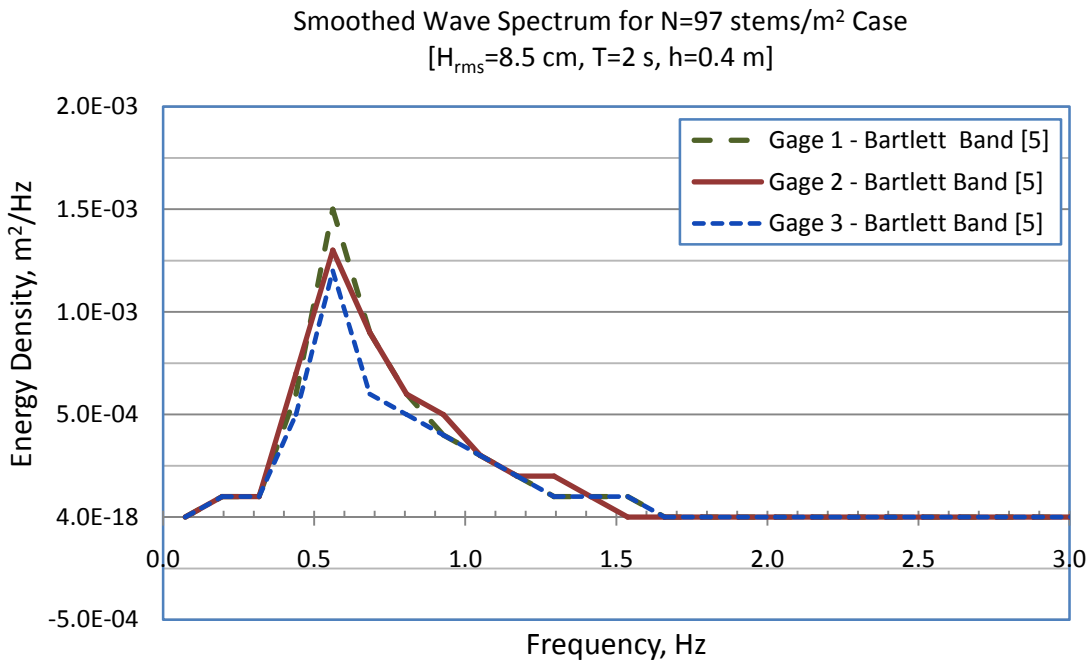
Smoothed Wave Spectrum for N=97 stems/m² Case
[H_rms=8.5 cm, T=2 s, h=0.4 m]
Energy Density, m²/Hz
2.0E-03
1.5E-03
1.0E-03
5.0E-04
4.0E-18
-5.0E-04
0.0
0.5
1.0
1.5
2.0
2.5
3.0
Frequency, Hz
Gage 1 - Bartlett Band [5]
Gage 2 - Bartlett Band [5]
Gage 3 - Bartlett Band [5]

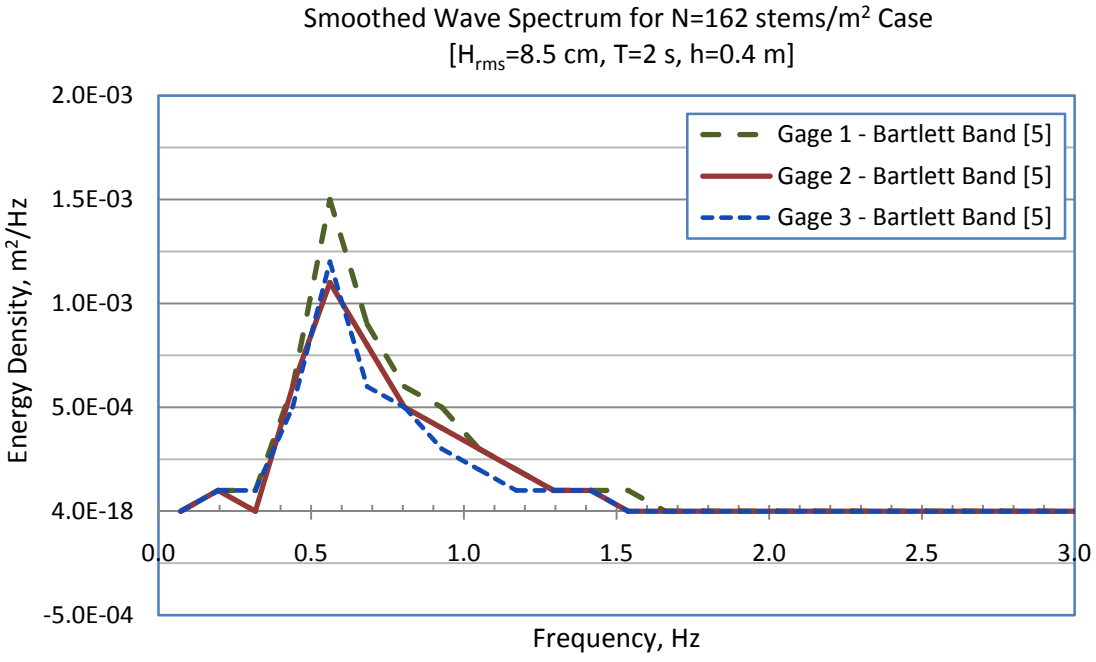
Smoothed Wave Spectrum for N=162 stems/m² Case
[H_rms=8.5 cm, T=2 s, h=0.4 m]
Energy Density, m²/Hz
2.0E-03
1.5E-03
1.0E-03
5.0E-04
4.0E-18
-5.0E-04
0.0
0.5
1.0
1.5
2.0
2.5
3.0
Frequency, Hz
Gage 1 - Bartlett Band [5]
Gage 2 - Bartlett Band [5]
Gage 3 - Bartlett Band [5]

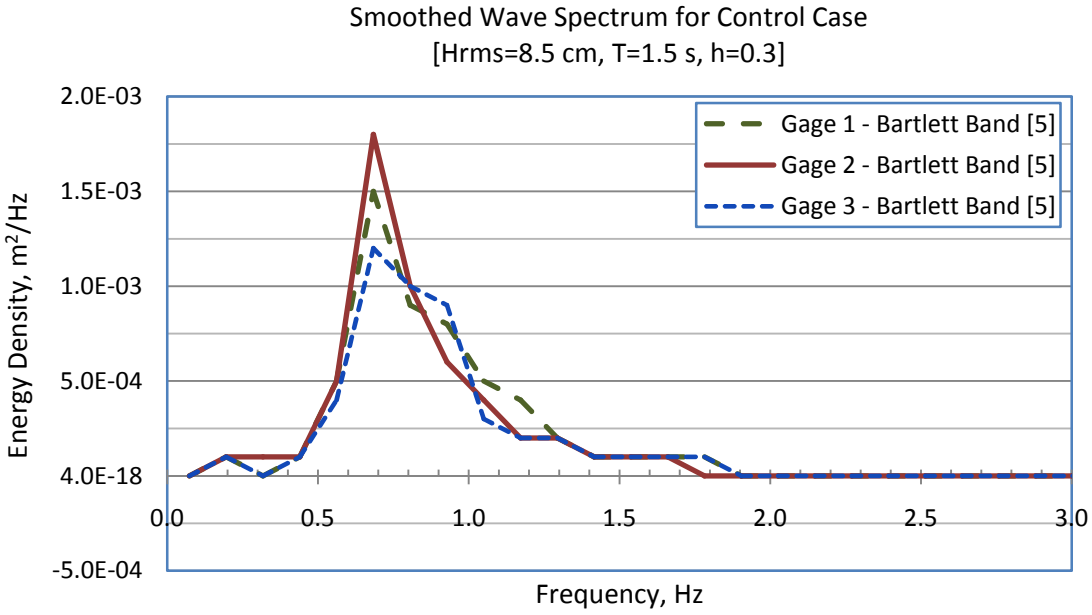
Smoothed Wave Spectrum for Control Case
[Hrms=8.5 cm, T=1.5 s, h=0.3]
Gage 1 - Bartlett Band [5]
Gage 2 - Bartlett Band [5]
Gage 3 - Bartlett Band [5]
Energy Density, m²/Hz
2.0E-03
1.5E-03
1.0E-03
5.0E-04
4.0E-18
-5.0E-04
0.0
0.5
1.0
1.5
2.0
2.5
3.0
Frequency, Hz

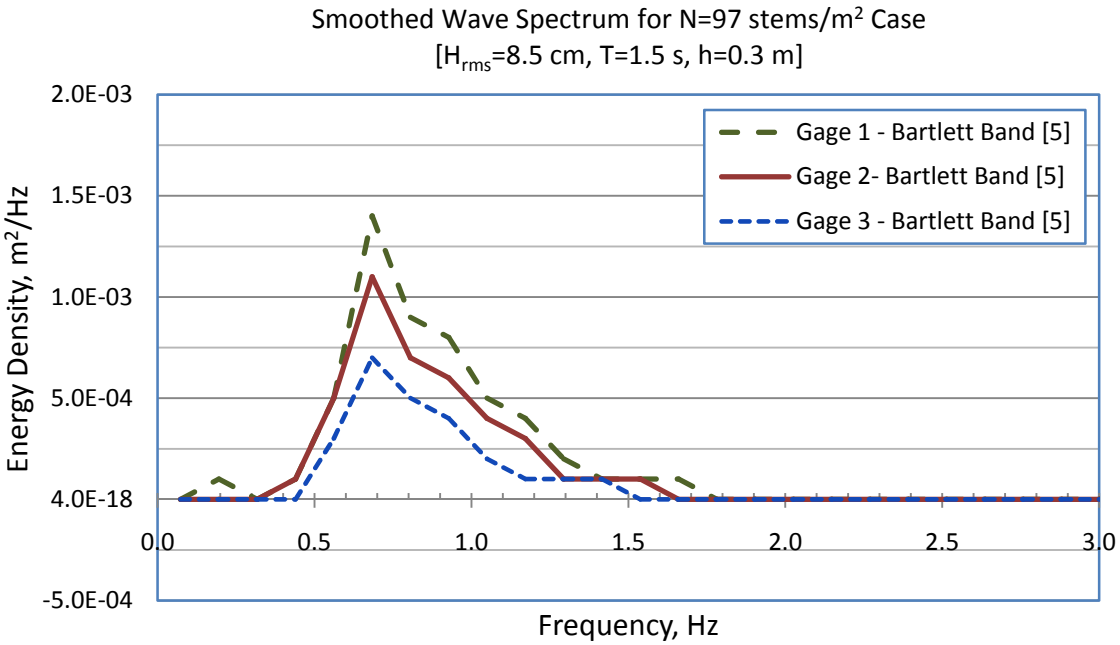
Smoothed Wave Spectrum for N=97 stems/m² Case
[Hrms=8.5 cm, T=1.5 s, h=0.3 m]
Gage 1 - Bartlett Band [5]
Gage 2- Bartlett Band [5]
Gage 3 - Bartlett Band [5]
Energy Density, m²/Hz
2.0E-03
1.5E-03
1.0E-03
5.0E-04
4.0E-18
-5.0E-04
0.0
0.5
1.0
1.5
2.0
2.5
3.0
Frequency, Hz

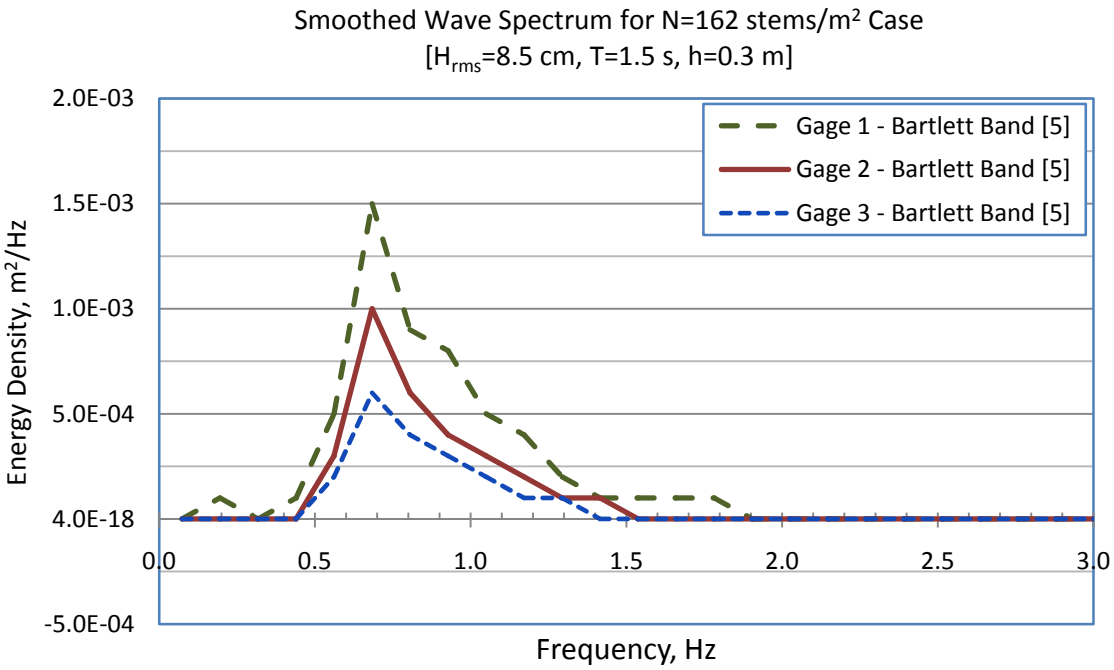
Smoothed Wave Spectrum for N=162 stems/m² Case
[Hrms=8.5 cm, T=1.5 s, h=0.3 m]
Gage 1 - Bartlett Band [5]
Gage 2 - Bartlett Band [5]
Gage 3 - Bartlett Band [5]
Energy Density, m²/Hz
2.0E-03
1.5E-03
1.0E-03
5.0E-04
4.0E-18
-5.0E-04
0.0
0.5
1.0
1.5
2.0
2.5
3.0
Frequency, Hz

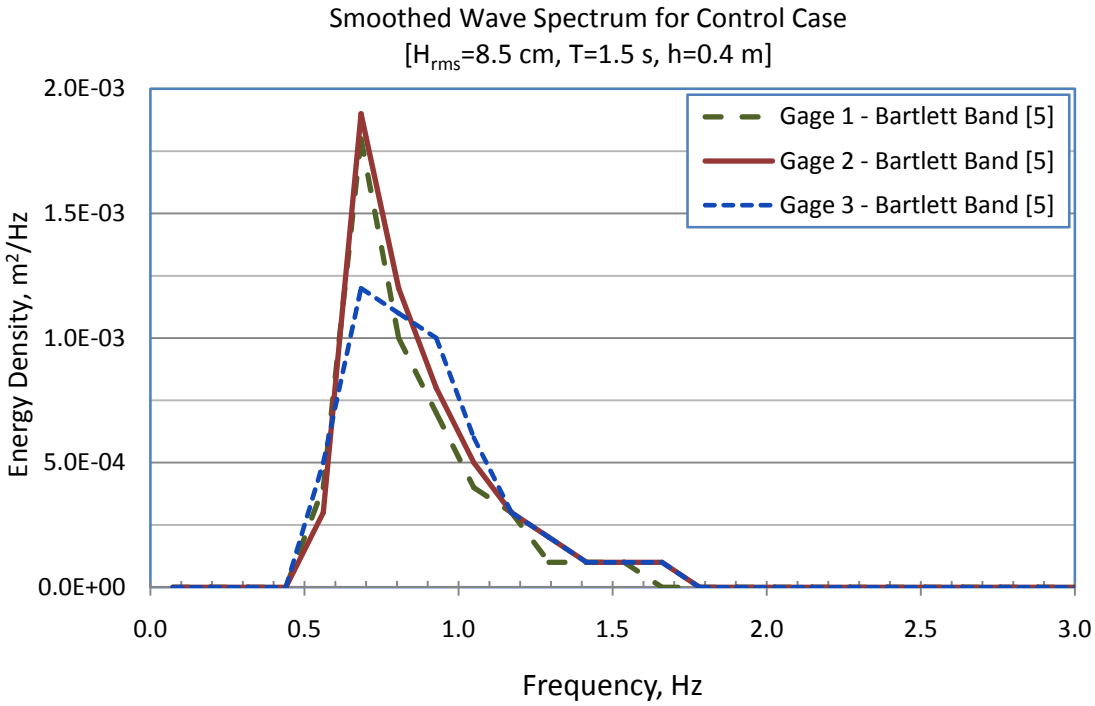
Smoothed Wave Spectrum for Control Case
[Hrms=8.5 cm, T=1.5 s, h=0.4 m]
Gage 1 - Bartlett Band [5]
Gage 2 - Bartlett Band [5]
Gage 3 - Bartlett Band [5]
Energy Density, m²/Hz
2.0E-03
1.5E-03
1.0E-03
5.0E-04
0.0E+00
0.0
0.5
1.0
1.5
2.0
2.5
3.0
Frequency, Hz

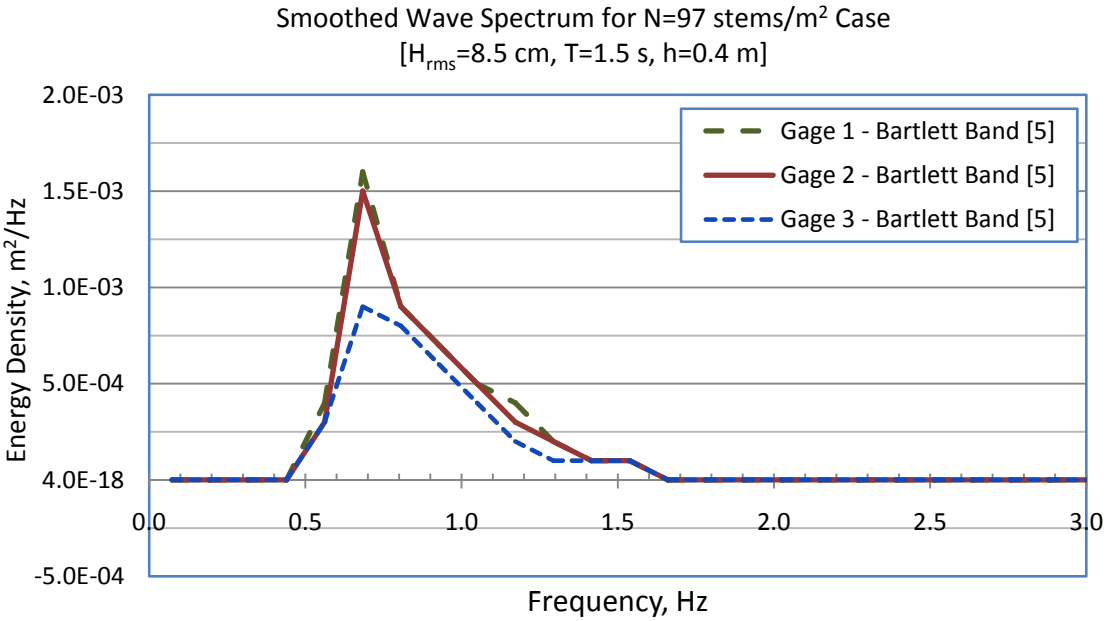
Smoothed Wave Spectrum for N=97 stems/m² Case
[H_rms=8.5 cm, T=1.5 s, h=0.4 m]
Gage 1 - Bartlett Band [5]
Gage 2 - Bartlett Band [5]
Gage 3 - Bartlett Band [5]
Energy Density, m²/Hz
2.0E-03
1.5E-03
1.0E-03
5.0E-04
4.0E-18
-5.0E-04
0.0
0.5
1.0
1.5
2.0
2.5
3.0
Frequency, Hz

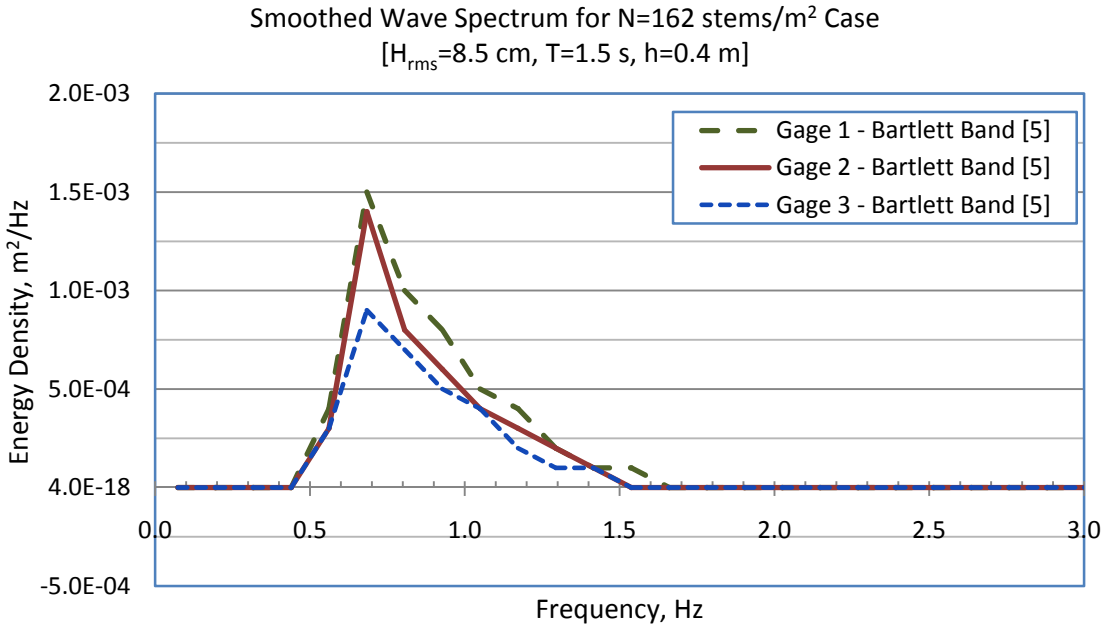
Smoothed Wave Spectrum for N=162 stems/m² Case
[H_rms=8.5 cm, T=1.5 s, h=0.4 m]
Gage 1 - Bartlett Band [5]
Gage 2 - Bartlett Band [5]
Gage 3 - Bartlett Band [5]
Energy Density, m²/Hz
2.0E-03
1.5E-03
1.0E-03
5.0E-04
4.0E-18
-5.0E-04
0.0
0.5
1.0
1.5
2.0
2.5
3.0
Frequency, Hz

APPENDIX D

NUMERICAL FRICTION FACTOR PLOTS

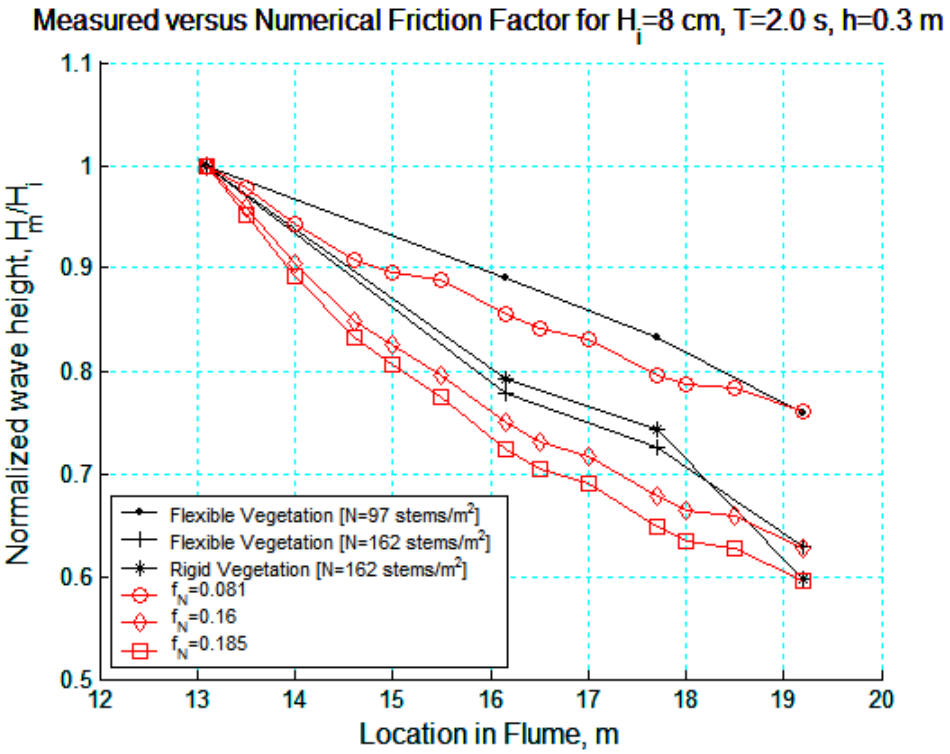
Measured versus Numerical Friction Factor for H_i=8 cm, T=2.0 s, h=0.3 m
Normalized wave height, H_m/H_i
Location in Flume, m
Flexible Vegetation [N=97 stems/m^2]
Flexible Vegetation [N=162 stems/m^2]
Rigid Vegetation [N=162 stems/m^2]
f_N=0.081
f_N=0.16
f_N=0.185

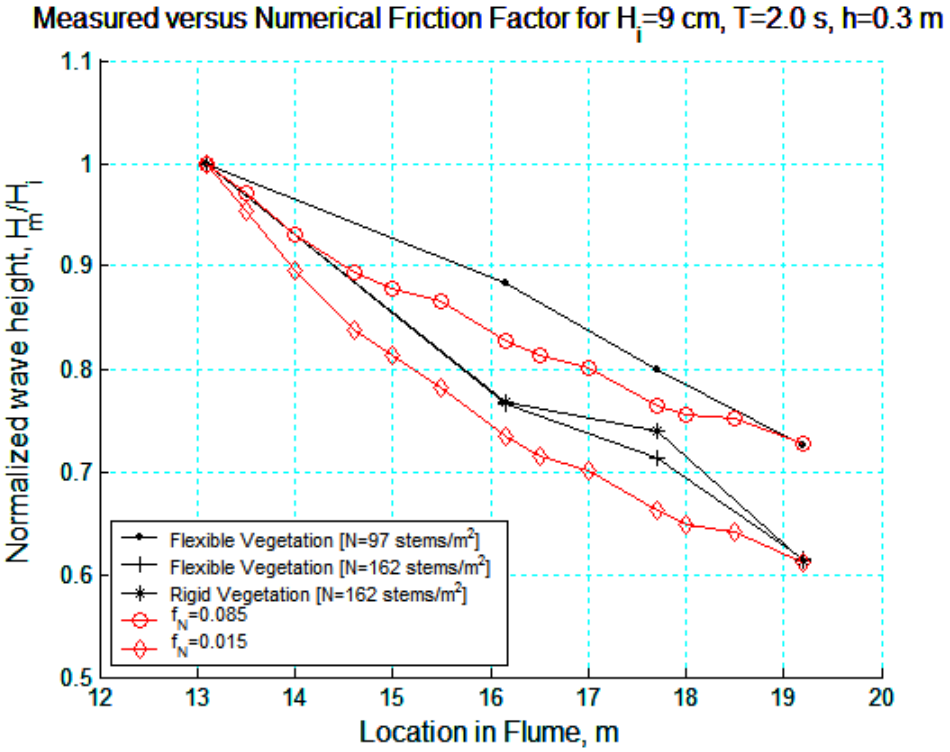
Measured versus Numerical Friction Factor for H_i=9 cm, T=2.0 s, h=0.3 m
Normalized wave height, H_m/H_i
Location in Flume, m
Flexible Vegetation [N=97 stems/m^2]
Flexible Vegetation [N=162 stems/m^2]
Rigid Vegetation [N=162 stems/m^2]
f_N=0.085
f_N=0.015

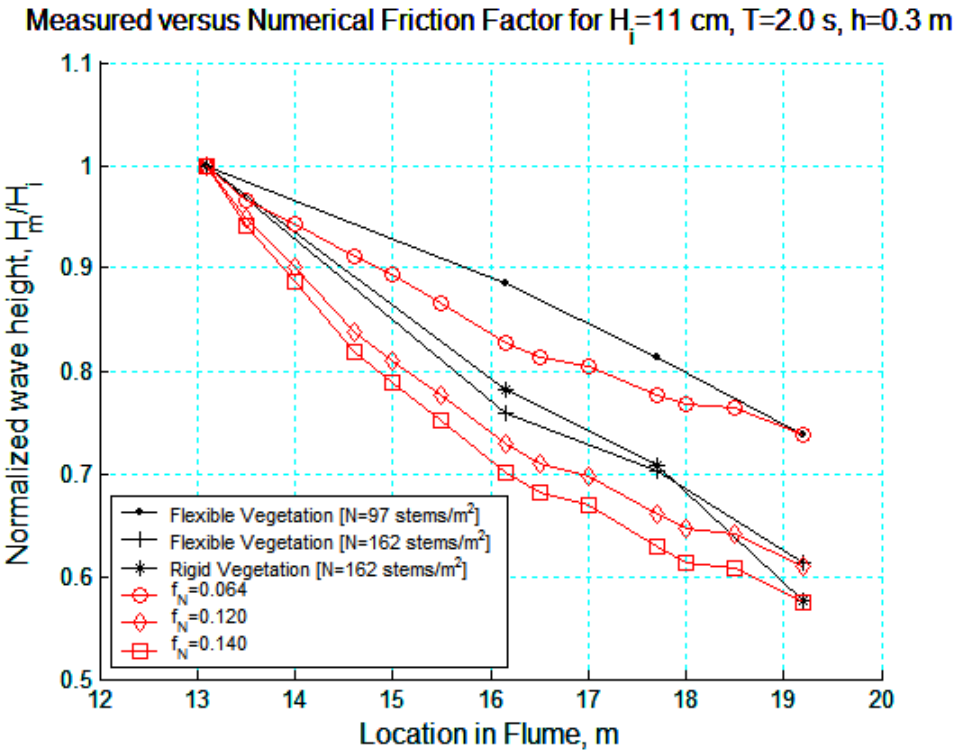
Measured versus Numerical Friction Factor for H_i=11 cm, T=2.0 s, h=0.3 m
Normalized wave height, H_m/H_i
Location in Flume, m
1.1
1
0.9
0.8
0.7
0.6
0.5
12
13
14
15
16
17
18
19
20
Flexible Vegetation [N=97 stems/m^2]
Flexible Vegetation [N=162 stems/m^2]
Rigid Vegetation [N=162 stems/m^2]
f_N=0.064
f_N=0.120
f_N=0.140

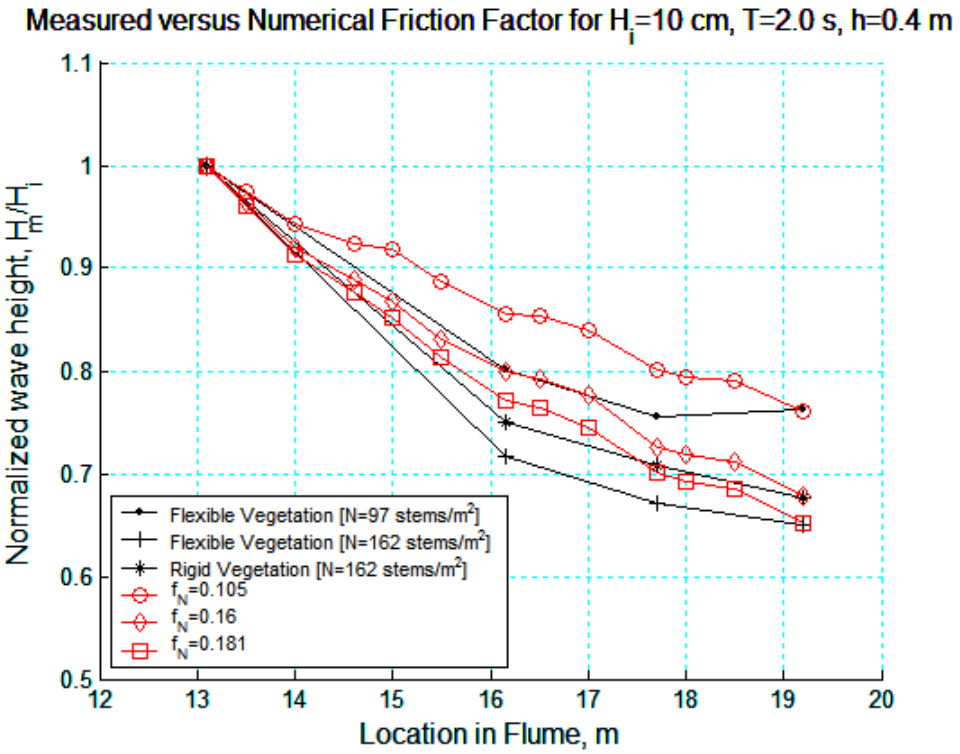
Measured versus Numerical Friction Factor for H_i=10 cm, T=2.0 s, h=0.4 m
Normalized wave height, H_m/H_i
Location in Flume, m
Flexible Vegetation [N=97 stems/m²]
Flexible Vegetation [N=162 stems/m²]
Rigid Vegetation [N=162 stems/m²]
f_N=0.105
f_N=0.16
f_N=0.181

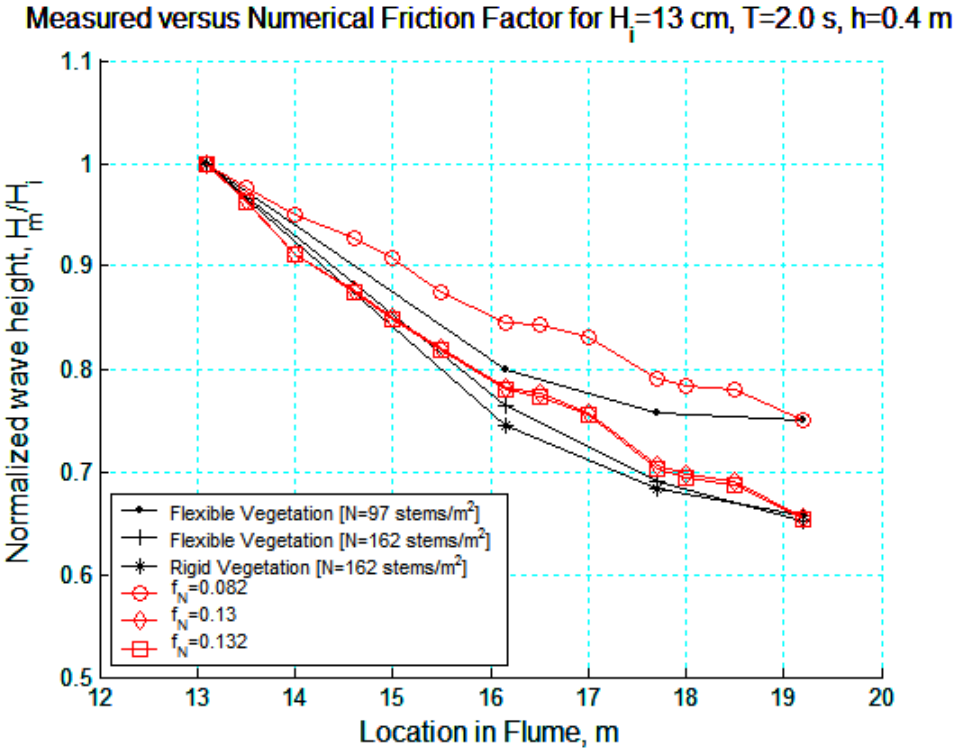
Measured versus Numerical Friction Factor for H_i=13 cm, T=2.0 s, h=0.4 m
Normalized wave height, H_m/H_i
Location in Flume, m
Flexible Vegetation [N=97 stems/m²]
Flexible Vegetation [N=162 stems/m²]
Rigid Vegetation [N=162 stems/m²]
f_N=0.082
f_N=0.13
f_N=0.132

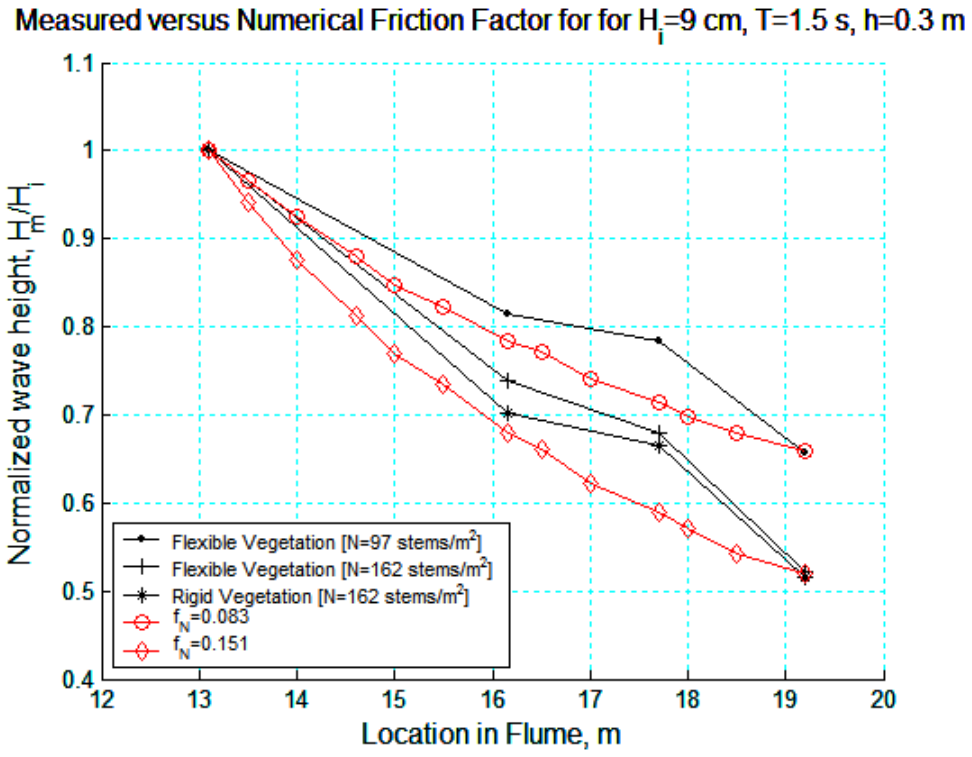
Measured versus Numerical Friction Factor for for H_i=9 cm, T=1.5 s, h=0.3 m
Normalized wave height, H_m/H_i
Location in Flume, m
Flexible Vegetation [N=97 stems/m^2]
Flexible Vegetation [N=162 stems/m^2]
Rigid Vegetation [N=162 stems/m^2]
f_N=0.083
f_N=0.151

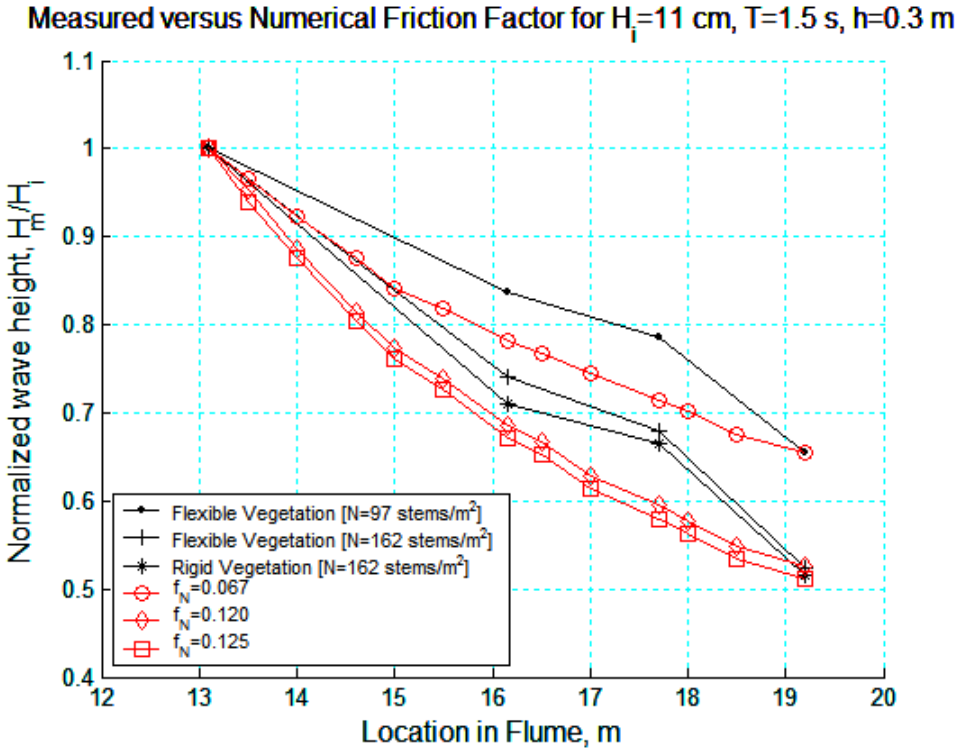
Measured versus Numerical Friction Factor for H_i=11 cm, T=1.5 s, h=0.3 m
Normalized wave height, H_m/H_i
Location in Flume, m
Flexible Vegetation [N=97 stems/m^2]
Flexible Vegetation [N=162 stems/m^2]
Rigid Vegetation [N=162 stems/m^2]
f_N=0.067
f_N=0.120
f_N=0.125

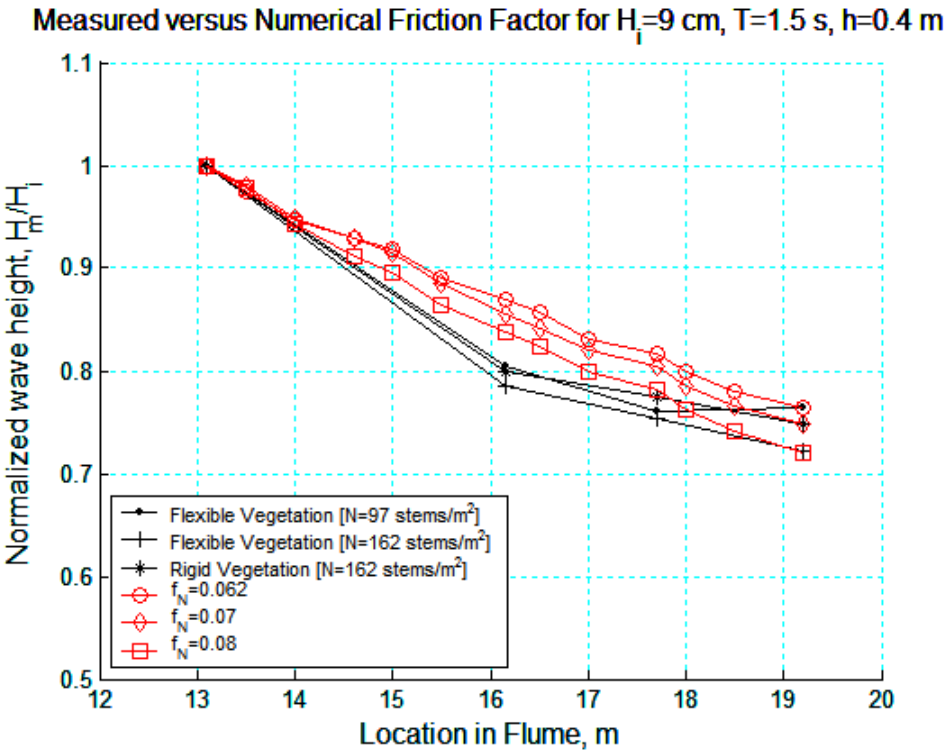
Measured versus Numerical Friction Factor for H_i=9 cm, T=1.5 s, h=0.4 m
Normalized wave height, H_m/H_i
Location in Flume, m
Flexible Vegetation [N=97 stems/m²]
Flexible Vegetation [N=162 stems/m²]
Rigid Vegetation [N=162 stems/m²]
f_N=0.062
f_N=0.07
f_N=0.08

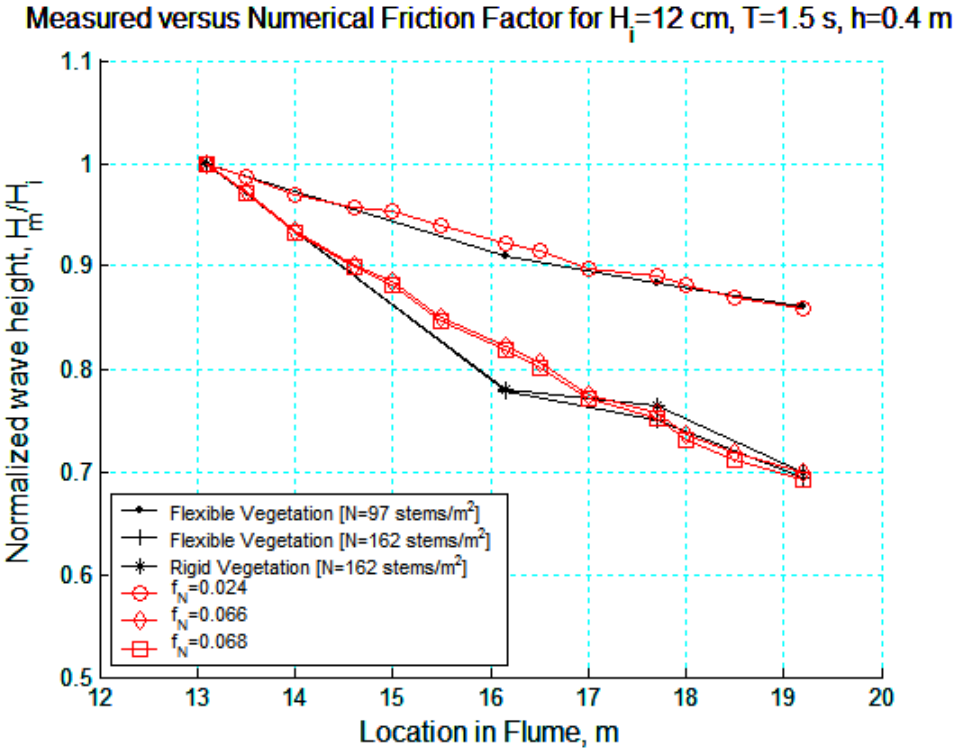
Measured versus Numerical Friction Factor for H_i=12 cm, T=1.5 s, h=0.4 m
Normalized wave height, H_m/H_i
Location in Flume, m
Flexible Vegetation [N=97 stems/m²]
Flexible Vegetation [N=162 stems/m²]
Rigid Vegetation [N=162 stems/m²]
f_N=0.024
f_N=0.066
f_N=0.068

APPENDIX E

ELECTRONIC SUPPLEMENT

This DVD contains a video file from the vegetation experiments conducted in the Haynes Coastal Laboratory and defines the flexibility of the artificial foam vegetation.

This file accompanies this thesis as a file available for downloading.

VITA

Name: Lauren Nicole Augustin

Email Address: Lauren.Augustin@gmail.com

Education:

B.S., Ocean Engineering

Texas A&M University, College Station, TX, (2005)

M.S., Ocean Engineering

Texas A&M University, College Station, TX, (2007)